CONFIDENTIAL

NATIONAL AERONAUTICS AND SPACE ADMINISTRATION
CONTRACT NO. NASw-6

Space Programs Summary No. 37-1

for the period 15 November 1959 to 15 January 1960

jpl JET PROPULSION LABORATORY
4800 OAK GROVE DRIVE, PASADENA, CALIFORNIA
CALIFORNIA INSTITUTE OF TECHNOLOGY

1 February 1960

Copy No._____

GROUP 4
Downgraded at 3 year intervals; declassified after 12 years

CONFIDENTIAL

Preface

The *Space Programs Summary* is a bimonthly publication of the Jet Propulsion Laboratory. Research and development activities conducted by JPL, having specific application to space programs under the sponsorship of the National Aeronautics and Space Administration, are reported in this publication.

The projects reported herein were undertaken in partial fulfillment of National Aeronautics and Space Administration Contract No. NASw-6.

W. H. Pickering, Director
Jet Propulsion Laboratory

This document contains information affecting the national defense of the United States within the meaning of the Espionage Laws, Title 18, U.S.C., Sections 793 and 794, the transmission or revelation of which in any manner to an unauthorized person is prohibited by law.

Copyright © 1960
Jet Propulsion Laboratory
California Institute of Technology

Contents

I. Synopsis 1

II. Ranger Spacecraft Program 2

A. Scientific Experiments 2

B. Communications 4

C. Telemetry and Command Systems 10

D. Guidance 24

E. Power 30

F. Packaging 35

G. Orbit Determination 37

III. Project Echo 40

A. Moon Bounce Experiments 40

B. Transmitter Exciter 42

IV. Vega Program 44

A. Spacecraft 44

B. Guidance and Control 46

Reference 51

I. SYNOPSIS

On 11 December 1959 the National Aeronautics and Space Administration announced the cancellation of the *Vega* program. This program, described in previous issues of *SPS*, was to have included the development of a three-stage vehicle using an *Atlas* booster, a second stage with a GE-405H engine, and third stage with a JPL-6K engine. Upon the notice of termination, the *Atlas* order was suspended, the GE-405H effort was cancelled, and the JPL-6K program was redirected to become an experimental powerplant development. Work on the *Vega* injection guidance system (VIGS) at JPL was also cancelled.

The Jet Propulsion Laboratory was subsequently requested to undertake a study which would result in the definition of a program of lunar and planetary experiments based on the use of the *Atlas-Agena B* and *Centaur* vehicles. Concurrently, the Army Ballistic Missile Agency was asked to form a survey group to determine the limits of *Atlas-Agena B* vehicle performance, and to investigate the availability of vehicles, launching facilities, and other necessities of a flight program.

The survey group, which included representatives from NASA Headquarters, ABMA, GSFC and JPL, visited agencies concerned with the U. S. Air Force *Agena* program, and received technical study results from Lockheed (the Air Force *Agena* prime contractor) and from JPL.

On the basis of the survey it was concluded that the *Atlas-Agena B* vehicle could perform useful spacecraft-development and lunar missions. It was then necessary to make more accurate studies in the areas of guidance and control, range instrumentation, and spacecraft-vehicle interactions. These studies are now in progress.

One of the conclusions of the *Agena* survey was that it is both technically possible and highly desirable to fly early. Therefore, the spacecraft design effort which was in progress for *Vega* has been continued with the hope of meeting or even improving on the proposed *Vega* schedule. At present it appears that the flight schedule depends primarily upon the time required for organization and contracting of the new program, and upon interactions with other U. S. Air Force efforts, rather than upon technical problems. Therefore, in order to take advantage of the earliest flight date that can realistically be achieved, the development of the first model spacecraft, called *Ranger* A-1, is being planned for production of a flight article by early 1961.

In addition to *Ranger*, this issue of the *SPS* contains a section on Project Echo. Echo is a NASA communications experiment utilizing a passive repeater satellite in the form of a 100-foot inflatable plastic sphere with a highly reflective coating of vapor-deposited aluminum. The objectives of Project Echo are: (1) to study the radio wave propagation in the space between the earth and the exosphere, and (2) to determine the feasibility of establishing long distance communication between various locations on earth.

Space Programs Summary 6 contains an introductory report and description of all elements of Project Echo. Preliminary tests of the Project Echo communications system have been made by bouncing radio signals off the surface of the moon. These tests were performed on 23 November 1959 and again on 6 January 1960; results of these tests have proved to be very satisfactory. A detailed description of Project Echo can be found in this report.

Reports on those studies conducted for *Vega* that are not applicable to *Ranger* are being concluded in this issue of the *SPS*. Other research studies, not immediately applicable to *Ranger* but having a potential future application to space programs, are being reported in the *Research Summaries* under these headings: Tracking and Communications, Space Navigation and Trajectory Studies, and Storable Liquid Propulsion Systems.

Beginning with this issue of the *SPS* a new numbering system is being introduced. Subsequent issues will each bear the 37 series designation, but the sequence number will change with each succeeding issue.

II. RANGER SPACECRAFT PROGRAM

The basic configuration of the *Ranger* spacecraft (A-1) is essentially the same as had been proposed for *Vega*; namely, a hexagonal frame containing the electronics packages, with erectable solar-power panels and a movable parabolic communications antenna. By a fortunate coincidence this structural configuration is easily adapted to one type of forward equipment compartment that is used in the Air Force *Agena* program.

The primary functional elements of the spacecraft, without which none of the proposed missions can be performed, are the following: attitude control, power, communications, and environmental control. Operation of these elements is now visualized as follows: immediately after injection the spacecraft is separated from the *Agena* propulsion stage. The solar panels are erected and the communication antenna is rotated to a preset hinge angle. The attitude-control system is activated and solar sensors point the roll axis of the vehicle toward the sun, thus placing the solar power system in operation. The vehicle then turns about the roll axis until the antenna beam points toward the earth. Upon earth acquisition by optical sensors which move with the antenna, the high-gain communication link is established. Provisions are made so that certain scientific equipment can also be kept pointed toward the earth. The spacecraft then continues to coast with its roll axis pointed toward the sun and its communication axis pointed toward the earth. The thermal environment will be controlled primarily by passive methods; i.e., surface emissivity of the equipment containers. Some items of equipment may be pressurized, but it is not now intended to pressurize the hexagonal structure as a whole, nor to use a circulating gas inside the electronics compartments.

A. Scientific Experiments

The scientific experiments for the first two deep-space missions are, understandably, in a more advanced stage of planning than are the subsequent missions. It is planned that the first two *Ranger* flights will be either very high apogee or escape trajectories. The choice of scientific packages for these flights is based on the viewpoint that these packages should constitute an experiment, not merely a collection of instruments. This outlook not only is consistent with the traditions of experimental science, but also helps to insure that spacecraft technology will develop in a direction compatible with space science.

The measurement of the solar corpuscular radiation, or solar atmosphere, is the primary experiment to be carried on the first JPL spacecraft. This measurement consists of six electrostatic analyzers, which look in six different directions; a magnetometer, a vehicle-charge measuring device; and some semiconductor radiation detectors. The electrostatic analyzers will be supplied by JPL. The detectors will measure the differential energy spectrum of electrons up to ~ 100 ev and protons up to ~ 5 kev. The semiconductor radiation devices, which were developed by the State University of Iowa, have electron and proton thresholds of less than 1 and 3 kev, respectively; the actual thresholds have not yet been established.

Magnetic field measurements are a necessary part of the experiment. The rubidium vapor and flux gate magnetometer system, which appears to be sufficiently advanced for use on the first flight, will be suspended from a 10-foot boom to reduce background fields originating in the vehicle. The vehicle-charge instrument will be supplied by either Goddard Space Flight Center or JPL.

This experiment will begin the most important part of its operation when at about 10 earth radii, and it will continue to be significant for as long as it supplies data. The importance of this experiment is based on the fact that the sun is the source of low-energy electrons and protons. As yet, it is not understood how these particle streams are produced or exactly what their relation is to other solar and terrestrial phenomena.

Some high-energy particle detectors are planned to accompany the solar-radiation experiment. It is planned to place a Neher ion chamber (CIT) on the same boom as the magnetometer. This detector will measure all particles with energies above a few mev. (The ion chamber will be accompanied by a single geiger tube.) It is also planned to fly two triple-coincidence cosmic ray telescopes which will be provided by the University of Chicago (UC). One telescope will be unshielded and will have thresholds for detection of ~ 10 mev for protons and of ~ 3 mev for electrons. The second telescope will be shielded by approximately 5 gms/cm^2 of lead which will put the proton and electron thresholds at 75 and 12 mev, respectively. Figure 1 shows the spectral ranges covered by the complete set of radiation detectors.

A Lyman Alpha detector accompanied by a 6-inch mirror and a scanning mechanism will be the second experiment to be carried. It shall be the objective of this experiment to determine the size and shape of the neutral hydrogen cloud which surrounds the earth. The hydrogen cloud experiment will consist of a nitric oxide gas ion chamber with a lithium fluoride crystal, a specially prepared 6-inch mirror, and a mechanical scanner. The ion chamber will be supplied by the Naval Research Laboratories, the mirror will be prepared by Fort Belvoir, and the scanner will be designed by JPL.

The measurement of micrometeorites on the spacecraft skin will be the third experiment. This will be a composite package that will measure both the energies and momenta of impacting micrometeorites. It will be supplied by the Goddard Space Flight Center.

The scientific objectives of the second JPL spacecraft will be essentially the same as for the first flight.

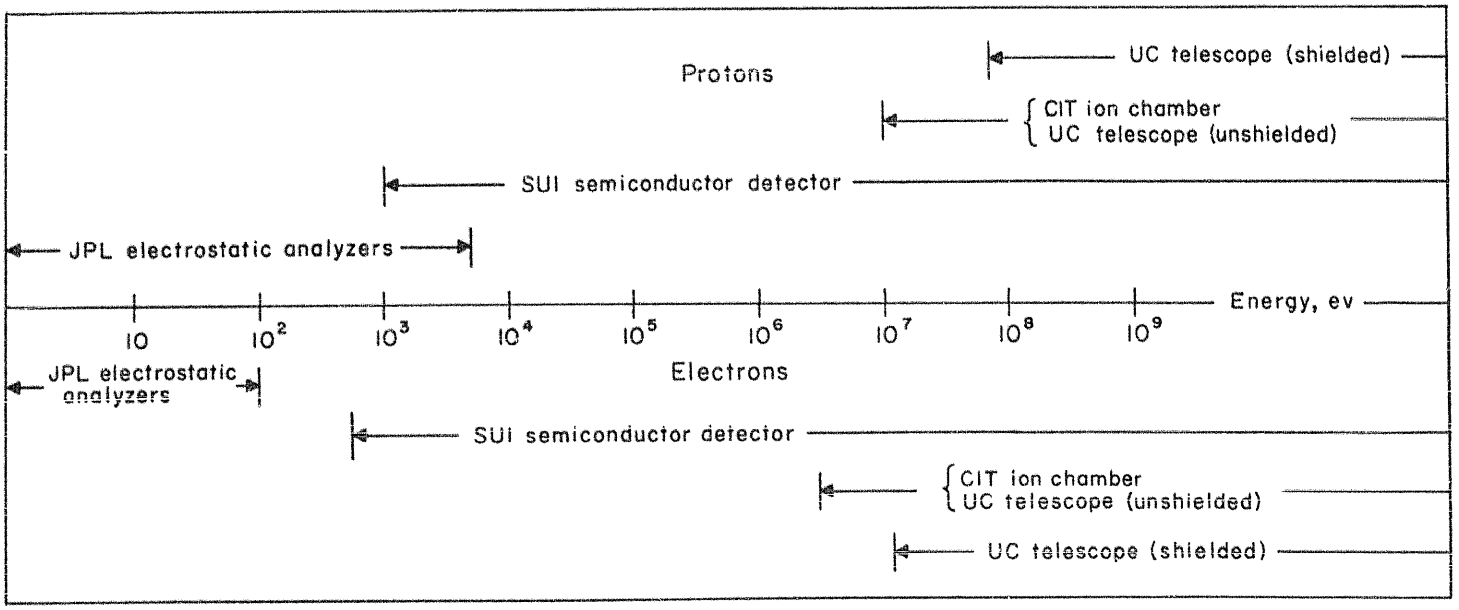

Figure 1. Detector energy spectrum

B. Communications

The communications system proposed for the first *Ranger* spacecraft will consist of a low-power transmitter and a high-power transponder (Fig 2). The low-power transmitter will operate on 960.10 mc and will radiate 0.25 watt essentially omnidirectionally. It will telemeter information about the gross operation of the payload and its scientific instrumentation for ½ million miles and is designed to be powered either by its own separate battery or by omnidirectional solar cells. The low-power transmitter, therefore, will function independently of the attitude of the spacecraft.

The purpose of the high-power transponder is to provide two-way doppler velocity information, to receive commands sent from the earth, and to provide telemetering to a maximum range. It will be powered by solar power (after the solar panels have been erected). Prior to erection the transponder is energized from batteries. The transponder will receive a signal at 890.046 mc using the same antenna as the low-power transmitter and will transmit a 960.05 mc signal using a directional antenna.

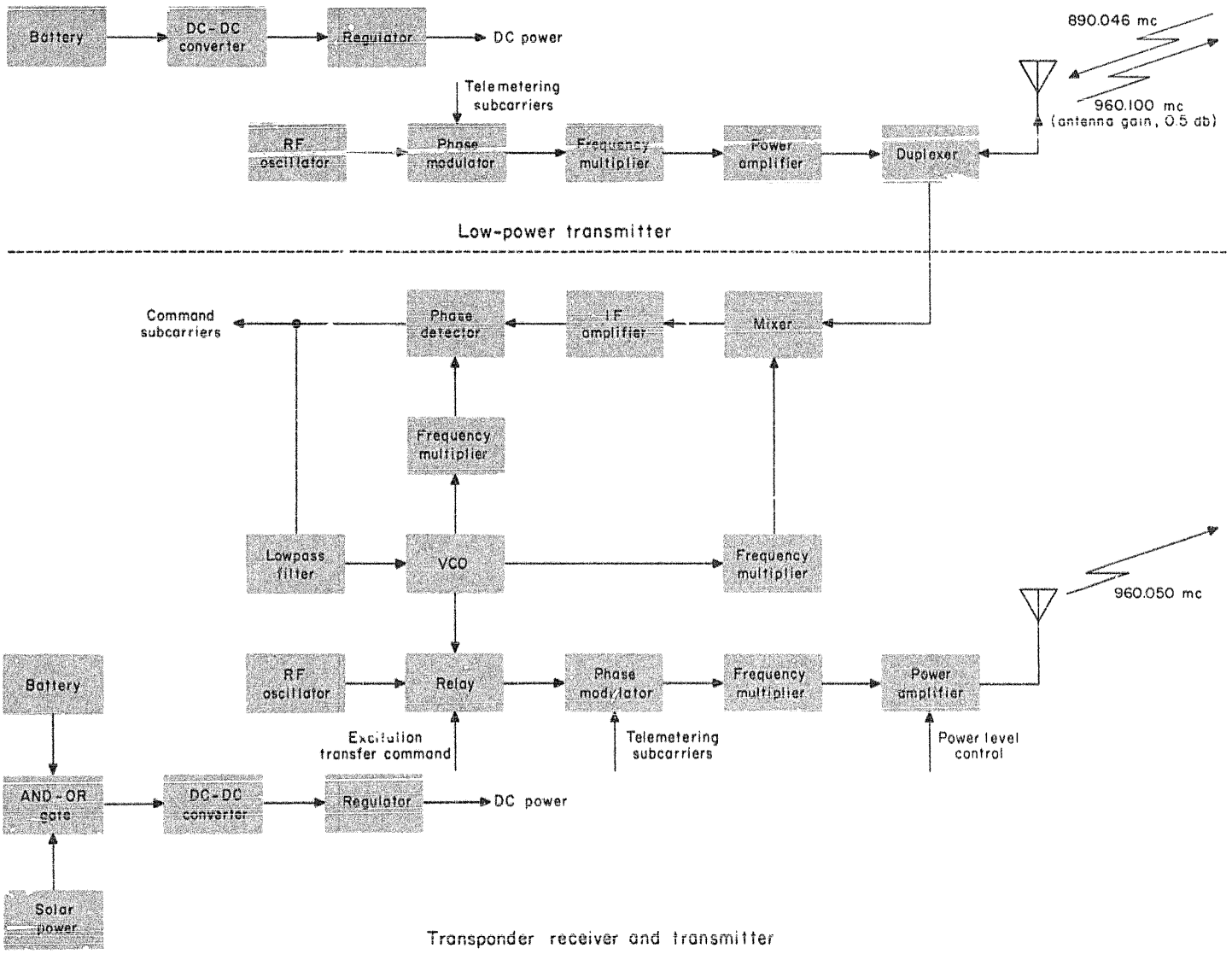

Figure 2. Spacecraft communications system

In order to guarantee communications to 5 million miles, two transponder systems are suggested depending upon the status of the attitude control systems. If a two-axis attitude control system is flown, the best design would incorporate a 25-watt transmitter and a 6-db antenna pattern symmetric about the sun line. If the third axis was considered experimental, a similar design would be used but with sufficient circular asymmetry to permit some instrumentation of the third axis position. If the third axis was considered operational, the transmitter power could be reduced to 3 watts by employing a 4-foot movable parabolic antenna, thereby reducing the dc power requirements from 85 watts (for the 25-watt system) to 20 watts. It is planned to develop both the 3-watt and 25-watt transmitters.

1. Transponder

a. Receiver. A prototype transponder receiver has been developed by JPL to evaluate new transistor circuits and to test their performance in a closed-loop phase-coherent receiver system. The production model is being designed and manufactured by Motorola, at Phoenix, Arizona. The first production unit is scheduled for delivery about 25 January 1960. Although the loop gains and noise figure of the prototype receiver are not identical to those of the production models, the prototype receiver has the same loop-noise bandwidth, and the following measurements of the response of the APC and AGC loops are applicable to both receivers.

The $|1 - H(j\omega)|$ response of the APC loop was determined by phase modulating the receiver's local oscillator and measuring the amplitude of the error signal at the output of the loop phase detector. The theoretical response of the APC loop is shown in Figure 3, together with the measured data. Both the calculated curve and the measured data represent the loop response at a high signal level (−70 dbm). Below 15 cps the signal at the phase-detector output was in the vicinity of the noise level, and accurate measurements could not be made. The response of the phase-detector output circuit was down 3 db at 1600 cps. This accounts for the falloff of the response curve in this region. A 6-kc bandwidth crystal filter in the 10-mc IF amplifier causes the sharp falloff above 3 kc. The favorable correlation between the measured data and the calculated $|1 - H(j\omega)|$ response curve indicates that the actual loop characteristics agree closely with the design. The loop-noise bandwidth, however, is a function of the area beneath the $|H(j\omega)|^2$ curve. Calculations from the measured $|1 - H(j\omega)|$ response indicate that the actual APC loop-noise bandwidth is within 0.5 db of the design value.

The AGC loop of the final receiver is being designed for a noise bandwidth of 1 cps at threshold and is not expected to exceed 10 cps at the maximum signal level of −50 dbm. To evaluate the performance of the AGC loop, the loop-filter time constant was selected to give a loop-noise bandwidth of 5 cps at a high signal level. The response of the loop was measured at a signal level of −70 dbm by amplitude modulating the input signal and measuring the loop output at the AGC bus. The measured data is shown in Figure 4, together with the theoretical response. Calculations from the measured $|H(j\omega)|$ response indicate that the actual APC loop noise bandwidth is within 1.0 db of the design value.

Evaluation of the early prototype receiver is continuing with emphasis on locating and eliminating any internally generated interfering signals. Measurements are also being made to determine the requirements of other portions of the communications system in order to be compatible with the receiver.

b. AGC amplifier. In order to determine the received signal level, it is desired to telemeter the transponder AGC voltage from the spacecraft. The received signal level may be determined indirectly by measuring the gain of the receiver. The accuracy of the measurement is

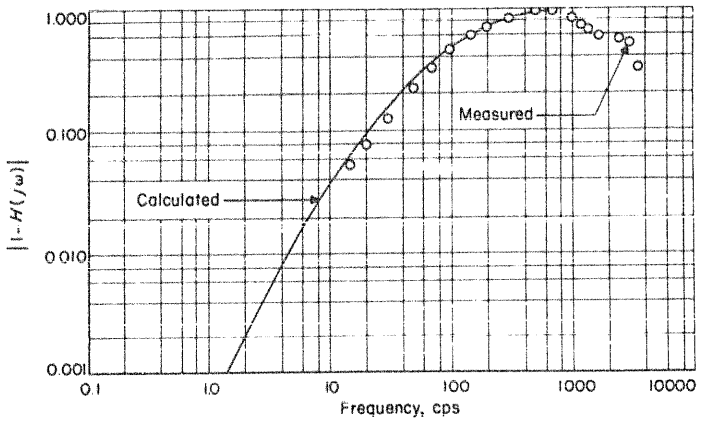

Figure 3. APC loop response

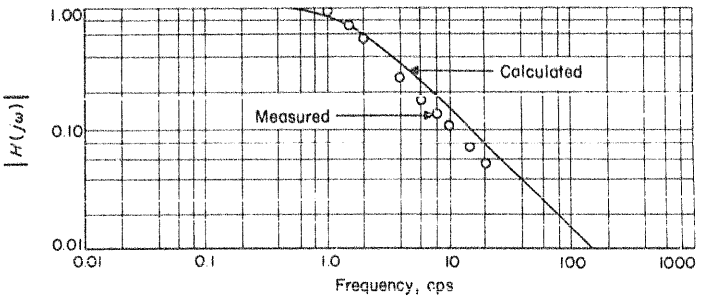

Figure 4. AGC loop response

expected to depend primarily upon the gain stability of the receiver, but it is also affected by the stability of other elements within the AGC loop. Included in the AGC loop is a dc amplifier, the primary function of which is to act as an impedance transformation device such that the receiver gain control circuit does not load the AGC loop filter. For the transistorized IF amplifiers, it was not possible to develop a gain control circuit that would not load the filter without appreciably decreasing the gain control constant K_r. The amplifier need not develop any gain.

Figure 5 is a diagram of the actual AGC loop and also of an equivalent linear loop. The constants of the equivalent loop are:

K_r = receiver gain control, db/v
K_d = amplitude detector gain, v/db
K_a = dc amplifier gain, v/v
S = signal constant for drift calculation

If the dc amplifier develops a drift V over the designed range of temperature (−10 to 82°C), the error in maintaining the receiver output constant will be:

$$e_r = \frac{VK_r}{1 + K_rK_dK_a}\,(\text{db}) \qquad (1)$$

The error in the telemetered information will be:

$$e_t = \frac{V}{1 + K_rK_dK_a}\,(\text{volts}) \qquad (2)$$

Figure 6 is a schematic of the present dc amplifier. For all practical purposes, the amplitude detector output impedance can be included in R_f. The leakage R_{1K} through the capacitor is assumed negligible. Therefore, the voltage gain of the amplifier can be determined as follows:

$$V_{in} = I_{in}R_f + V_{be_1} + V_{be_2} + \frac{\beta_1\beta_2 R_L R_e}{R_L + R_e} I_{in} \qquad (3)$$

Since Q1 is an NPN transistor and Q2 a PNP, the polarities of their emitter to base junction voltages are opposite ($V_{be_1} \simeq -V_{be_2}$). Considering this along with the fact that R_f is small compared with $\beta_1\beta_2 R_e R_L/(R_e + R_L)$, the amplifier gain is essentially unity, and the input impedance is $\beta_1\beta_2 R_e R_L/(R_e + R_L)$. Amplifier drift due to change in temperature will result due to two phenomena. As the temperature increases, the emitter-to-base diode resistance decreases causing a voltage drift from emitter to base of approximately 2 mv/°C for silicon transistors. However, due to the cascading of the NPN and PNP transistors, these drifts are in opposite directions and tend to cancel. The second temperature-producing effect is the

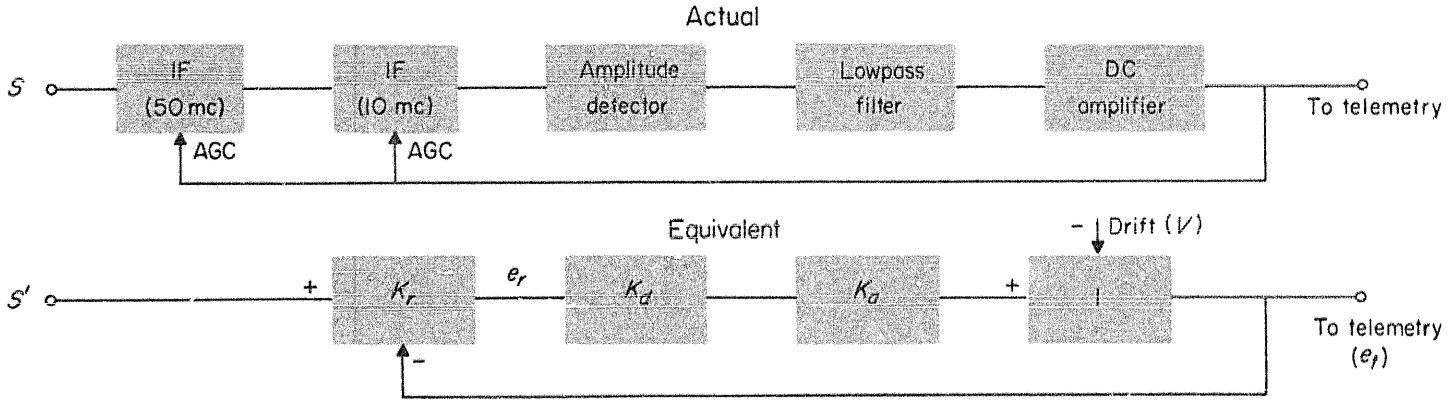

Figure 5. AGC loop

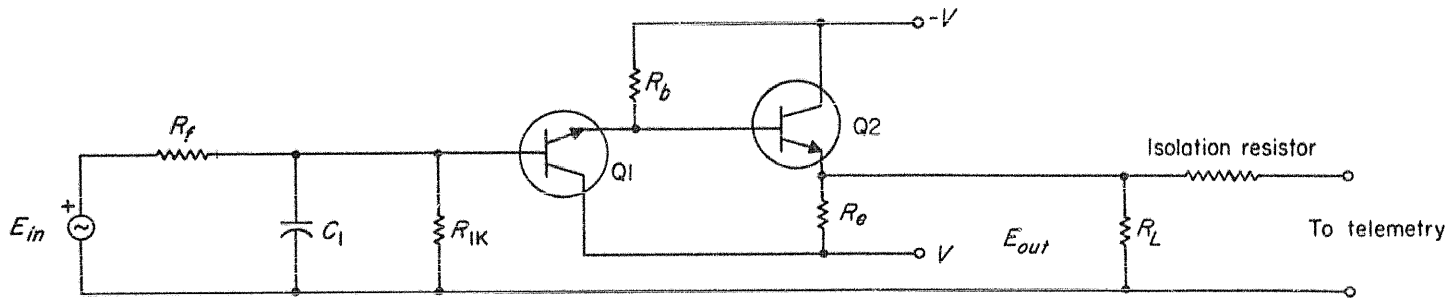

Figure 6. AGC dc amplifier

increase with temperature of the collector to base reverse diode leakage current (I_{co}) which tends to increase the transistor collector currents. Since the current through R_b is practically constant, the increase with temperature of the emitter current in Q1 tends to cancel the increase in emitter current of Q2.

Figure 7 is a graph of the gain of the amplifier at room temperature. It is noted that the gain is extremely linear and very close to unity over the range of operation (0 to 3 volts). Figure 8 is a graph of the millivolt drift of the amplifier over the design temperature range. It is noted that the total drift is in the order of 50 millivolts. Typical values for K_r and K_d would be 50 db/v and 2 v/db.

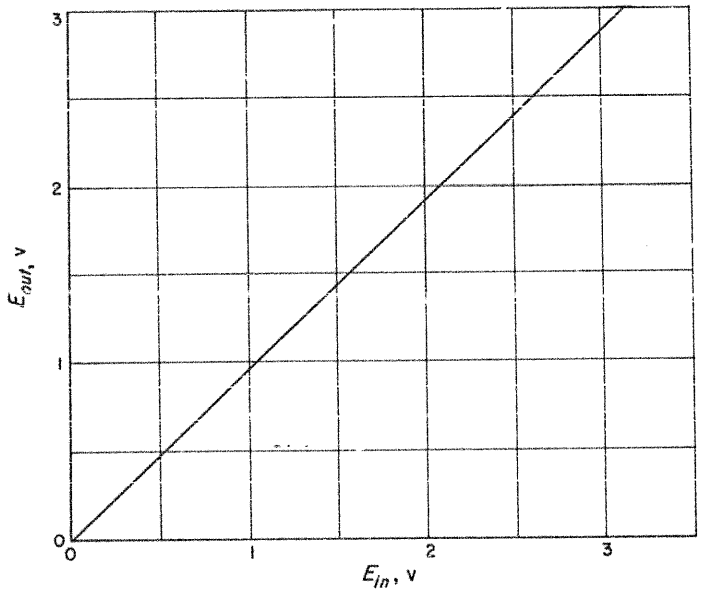

Figure 7. DC amplifier gain

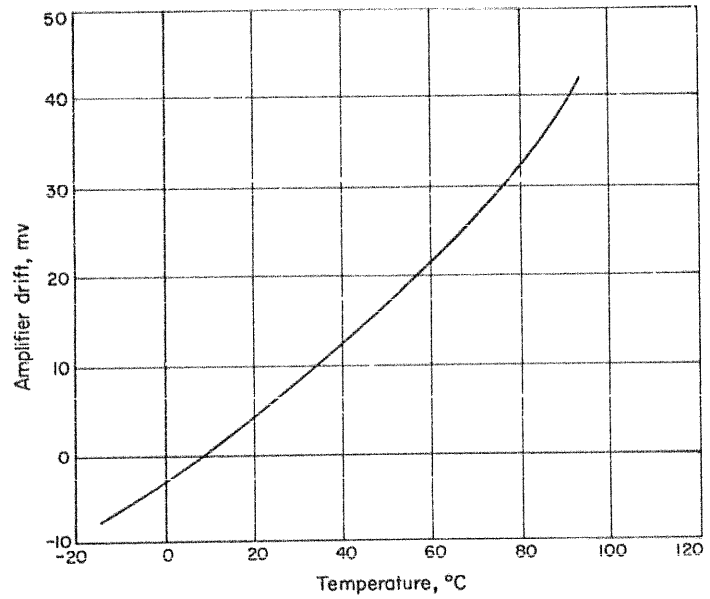

Figure 8. DC amplifier drift

Referring to Equations (1) and (2) and using the above constants, the receiver error and telemetered error would be 0.025 db and 5×10^{-4} volts, respectively. As expected, this error is small enough to be neglected.

c. UHF cavity amplifier. The cavity amplifier described herein is the first in a series of three UHF amplifiers which will comprise the high-power transmitter section of the spacecraft transponder. The purpose of this unit is to amplify the 960-mc, 5-milliwatt transponder output signal to a nominal level of 0.25 watt. The other two cavity amplifiers are expected to have nominal power outputs of 2.5 to 25 watts.

The principal criteria affecting the design of the cavity amplifier were reliability, high efficiency, high gain, wide bandwidth, and low incidental phase modulation as a function of vibration. Design, fabrication, and testing have been completed on the first amplifier. Figure 9 shows an assembly view of the amplifier. The electrical characteristics of the unit have been measured and are compared with the specifications in Table 1.

The amplifier is designed to operate in a partially saturated condition to provide some stabilization of the output signal for variations of the input signal. The RF power output vs RF power input curve of Figure 10 shows the saturation characteristic. The data in Figure 10 indicates that a 3-db decrease in drive level will result in a 1.4-db decrease in output power. Figures 11 and 12 show the effects of B + and filament power supply variations on amplifier performance. Within the spacecraft B+ and filament power supply regulation tolerance of ±5%, the

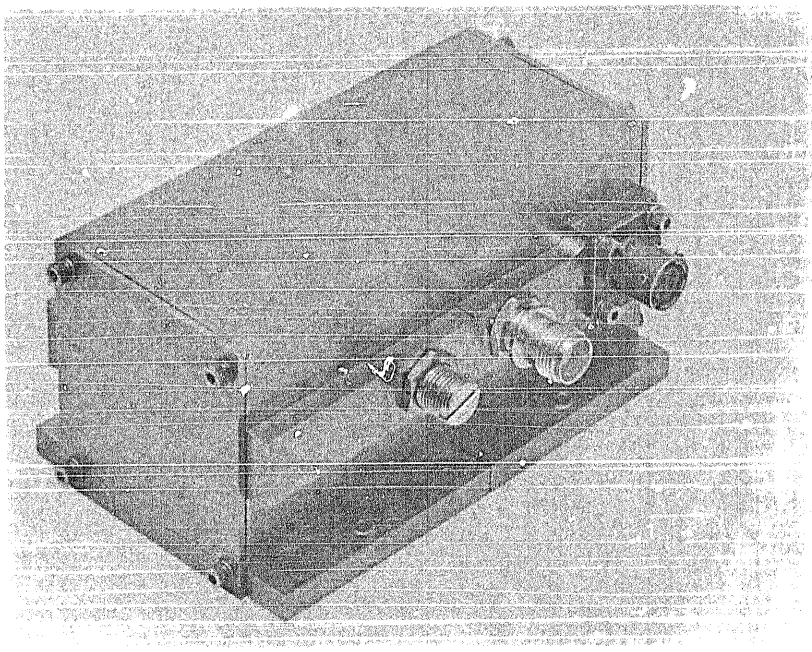

Figure 9. UHF cavity amplifier

Table 1. UHF cavity amplifier characteristics

Characteristic	Design	Measured
Power input, mw	5	5
Power output, mw	250	300
Gain, db	17	17.8
Bandwidth, mc	5	5
Plate efficiency, %	31	41.6
Overall efficiency, %	8	8.4
Input impedance (nominal), ohms	50	50
Input VSWR	1.5	1.25
Output impedance (nominal), ohms	50	50
Output VSWR	1.5	1.06
Plate voltage, v	100	100
Plate current, ma	8	7.2
Filament voltage, v	4.75	4.75
Filament current, ma	600	600

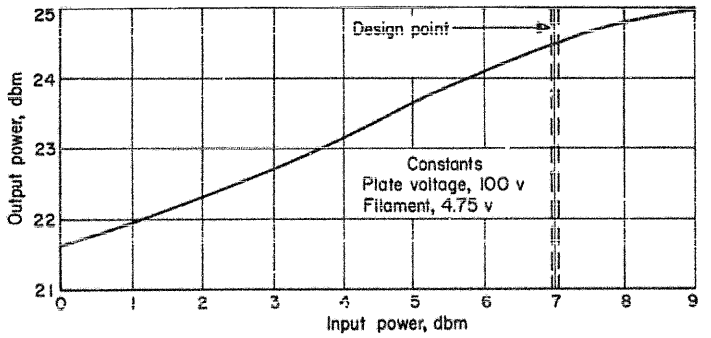

Figure 10. Input vs output power

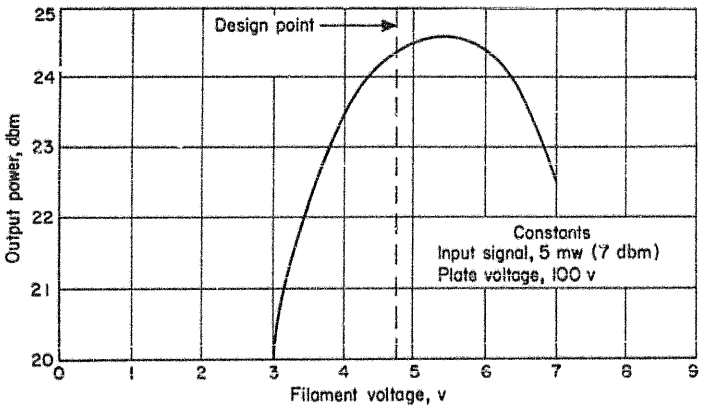

Figure 11. Output power vs filament voltage

curves show that the output of the amplifier will vary ±0.25 db. The actual supply voltages were chosen for highest efficiency and greatest life expectancy.

The thermal characteristics of the unit are shown in Figure 13. It can be seen that the output power will decrease 2 db at the temperature extremes of −10 and 80°C. The mechanical parts of the cavity are fabricated from 2024 aluminum alloy. This material was chosen for light weight and ease of machining and surface plating.

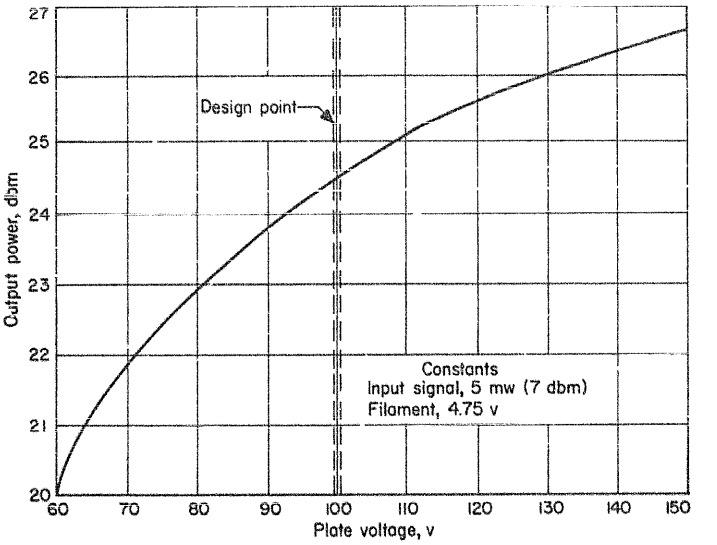

Figure 12. Output power vs plate voltage

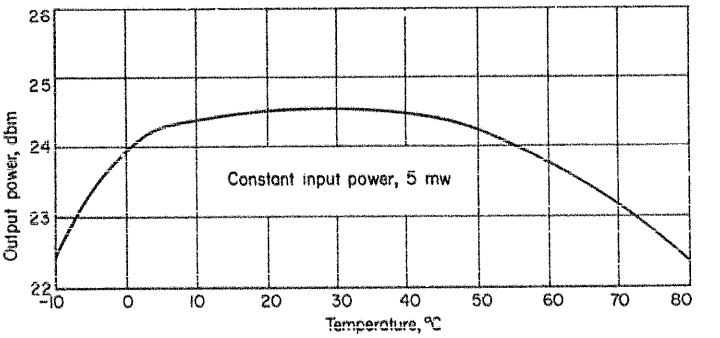

Figure 13. Output power vs temperature

The thermal expansion and contraction of this material de-tunes the cavity and causes the power to drop as indicated in Figure 13. It is desired that the effect of temperature on the power output be limited to 1 db. To accomplish this, an effort is now being directed toward temperature stabilization by means of thermally sensitive tuning adjustments.

The unit was tested environmentally to the flight equipment specifications listed in Table 2. As a function of mechanical shock and vibration, the amplifier was required to meet that portion of JPL design specifications No. 30317 covering performance. The results of the tests are compared with the specifications in Table 2.

The results shown in Table 2 indicate that the amplifier exceeds what may be regarded as a typical flight equipment specification. It is anticipated that this design will also be used as the second amplifier (2.5 watts) in the transmitter chain. In this mode, higher supply voltages as well as minor electronic component changes are required. It is expected that greater efficiency will be realized at the higher level of operation.

Table 2. UHF cavity amplifier environmental test specifications and performance

Test	Definition of limits	Maximum phase jitter, deg	
		Design	Measured
Vibration	3 planes, complex wave		
	12.5 *g* rms noise, 4 sec	2.5	0.7
	5 *g* rms noise / 5 *g* rms sinusoid } 10 min	1.0	0.5
	5 *g* rms noise / 8 *g* rms sinusoid } 10 min	1.6	0.6
	4 *g* rms sinusoid, 20 to 2000 cps, 10 min	0.8	0.5
Shock	3 planes		
	50 *g*, 6.0 millisec	10.0	1.0
Thermal	−10 to 82°C at 1 micron pressure	—[a]	—[a]

[a]See Figure 13.

2. Antenna System

The basic requirements that the spacecraft antennas will have to meet have undergone re-evaluation. Originally, circularly polarized antennas were to be used so as to be compatible with the circularly polarized antennas on the ground. The polarization for the spacecraft antennas will now be linear.

It is planned to have the space net ground antennas circularly polarized only during the initial portions of the vehicle flight. During this time, the 3-db loss (which results from the fact that the antennas at the opposite ends of the communication links will not have similar type of polarizations) can be tolerated. Later in the vehicle flight it is planned to switch the space net ground antennas from a circularly polarized monopulse tracking system to a linearly polarized listening feed system. The rate of change of the polarization angle will be small enough to make it feasible to rotate the feed to maintain proper alinement with the polarization plane of the incoming signal. Also by this time the trajectory will be established so that *auto-track* will no longer be necessary and the antenna can be programmed to follow the vehicle. The polarization and tracking changeover does not, however, apply to the downrange station since that station will be utilized only during a short interval after injection.

A second requisite imposed upon the spacecraft antennas is that their radiation patterns be uniform and easily predictable in order that variations in the received signal strength can be used for propagation studies and for evaluation of the communication system. Two antenna systems are still necessary and there are other requirements peculiar to each antenna. The communication system requires that a high-gain antenna be used with the transponder-transmitter and a low-gain antenna be used with the primary telemetry-transmitter and transponder-receiver.

a. High-gain antenna. The high-gain antenna will be a 4-foot parabolic reflector which will provide a pencil beam of 18 degrees half-power beamwidth and a gain of 18.5 db over an isotropic radiator. Physically, it will be constructed of a ¼ by ¼ inch mesh giving a surface covering of 19% supported by six radial arms and three concentric hoops.

The feed for the antenna consists of a half-wavelength dipole mounted on a coaxial transmission line with a double-ended balun slot. At one end of the balun slot is a 9-inch diameter groundplane, ¼ wavelength from the dipole. The other end of the transmission line goes through the center of the reflector and acts as the support of the feed system. The reflector shape is defined by a focal length to diameter ratio of 0.35. Weight is to be approximately 10 pounds. Whereas the original configuration called for a stationary antenna, the antenna must now be slewable along an axis off to one side. This requirement poses several problems in addition to the obvious mechanical ones. One problem concerns the spacecraft configuration. No hardware may be in the path of the moving antenna or can obstruct its field of view. A second problem is in providing a rotary joint or a flexible cable service loop for the transmission line between antenna and transmitter.

An investigation will be carried out to determine which of the two methods is more feasible; at the present time, however, the rotary joint seems a simple approach. The probability of finding a highly flexible cable which can survive the extremes in temperatures and possible radiation environments is not too high.

A ¼-scale working model of the antenna has been constructed for testing on a spacecraft scale model, and pattern measurements are being made on this model. A full-scale antenna is under construction.

b. Low-gain antenna. The low-gain antenna will consist of a half-wavelength coaxial dipole mounted in front of and on the axis of the spacecraft (Fig 14). The basic design requirement is that the radiation pattern must be uniform over the expected communication angles of plus or minus 50 degrees from the equator of the vehicle (i.e., look like a donut-shaped pattern symmetrical about the vehicle axis). Two requirements are imposed on this antenna. First, no obstructions can be mounted on the spacecraft that would fall within the specified communication angles. Second, the bulk of the spacecraft below

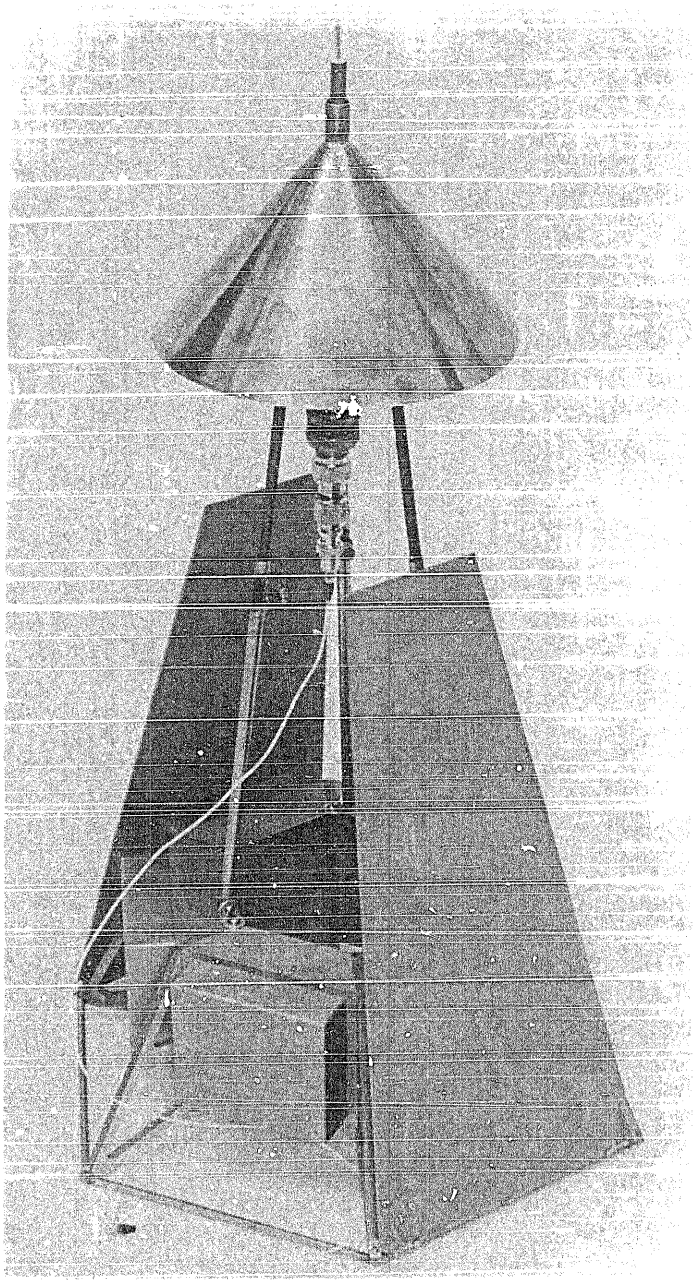

Figure 14. Low-gain spacecraft antenna, ¼-scale model

the antenna should appear symmetrical in order to avoid obtaining a pattern with many lobes and nulls. The necessity for accurately calibrating the pattern in order to verify the communications system parameters does not require that the pattern be complex. The approach being used to make the spacecraft appear symmetrical is to mount a cone shield below the antenna to mask the vehicle from the antenna.

A problem arises with the additional requirement that this antenna move out on a boom with a scientific experiment package. An investigation will be made to determine the best way of providing a transmission line between the antenna and spacecraft proper that will allow a boom travel on the order of 6 to 8 feet. Measurements are now in progress on a ¼-scale model to determine what effect various parts of the spacecraft have on the antenna radiation patterns such as various solar panel configurations, various locations of the antenna along the spacecraft axis, and shroud sizes and shapes.

c. Antenna accessories. A mixer-diplexer is required in the communications system. Preliminary specifications have been made and a survey completed on the availability of subcontractors to perform the work. As soon as the specifications can be finalized, the contracts will be let. It is expected that this will be accomplished within the coming month.

C. Telemetry and Command Systems

In addition to other functions, the spacecraft two-way communications system will be utilized as a carrier for command information and for both scientific and vehicle engineering telemetry data. The relationship of these systems to the communications system is shown in Figure 15. The following paragraphs discuss the theory and planned mechanization of the command and telemetry systems for the first *Ranger* spacecraft vehicles as presently envisioned.

In order to provide capability for a first spacecraft flight in January of 1961, the systems are mechanized to use currently available system components. It is anticipated that the Engineering Model flight equipment will be constructed and tested by April and that the Engineering Model of the ground equipment will be available about 1 month later.

The commands required for the first spacecraft are three separate on-off signals. The system must have the capability of reliably receiving and detecting these commands at threshold distances.

The telemetry data requirements for the first spacecraft are indicated in Table 3. The first telemetry system will provide approximately 25 engineering measurements which are divided among the attitude control, power, communications, and missile environment systems. This

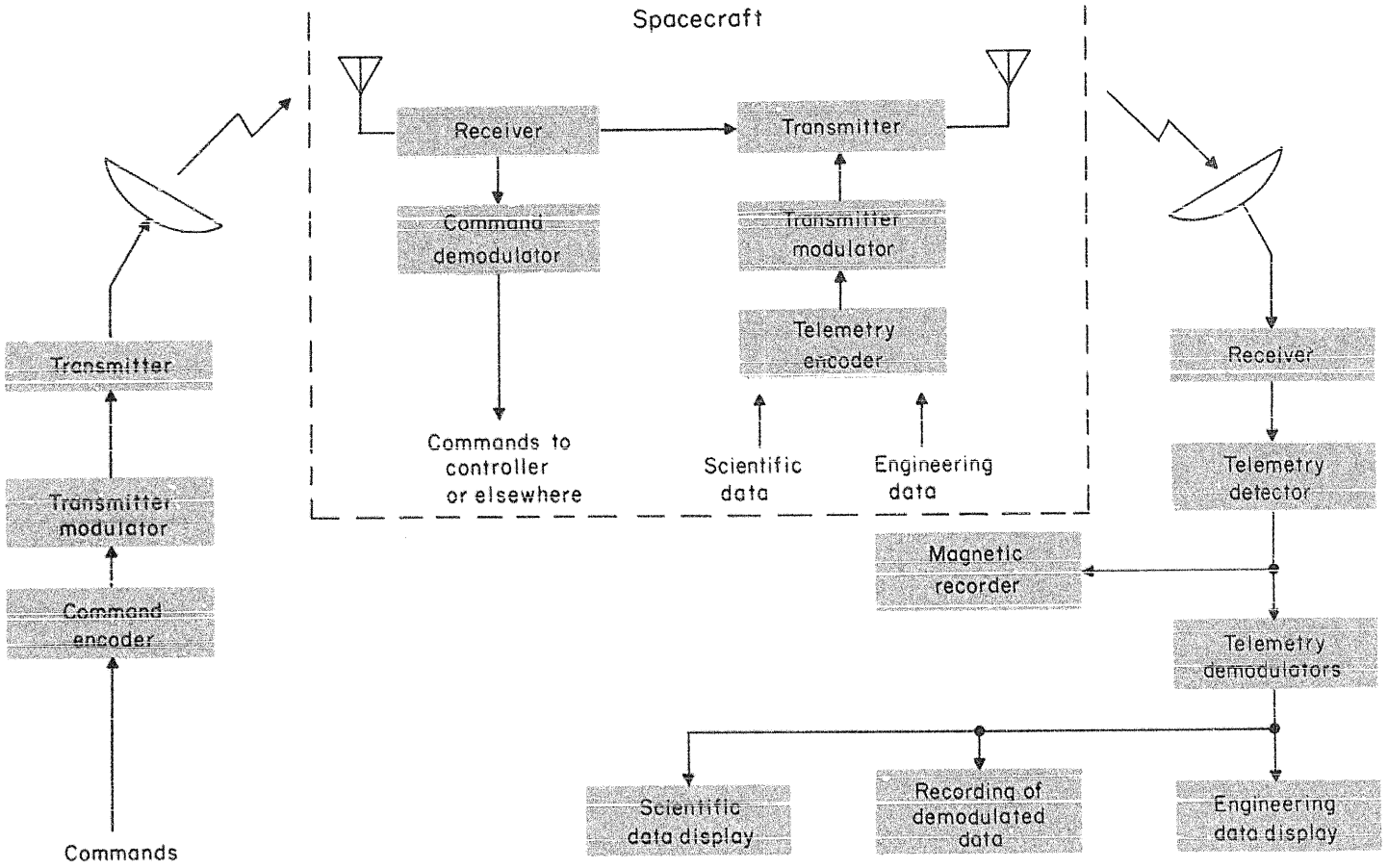

Figure 15. Command and telemetering system

telemetry system will also provide data encoding for nine scientific instruments.

The primary site for command transmission and data reception will be the Goldstone facility. Other Deep Space Network stations will receive only telemetry data.

1. Telemetry Data System

The presently proposed telemetry data encoding and decoding systems are shown in Figures 16 and 17. These systems represent some significant changes from the system discussed in *SPS 6*. Two types of frequency-multiplexed channels are used to provide the maximum data communication efficiency. One type of subcarrier (Channels 2, 3, and 4) carry analog-type data, whereas the remaining channels (B-10 through B-15) carry binary or two-state information. Spectrum relationship for these channels is shown in Figure 18.

The binary data is prepared in serial form by the scientific instrument electronics which modulates the binary channel with a very low-frequency deviation. This binary data is reconstructed by the ground discriminators into binary pulse data of the form presented to the flight encoder.

The engineering data is commutated onto Channels 2, 3, and B-10, in a manner discussed in *SPS 6*. Synchronization of the commutated data is obtained by (1) modulating appropriate segments of the commutator with a synchronization tone, (2) detecting this high-frequency modulation (with respect to the phase-lock-loop discriminator loop bandwidth) at the discriminator multiplier output, (3) routing this detected synchronization pulse through logic which appropriately reconstructs the flight-commutator data program, and (4) gating each specific subcarrier frequency readout to the individual read-and-hold displays for each measurement.

a. Theoretical design. In the design of a data communication link, either one of two general approaches may be taken. In the first approach, the number of data channels available as well as power available per channel may be arbitrarily fixed and the data then conditioned so as to pass through these channels. In the second method, the data rates and waveforms are fixed and then the channel power allocated for most efficient use of the available power. The *Explorer* satellites were an example of the former approach; an arbitrary division of power was made among the subcarrier channels with the thresholds allowed to fall where they might, as a function

Table 3. Engineering and scientific measurement requirements

Engineering measurement requirements	
Measurement	**Time between commutated samples, sec**
Attitude control system	
Yaw rate gyro	10
Yaw rate gyro	100
Pitch rate gyro	10
Pitch rate gyro	100
Roll rate gyro	10
Roll rate gyro	100
Fuel totalizer	1000
Power supply system	
Primary system voltage	1000
Solar panel No. 1 current	1000
Solar panel No. 2 current	1000
Solar panel No. 1 temperature	1000
Solar panel No. 2 temperature	1000
Battery temperature	1000
Converter No. 1 voltage	1000
Converter No. 2 voltage	1000
Solar panel erection	1000
Environmental	
Case No. 1 temperature	1000
Case No. 3 temperature	1000
Case No. 5 temperature	1000
Gas bottle temperature	1000
Radio communication system	
¼-watt transmitter power output	10
Transponder power output	10
Transponder-driver power output	10
Command receiver AGC voltage	10
Command receiver phase error	10
Command receiver mixer current	100
Transponder temperature	100
275 to 600 v dc	100

Scientific measurement requirements	
Measurement	**Binary, bps**
Solar corpuscular radiation	3.6
Flux gate magnetometer	2.6
Vehicle charge	0.2
Cadmium sulfide proton detector	0.4
Triple-coincidence ionization chamber	0.5
Integrated ionization chamber	0.1
Anton Geiger counter	0.15
Neutral hydrogen cloud (if digital measurement)	1.0
Micrometeorite	1.0

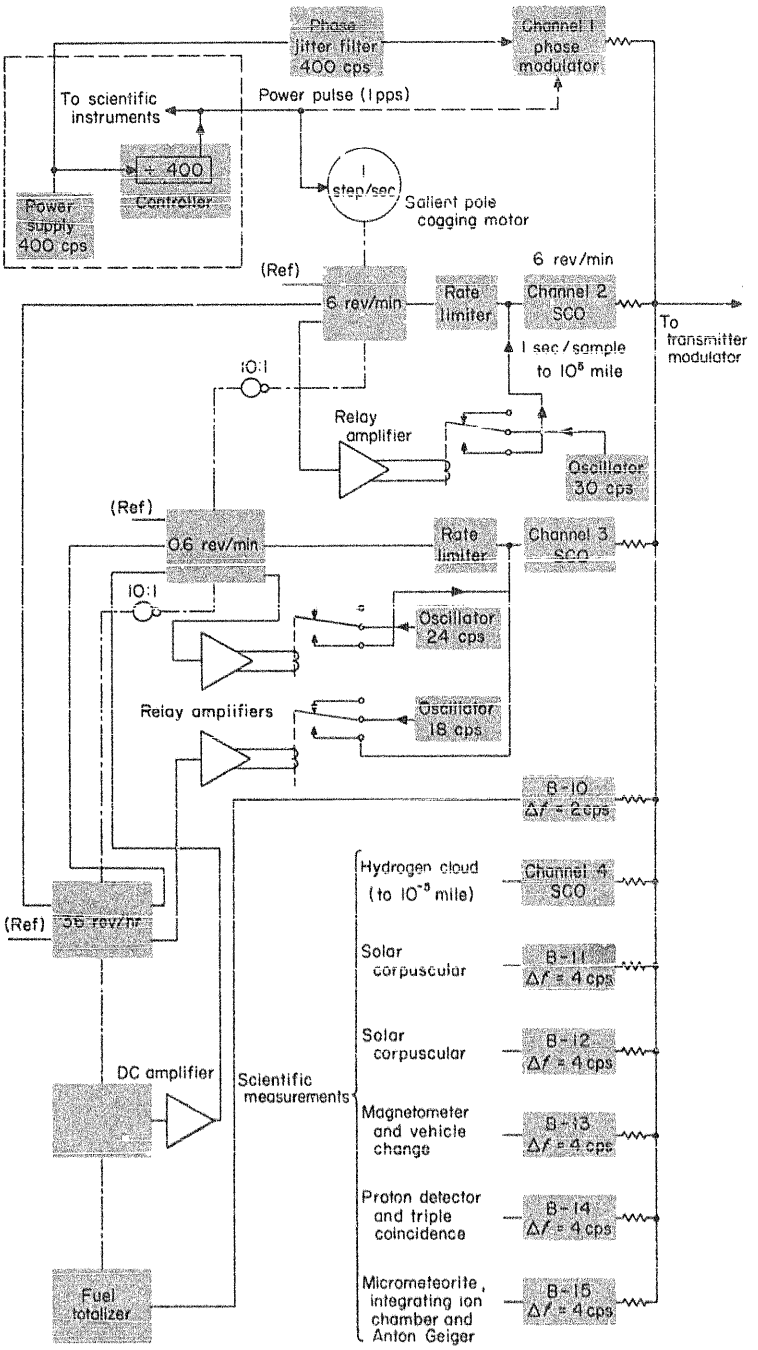

Figure 16. Telemetry data encoding system

of the data rates and waveforms. In the *Pioneer* lunar probes, the first approach was again used but much more sensibly. In this case, the available channel bandwidths were chosen to achieve a specified threshold and the data conditions so as not to exceed the allowable rate.

In designing the spacecraft communications system, the second approach has been taken. The data waveforms, sampling rates, accuracies, and threshold distances were chosen and then the power required to achieve this data rate and fidelity was allocated to each channel.

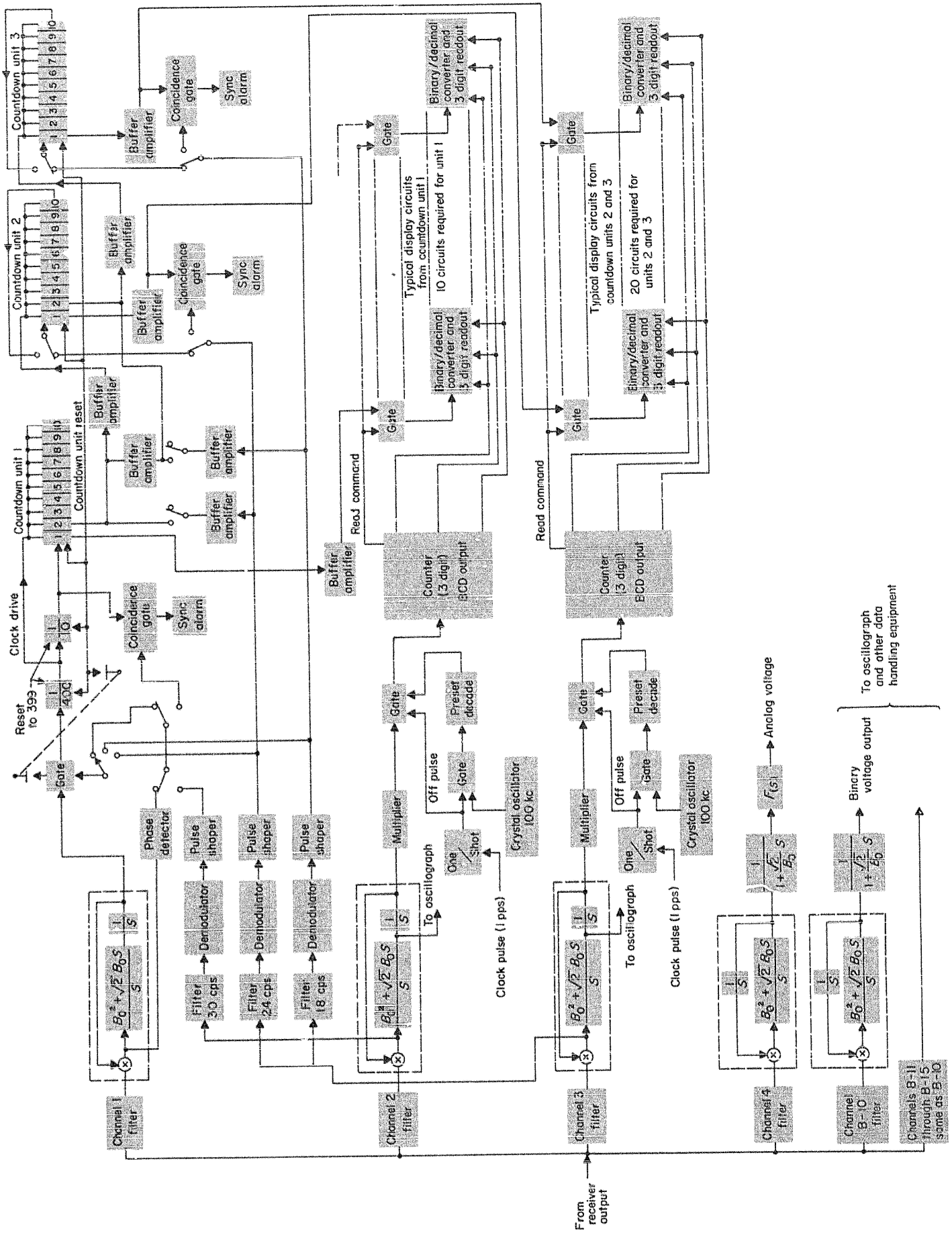

Figure 17. Telemetry data decoding system

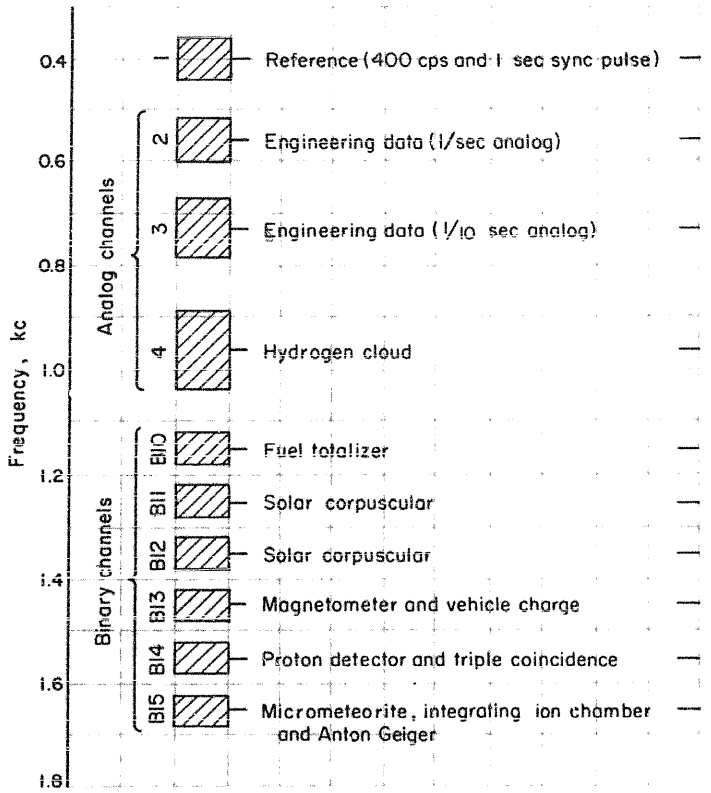

Figure 18. Tentative channel assignments

It can easily be shown that the following system equation holds for this communication link, as well as for the earth-to-space command system:

$$P_t + G_t + G_r = 2B_{L_0} + \left(\frac{S}{N}\right)_{2B_{L_0}} + \Phi_{KT} + \Phi_{NF} + L_s + L_p + \sum L_m$$

where

P_t = total transmitted carrier or subcarrier power, dbm.

G_t = transmitting antenna gain, minimum, db.

G_r = receiving antenna gain, db.

$2B_{L_0}$ = either phase-coherent loop noise bandwidth, or in a synchronous case, predetection noise bandwidth, with respect to 1.0 cps, db • cps.

$\left(\frac{S}{N}\right)_{2B_{L_0}}$ = required signal-to-noise ratio into $2B_{L_0}$ at threshold, db.

Φ_{KT} = noise power per cycle at 290°K, −174.0 dbm/cps.

Φ_{NF} = excess noise power per cycle above 290°K, db.

L_s = path (space) loss at threshold distance, db.

L_p = system design safety factor (pad), db.

$\sum L_m$ = miscellaneous losses, cable, etc., db.

Of the ten variables given by this equation, six can be called given system parameters as they must be known before the design of the subcarrier channels can begin. These are G_t, G_r, Φ_{KT}, Φ_{NF}, $\sum L_m$, and P_t, where P_t in this case implies the total available transmitter power, P_{tot}. Another boundary condition which must be determined is the amount of power allocated to the carrier itself; in the past this has usually been held to at least 50% of the total unmodulated power, but in the design to follow, a 40% figure was agreed upon. This leaves the carrier 4 db below the total system power, but at least 1.5 db above either subcarrier sideband in the worst case, if only one subcarrier is used.

To determine the relationship between the suppression of the carrier by subcarrier modulation (N being the number of subcarriers used) and the total rms phase modulation of the carrier, Figures 19 through 22 were plotted for N subcarriers with equal modulation indices $\Delta\theta_n$. Figure 19 gives the carrier power P_c with respect to P_{tot}, for 0 to 9 subcarriers and 0.5, 0.6, 0.7, 0.8, 0.9, and 1.0 radian rms modulation of the carrier. Figure 20 gives the individual subcarrier sideband power (the sum of both sidebands) with respect to P_{tot} and the same parameters. In Figure 21, the total subcarrier power is plotted as a percentage of the total available power P_{tot}. In Figure 22, the theoretical efficiency with which the system power is used is plotted against the same parameters. During the many numerical iterations required by the frequent *Vega* system changes, it was found that even when the modulation indices $\Delta\theta_n$ are not equal (but all fall within a relatively narrow range with respect to each

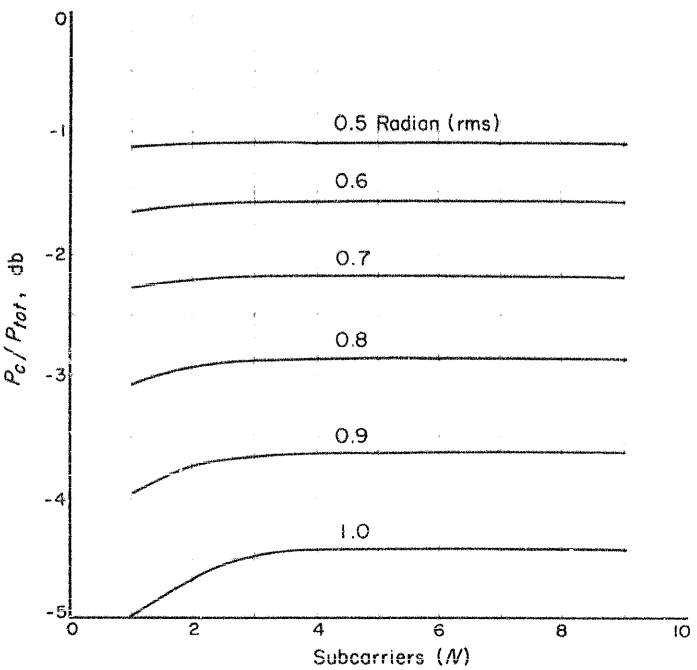

Figure 19. P_c/P_{tot} for various phase modulation indices

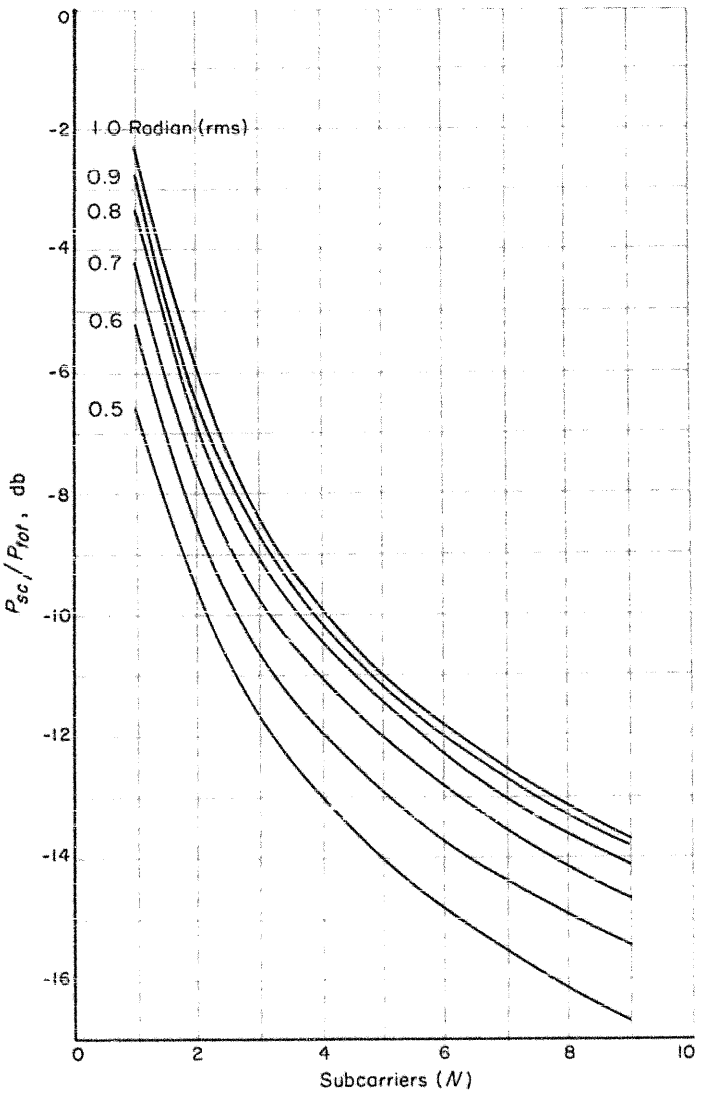

Figure 20. P_{sc}/P_{tot} for various phase modulation indices

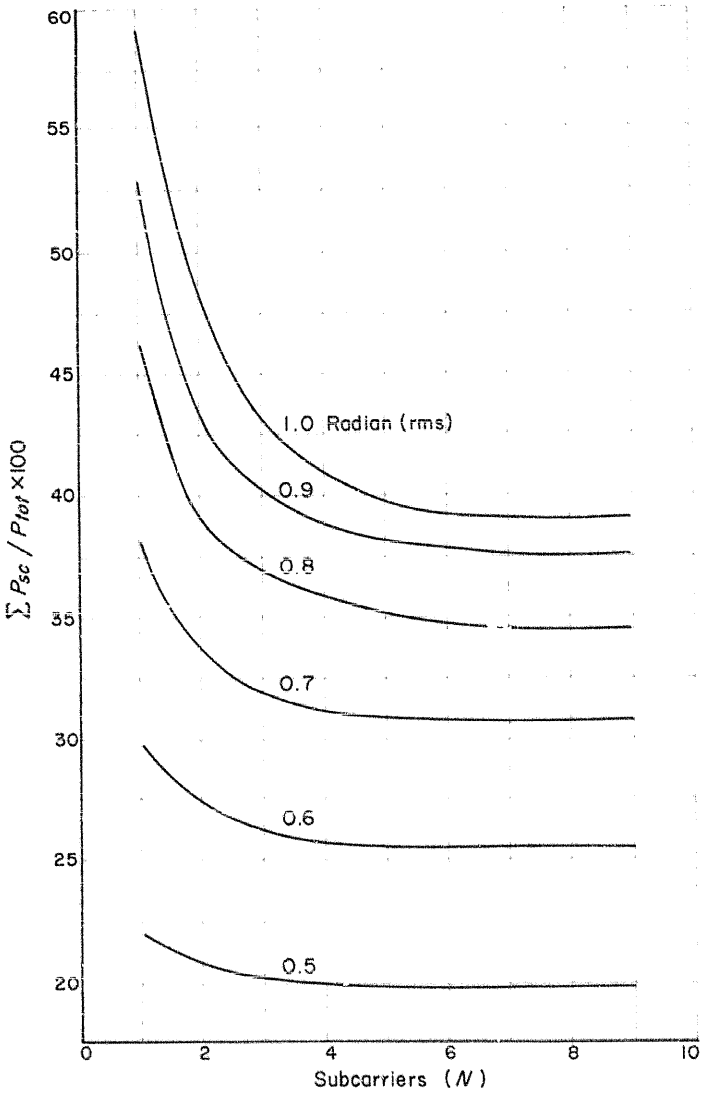

Figure 21. $\sum P_{sc}/P_{tot}$ for various phase modulation indices

other, approximating a factor of 5 to 6) Figures 19, 21, and 22 still hold to within a few percent. Note from Figure 19 that a 4-db suppression of the carrier by four or more subcarriers is equivalent to approximately 0.95 radian rms phase modulation; this fact will be used later in the actual system design.

b. Engineering data encoding. Since the first spacecraft (A-1) has as its prime mission the engineering evaluation of the entire spacecraft system, the telemetry encoding system was designed to reflect this priority. For the first series of spacecraft experiments, the engineering measurements will be time-multiplexed analog voltages which modulate airborne subcarriers. The length of the missions has made it impractical to consider recording the analog discriminator outputs. To facilitate the presentation of analog data a technique of sampling the local oscillator in the discriminator and printing out the subcarrier frequency as a function of time will be used. With such a technique the normal analog system recording and reduction errors can be eliminated. The effective system measurement accuracy, aside from airborne equipment drifts with time and temperature, is a direct function of the granularity of the frequency counter (± 1 count) and the noise error in the loop near threshold. The later effect can be ± 0.25 cycles at the beginning and end of the EPUT gate, or contribute a maximum count error of $+0.5$ count near threshold. Thus, even at threshold, the accuracy with which data can be presented is $\pm 1/\Delta f$, where Δf is the total full-scale frequency deviation.

Figure 23 is a sketch of a single sample of analog data with sample-length equal to T_s seconds. For the sake of analysis, the sample has been broken into three portions: t_R, the time required for the full-scale frequency ramp; t_T, the transient, or settling time in the ground system;

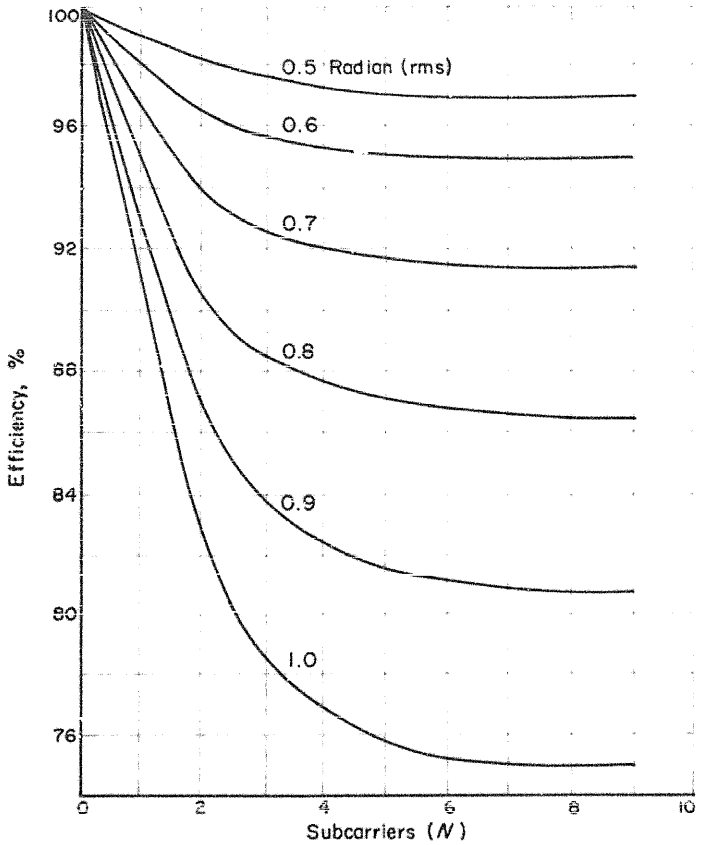

Figure 22. Percent efficiency for various phase modulation indices

and t_{ss}, the available or required steady-state data during which a frequency count is made. If the input to the ground phase-coherent discriminator is nearly a pure frequency-ramp, given by $\omega_i(t) = \dot{\omega}t$, the exact expression for the frequency of the loop oscillator (based on the linearized loop) can be shown to be

$$\omega_0(t) = \frac{\dot{\omega}}{B_0}\left(B_0 t - \sqrt{2}\, e^{-B_0 t/\sqrt{2}} \sin \frac{B_0 t}{\sqrt{2}}\right)$$

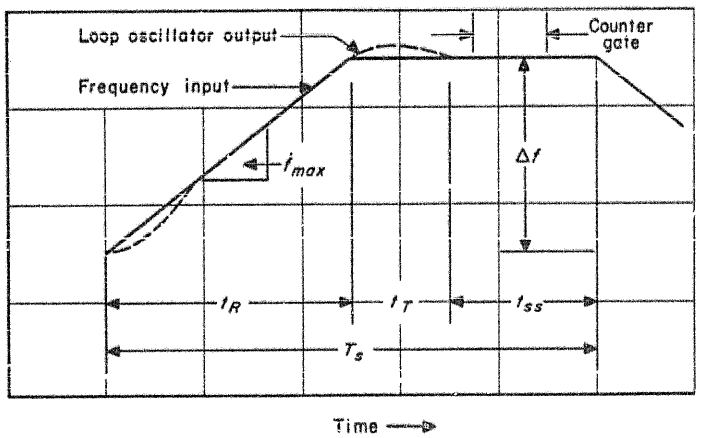

Figure 23. Sample analog data waveform

Figure 24 is a plot of the normalized $\omega_0(t)$ as a function of $B_0 t$ (B_0 being the usual natural frequency of the second-order phase-coherent servo, given in rad/sec). From this plot, it can be seen that the transient response is approximately zero for $B_0 t = 5$. Thus, a conservative figure for the transient time t_T would be $t_T = 10/B_0$, or $1.6/f_0$, where $f_0 = 2\pi B_0$.

The required ramp-time t_R is obtained by noting (1) that $\Delta f = \dot{f} t_R$ and (2) that by restricting the loop phase error to 30 degrees steady-state, the following equation holds: $\dot{f} = 3.28\,(f_0)^2$. Eliminating the common term $\dot{f}$ from these two equations yields

$$t_R = \frac{\Delta f}{3.28 f_0^2}$$

Or, since the percent accuracy is given by $100/\Delta f$, one finds that

$$t_R = \frac{30.5\,(\text{acc})}{f_0^2}$$

It is now possible to relate sampling-rate, accuracy, loop bandwidth, and steady-state data length, since

$$T_s = t_R + t_T + t_{ss}$$

or

$$T_s = \frac{30.5\,(\text{acc})}{f_0^2} + \frac{1.6}{f_0} + t_{ss}$$

After manipulating, substituting $2B_{L_0}$ (the loop noise bandwidth at threshold) for $6.66 f_0$, and solving the quadratic for $2B_{L_0}$, one has the result

$$2B_{L_0} = 5.33\left\{\frac{1 \pm [1 + 47.6\,(T_s - t_{ss})/(\text{acc})]^{1/2}}{(T_s - t_{ss})}\right\}$$

Only the positive root is of practical interest in the design of such an analog channel. In Figure 25 the required

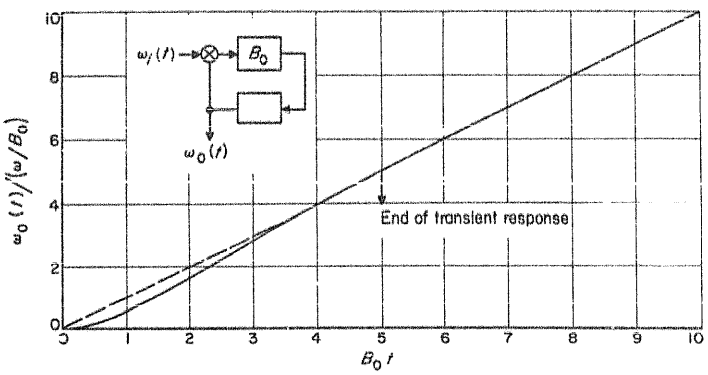

Figure 24. Frequency output for ramp input

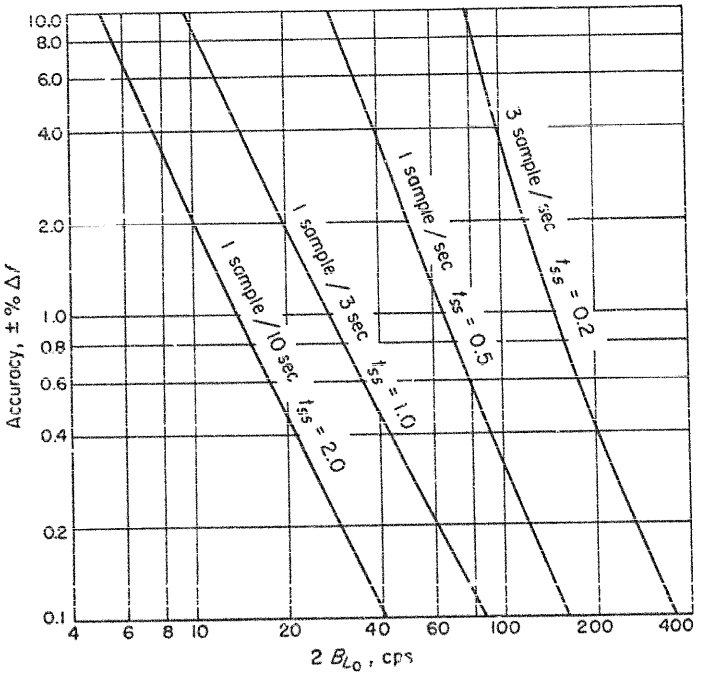

Figure 25. Loop noise bandwidth vs sampling rate accuracy

loop noise bandwidth has been plotted as a function of data (frequency-count) accuracy for sampling rates of 3.0, 1.0, 0.33, and 0.1 samples/sec.

As in any time-shared (commutated) analog system, a time reference must be obtained with respect to a complete cycle of the sampling device. The narrow loop bandwidths being used in this system design made the common out-of-band signal synchronization extremely difficult to mechanize; thus an alternate system was devised which appears to be practical. This mechanization is shown in Figure 26 and makes use of the fact that a modulating sinusoid whose frequency is sufficiently higher than the loop natural frequency f_0 will appear wholly as phase error at the multiplier output. This is an audio equivalent of the microlock technique. From Figure 27 it is seen that, under threshold conditions, the sync frequency must

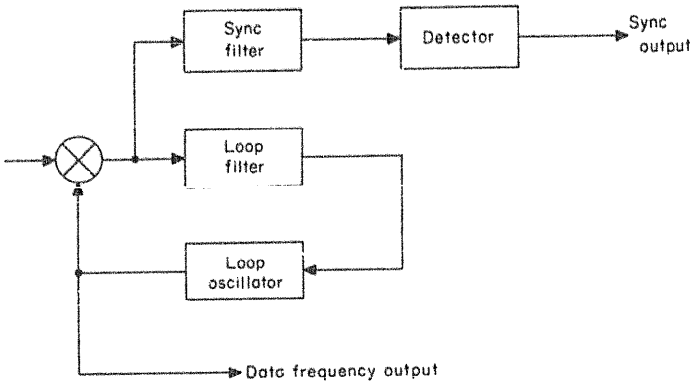

Figure 26. Phase-error synchronization

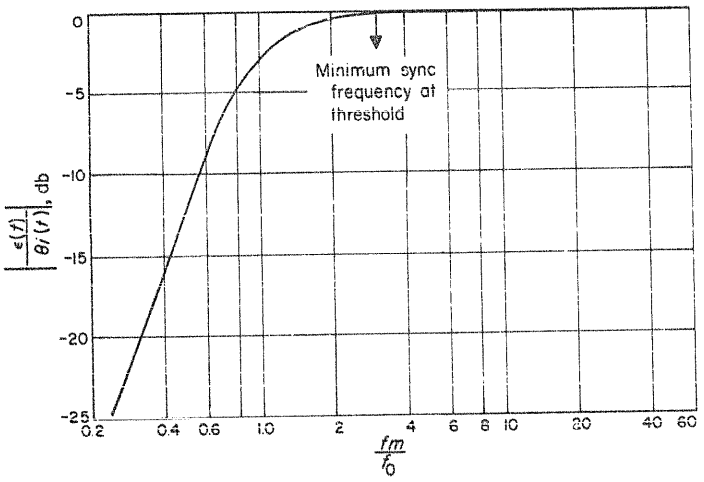

Figure 27. Loop phase error vs input phase modulation

be at least $3f_0$ in order that the loop filter effectively reject it. The over-damped loop behavior above threshold must be taken into account in the use of such a technique.

c. Scientific data encoding. In the process of selecting the optimum encoding method to accommodate the requirements of the scientific measurements it was desirable to transmit only two-state, or binary, data in most cases. An analog commutation technique is inefficient in such an application. In the theoretical derivation of the phase-coherent loop, since a pure frequency-step input in the presence of noise was assumed, it would appear that the use of such an input would make near-optimum use of any design loop bandwidth. A binary or two-state subcarrier oscillator was developed for use in the *Sergeant* PCM telemetry system, and given the name *frequency-switch*. With such an oscillator it is possible to hold the step-amplitude in frequency Δf to close tolerances; also it is relatively light in weight, requires no output filtering, and is frequency stable (0.1%) over a wide temperature range.

If the peak phase error in the discriminator loop is held to approximately 30 degrees at threshold the following equation holds

$$\Delta f_{max} = 1.2 f_0$$

The voltage at the discriminator output will be the data of interest; the expression for this voltage output in response to a pure frequency step input is

$$v_0(t) = \Delta\omega \left[1 - e^{-B_0 t/\sqrt{2}} \left(\sin \frac{B_0 t}{\sqrt{2}} + \cos \frac{B_0 t}{\sqrt{2}} \right) \right]$$

This expression is plotted as a function of $B_0 t$ in Figure 28 both for the condition at threshold (when the loop

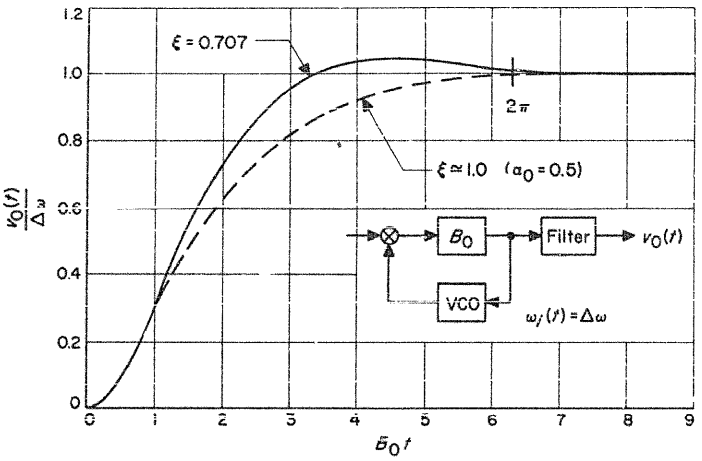

Figure 28. Voltage output for pure frequency step input

damping ratio is 0.707 of critical) and for a situation considerably above threshold (when the loop is overdamped, with a damping ratio of 1.00). From this figure it can be seen that it would be desirable to allow the voltage to settle to steady-state before allowing the input to change state again. This occurs if B_0t is set equal to 2π, or if $f_0t = 1.0$. It appears, then, that such a system waveform will allow a bit rate of 1 bpc of f_0.

It now remains to calculate the rms output noise to determine the output S/N of such a binary channel. If an in-lock confidence level of 2σ is chosen for the worst case (at threshold) for the discriminator loop, the normalized phase noise spectral density Φ may be calculated from the expression:

$$\left(\frac{N}{S}\right)_{2B_{L_0}} = 2B_{L_0} \cdot \Phi$$

Based on linear loop theory, the required S/N in $2B_{L_0}$ is 5.6 db, and since $2B_{L_0} = 6.66f_0$

$$\Phi = \frac{1}{25.1f_0}$$

The 1-σ output noise power is given by the expression, $(\sigma f)^2 = 2.22f_0^3 \cdot \Phi = 0.0884f_0^2$ and since it is known that $\Delta f = 1.2f_0$, then $(\sigma f)^2 = 0.0614\Delta f^2$, or

$$\left(\frac{\Delta f}{\sigma f}\right)^2 = \left(\frac{S}{N}\right)_{out} = 12.1 \text{ db (at threshold)}$$

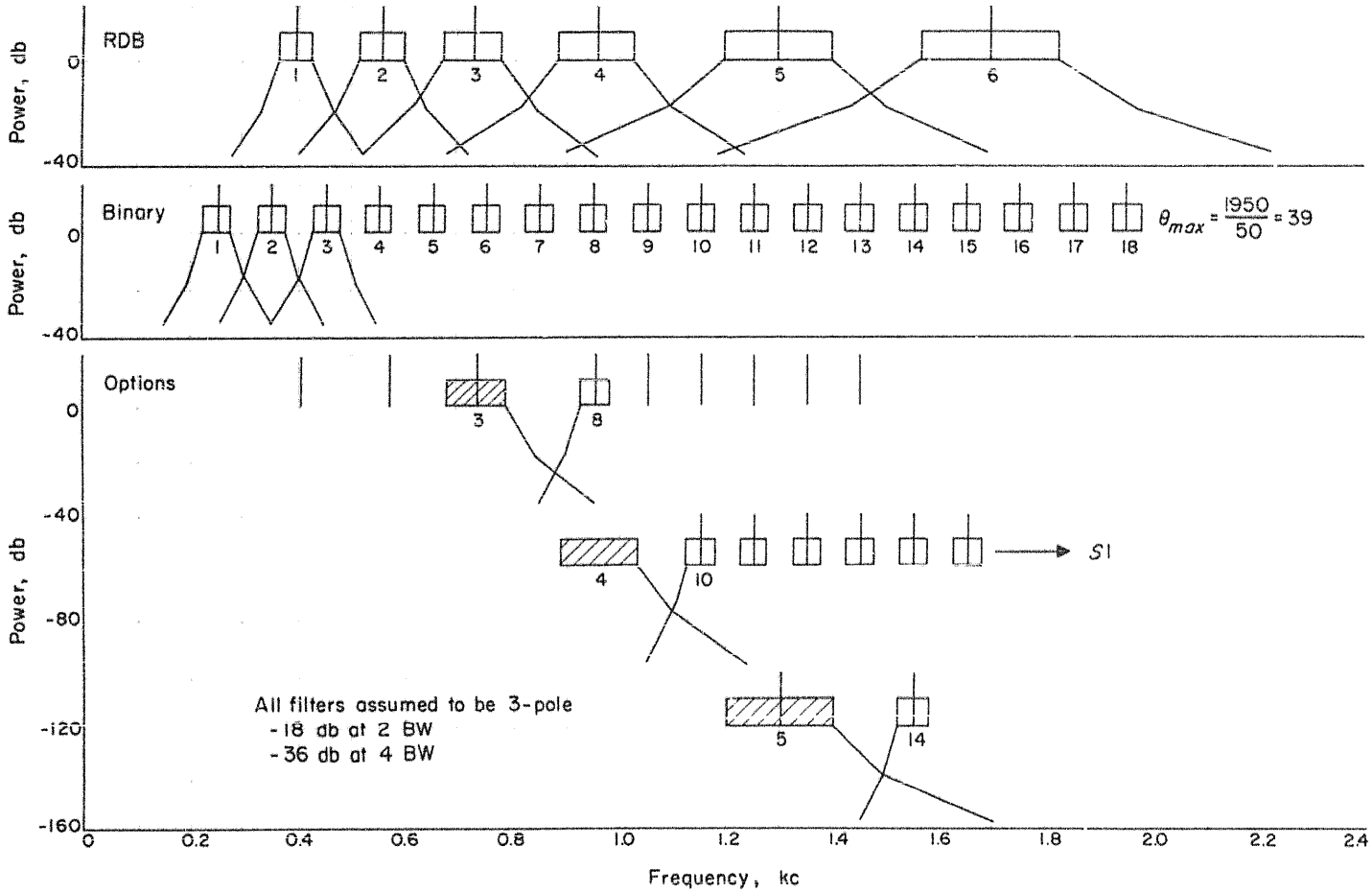

Figure 29. Proposed new channel assignment

This S/N ratio appears to be adequate for the operation of the binary code and decision-making detector required in the ground system.

It would not be wise to use standard RDB channel bandwidths for the binary channels as presently required; therefore, a new set of channels has been proposed (Fig 29). Equal predetection bandwidths of 50 cps were chosen, with equal spacing between channels, such that a moderate guard-band attenuation was possible with physically reliable 3-pole filters of moderate (approximately 40, maximum) Q. Note that when required standard RDB channels and the new binary channels may be combined by the options shown when both analog and binary data waveforms are required.

d. Overall system integration. Since at this time it is not definitely known whether two- or three-axis vehicle stabilization will be possible, two RF systems have been proposed which incorporate different vehicle antenna gains and total available powers. Table 4 lists these characteristics, as well as those of the ¼-watt omnidirectional system. Note that the algebraic sum of these five parameters, properly signed, is a direct means of comparing Systems A and B. If System A is flown, the actual threshold distance will be 3.9 db further (a distance factor of 1.57) than the System B design threshold. If either system is flown and fails, the omnidirectional system will have a distance threshold only 0.052 times the design System B distance.

Table 4. A-1 given communications system parameters

Parameter	System A	System B	Omnidirectional system
P_{tot}, watts	3.0	25	0.25
P_{tot}, dbm	34.8	44.0	24.0
G_t, db	18.5	6.0	0.5
G_r	41.3	41.3	41.3
L_m, db	1.1	1.7	1.9
Φ_{NF}, db	8.0	8.0	8.0
Effective usable power, dbm	85.5	81.6	55.9
Comparison with System B, db	3.9	0	−25.7
Relative threshold distance	×1.57	1.00	×0.052

To establish a system "clock" a 400-cps reference channel will be flown which will permit all sampling and bit rates to be related in an integer fashion. The sampling rates and accuracies required to adequately satisfy the engineering measurements have been chosen. The required bandwidths for these measurements are shown in Figure 25. The design system pad which is necessary to guarantee these measurements is 10 db, and the required S/N in $2B_{L_0}$ for a 2-σ in-lock confidence level at threshold is 5.6 db. Since the 400-cps reference channel provides the clock for the entire system, it has been given a 4-σ in-lock confidence level at threshold. Table 5 lists the remaining system design parameters.

Table 5. Spacecraft communications system design parameters

Parameter	Carrier	RDB				Binary	
		Ch 1	Ch 2	Ch 3	Ch 4	B-10	B-11 thru B-15
f_c, cps	960×10^6	400	560	730	960	1150	—[a]
BW, cps	7×10^9	60	84	110	144	50	50
Experiment[b]	—	Ref	E	E	S	E	S
Design T, miles	10^6	10^6	10^6	10^6	10^5	10^6	10^6
Sample or bps	—	—	1.0	0.1	—[c]	2	4
Δf, cps	—	—	50.0	50.0	120	2.4	4.8
Accuracy or $(S/N)_{out}$, db	—	—	±2%	±2%	36	12	12
$\dot{f}_{max}$, cps/sec	—	—	185	7.4	∞	—	—
$2B_{L_0}$, cps	20	1.0	50	10	—[d]	13.3	26.6
$(S/N)\ 2B_{L_0}$, db	0	8.1	5.6	5.6	18	5.6	5.6
In-lock probability, σ	~1	4	2	2	100%	2	2
Design pad, db	—	10	10	10	6	10	6
Design P_t, dbm	40.0	23.1	17.6	30.6	30.5	31.8	30.9
Design $\Delta\theta$,[e] radians	—	0.20	0.10	0.46	0.46	0.50	0.46
Actual P_t, dbm	40.1	23.1	17.1	30.5	30.5	31.3	30.5
Actual P_t,[f] % P_{tot}	40.6	0.8	0.2	4.6	4.6	5.4	4.6
Actual pad, db	22.1	10.0	9.5	9.9	6.0	9.5	5.5

[a] Values of f_c for B-11 through B-15 are 1250, 1350, 1450, 1550, and 1650 cps, respectively.
[b] Type of experiment is indicated by E for engineering and S for scientific.
[c] Overall discriminator response is −3 db at 50 cps.
[d] Theoretically 666 cps; in practice limited by input bandwidth to 144 cps.
[e] $\Delta\theta_{rms} = 0.945$ radian.
[f] Efficiency = 79.2%.

e. Specific examples of channel design. Sample calculations for RDB Channel 2 are as follows:

(1) Design threshold distance = 10^5 miles, thus

$$L_s = 196.6 \text{ db}$$

(2) For a 1-sample/sec, ±2% channel

$$2B_{L_0} = 50 \text{ cps} = 17.0 \text{ db} \cdot \text{cps}$$

(3) For 2-σ in-lock confidence level

$$\left(\frac{S}{N}\right)_{2B_{L_0}} = 9.6 \text{ db}$$

(4) Design pad

$$L_p = 10 \text{ db}$$

(5) Required subcarrier power

$$P_{sc} = 2B_{L_0} + \left(\frac{S}{N}\right)_{2B_{L_0}} + L_p - 15.0$$

$$= 17.0 + 5.6 + 10.0 - 15.0 = 17.6$$

Therefore the total transmitted subcarrier power required is $P_{sc} = 17.6$ dbm.

Channels 1 and 3 were designed in a similar manner.

For the engineering binary channel, B-10 was designed in much the same manner by choosing a bit rate of 2 bps, requiring $f_0 = 2.0$ cps, $2B_{L_0} = 13.3$ cps, or 11.2 db • cps. The remainder of the calculation is identical to that for Channel 2.

Once the required subcarrier power for the engineering channels was determined, modulation indices were chosen for these channels, and then the rms value of these calculated

$$\Delta\theta_{rms} = \left[\sum_{n=1}^{4}\left(\frac{\Delta\theta}{\sqrt{2}}\right)\right]^{1/2} = 0.506 \text{ radian (rms)}$$

It can be determined (Fig 19) that a 4-db suppression of the carrier by the modulation is equivalent to 0.95 radian rms phase modulation. Therefore it is possible to solve for the effective rms phase modulation of the carrier for the scientific channels. Six scientific channels were chosen to satisfy the scientific requirements of the spacecraft. The following modulation index calculation is based on the six-channel assignment:

$$0.95 = \left[(0.506)^2 + 6\left(\frac{\Delta\theta}{\sqrt{2}}\right)\right]^{1/2}$$

or

$$\Delta\theta = 0.46 \text{ radian (peak)}$$

These modulation indices, of 0.46 radian each, allow approximately 4 bps per binary channel. The RDB Channel 4 was given the scientific section for the hydrogen cloud measurement. Since its threshold is only 10^5 miles instead of 10^6, the loop bandwidth has been widened to accommodate a full-band frequency step; with narrower output, however, filtering yields an output S/N of approximately 36 db.

Once the modulation indices have been chosen, the actual carrier and subcarrier powers may be calculated (Table 5). An attempt was made to make the actual subcarrier power agree with the design to within 0.5 db. A system can be designed with a pad of 10 db for the engineering channels, for example, and a threshold slightly less than design, or think of the difference between the design and actual sideband power as a loss in channel safety factor, or pad.

f. System test. During the next month a communications system breadboard will be constructed to evaluate the foregoing encoding theory. If possible, differences between practice and theory will be corrected or adjusted by changing system parameters. Results of these tests will be used in designing flight and ground equipment for the first spacecraft flights.

2. Command System

As presently envisioned, future spacecraft missions will require two types of commands: off-on and proportional controls. Since the projected accuracy requirements on proportional control functions are in the order of 1% or better, it appears that, within the time allotted for preparation of Spacecrafts A-1 and A-2, development should be concentrated on an immediate system capability for only on-off functions.

Two types of systems have been considered for on-off functions; namely, tone burst and discrete pulse modulation. Some advantages of a tone approach which may be cited are the following: experience and familiarity with these techniques at JPL, relative simplicity for a small number of commands, and its adaptability to parallel redundancy. Also, tone systems of control are extensively used at most missile test ranges. Disadvantages include the possible weight penalties associated with filter components and the bandwidth limitations imposed by temperature or aging drifts in filter and/or local oscillator frequencies.

Any pulse-modulation system is necessarily time multiplexed so that simultaneous transmission of more than one command is not possible unless coding logic is employed. Advantages of this type of system are use of simple digital building blocks (practically all switching mode operation) and a capability for extension to com-

plex control functions (e.g., proportional step-wise control with the addition of a digital-to-analog converter). Among the disadvantages are the following: (1) need for complete system development, possibly serial information flow, and (2) most important, present indication of no worthwhile performance improvement over a tone system for the simple functions required for early spacecraft missions. Based on these considerations, the conclusion is that a frequency division multiple-tone command system is the most logical way to implement early spacecraft command functions.

A tone-burst system would logically take the form indicated in Figure 30. The ground system consists of an ensemble of tone generators (in this case, three) which are keyed independently to achieve a command.

In practice, a command will be initially generated with a push button having maximum and minimum required holding times of 3 and 0.1 seconds, respectively. An electronic timer will provide a standard command duration of 3 seconds which can be lengthened by continued closure of the push-button switch. In the event the electronic timer fails, the same function can be achieved by pushing the button for at least 3 seconds. These tone signals are used to phase-modulate an 890-mc transmitter at a nominal total rms phase deviation of 0.8 radian. Combinational switching arrangements will insure that total rms phase deviation remains constant for simultaneous generation of more than one command tone.

Salient vehicle system components would consist of a coherent transponding receiver capable of furnishing a phase-error reproduction of the transmitted tones, together with an audio decoding channel corresponding to each of the tones used. Each decoder channel will consist of a suitable amplifier, a narrow-band tone-matched filter, and a threshold detector. Initiation of commands is accomplished by relay closures. Since the maximum tolerable delay between reception of a command tone and conversion of this information into a relay closure is 2 seconds, the minimum permissible decoding channel bandwidth is approximately 1 cps, which is fortunately compatible with the required system reliability (in a noisy environment) and available pre-decoder signal-to-noise ratios.

To guard against false operation, inhibiting functions, derived from a receiver-coherent AGC loop, interrupt signal paths on both ends of all channels in the event that carrier lock is lost or insufficient signal strength is obtained.

Implementation of airborne system hardware is presently progressing along two lines: one involving a tuning-fork filter approach, and the other, a heterodyning technique using magneto-strictive resonators for local oscillators and mixers. Since both techniques appear likely to satisfy requirements, final decision will most likely be made on the basis of performance against weight, power consumption, and complexity.

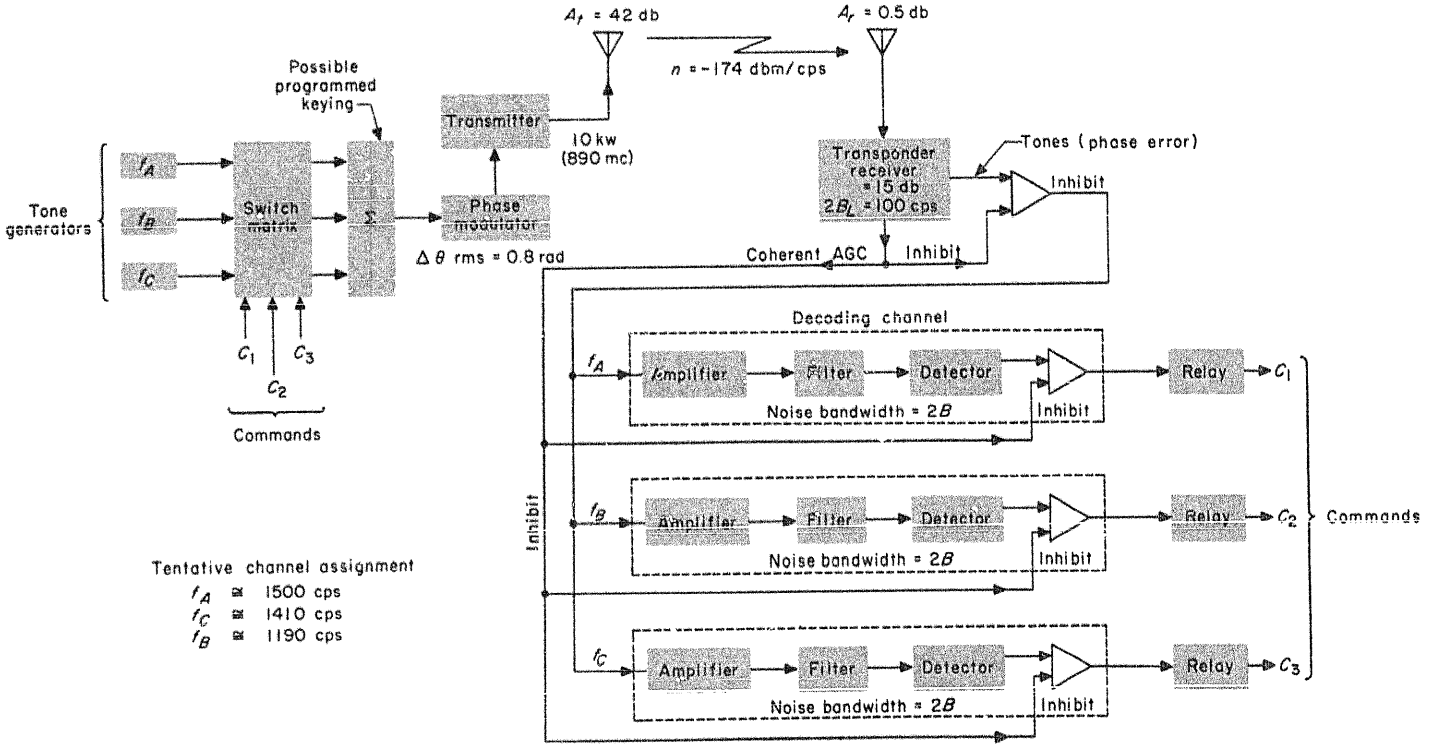

Figure 30. Command system

Tones have been chosen which conflict with neither the standard telemetry channels nor the narrow-band binary channels to be used on these missions. Consistent with a bandwidth available from the transponder of 370 to 2000 cps and the use of higher frequencies to minimize vibration problems, channel assignments for the tuning fork approach have been placed at 1500, 1410, and 1190 cps (1080 cps available if a fourth channel is used).

a. System reliability. Two important command-system decoder parameters are the probability of initiating a false command signal and the probability of recognizing and acting upon a received command. These types of errors may arise from two sources: first, an electrically noisy environment, and second, failure of one or more components in the group of decoding circuits. Whereas solution of the problems associated with the latter is largely a matter of recognizing and designing around undesirable detailed circuit configurations, constraints in the noise area are imposed by general transmission system performance and are therefore amenable to predesign calculations. The calculations which follow are based on a single decoding channel of the type which would be used in a tone-burst system. Such a channel includes a narrow-band filter followed by a threshold envelope detector.

b. False command probability. The average number of defined noise perturbations through a narrow-band filter having noise bandwidth B (Table 6) is 2 bps. This follows from the fact that the information capacity of a filter is 2 bpc of bandwidth. For a total operation time of T_0, the total number of noise bits during T_0 is $2BT_0$; therefore, the probability of a false command due to noise alone in one channel P_{en} is

$$P_{en} = (2BT_0)\,P_n(\delta)$$

where $P_n(\delta)$ is the probability that noise exceeds detector threshold, $\delta = K\sigma$, and σ is the maximum rms noise voltage expected at the detector input.

For spacecraft missions A-1 and A-2,

$$T_0|\,\text{A-1} = T_1 = 70 \text{ days} = 6 \times 10^6 \text{ seconds}$$

and

$$T_2 = 60 \text{ days} = 5 \times 10^6 \text{ seconds}$$

If $P_{en} = 10^{-2}$,

$$P_n(\delta)|\,\text{A-1} \cong \frac{1}{B}\,(10^{-9}) = P_n(\delta)|\,\text{A-2}$$

c. Threshold requirements. For reasonable bandwidths ($\geq$1 cps), achievement of required values of $P_n(\delta)$ indicates that $K = S/\sigma$ must be ≥ 6. To assure that commands are acted upon most of the time [$P_s(\delta) \geq 0.9$] it is apparent that the minimum expected peak signal S must exceed δ, and therefore σ, by an appreciable amount. Under these conditions, $K >> 1$ and $\beta = S/\sqrt{2\sigma} >> 1$, the signal plus noise characteristics at the detector input have a normal distribution with mean = S.

A set of curves showing the inter-relations between $P_n(\delta)$, $P_s(\delta)$, and β^2 is shown in Figure 31 (Ref 1).

Table 6. Glossary of terms used in command system

B	= tone decoder channel noise bandwidth, cps
T_0	= mission time, seconds
P_{en}	= probability of a false command due to noise alone in one channel
$\overline{P}_{es}$	= probability of recognizing and acting upon a command with one channel
$P_n(\delta)$	= probability that noise exceeds detector threshold δ
$P_s(\delta)$	= probability that signal and noise exceed threshold δ
σ	= maximum expected rms noise voltage at input to threshold detector
S	= minimum expected peak signal at detector input
$(P_e)_n$	= probability of a false command over mission time with a multiple-channel system
$(\overline{P}_e)_s$	= probability of recognizing and acting upon command with a multiple-channel system
δ	= detector threshold

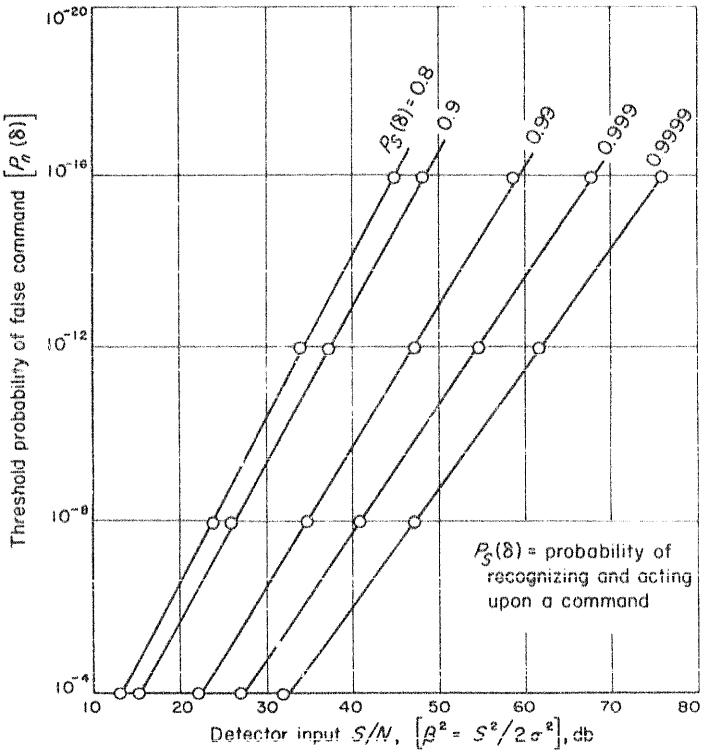

Figure 31. Relationship between error probability and S/N ratio

Preliminary system parameters. A compilation of approximate system parameters based on figures presently available is given in Table 7. Note that for A-2 range, anticipated performance is rather marginal since only 7.2-db deterioration in signal level anywhere in the system results in a good possibility of objectionable operation. Consistent with a maximum command delay of 2 seconds and reasonable tone generator and filter stabilities, it appears that it might be possible to reduce decoding channel noise bandwidth to 1 cps, in which case an additional 7-db margin could be added to those figures shown.

Table 7. Command system parameters

Parameter	A-1 = 10^6 miles	A-2 = 5×10^6 miles
Effective received subcarrier power, dbm	−115.8	−127.8
Subcarrier S/N ratio in RF loop bandwidth ($2B_L$ = 100 cps), db	24.2	10.2
Decoding channel noise bandwidth (2B = 5 cps), db-cps	7	7
Tone S/N ratio (in 2B), db	37.2	23.2
Required S/N ratio,[a] db	16	15
Subcarrier S/N margin, db	21.2	7.2

[a]For probability of false command, this value equals 0.01, and for failure to recognize and act on command, it equals 0.1.

Possible system extension. Although the system as outlined in the preceding sections (i.e., using a 1-to-1 correspondence between command functions and tones) appears to adequately satisfy all anticipated requirements, a theoretically greater reliability, if required, may be obtained by using a multiplicity of simultaneous tones to initiate a command through suitable digital logic. A probable implementation of this technique would involve (Fig 15) the use of additional tone generators, decoding channels, and some diode logic between the channel detectors and command relays.

In specific terms, assume that each command can be initiated by the simultaneous presence of N tones and that there are M possible combinations of N tones for each command, with no tone used more than once for a given command.

For this situation the overall probabilities of false command and failure to recognize and act upon reception of at least one of the M possible combinations become

$$(P_e)_n = 1 - [1 - (P_{en})^N]^M$$

and

$$(P_e)_s = [1 - (P_{es})^N]^M$$

where P_{en} = probability of a false command with one channel decision.

N = number of independent channel decisions required per command (decisions *ANDed*).

M = number of independent ways of implementing a particular command (possibilities *ORed*).

$(P_e)_n$ = overall probability of a false command.

P_{es} = probability of recognizing and acting upon a single channel decision.

$(P_e)_s$ = overall probability of failing to recognize and act upon a command.

The net result of this technique is to increase system reliability in a given signal and noise environment for a negligible decrease in the mean time before failure, resulting from slightly increased system complexity.

For example, for Missions A-1 and A-2, assume that three commands are necessary and that over the mission time, probability of false command $(P_e)_n = 0.01$ and probability of recognizing and acting upon a command $(P_e)_s = 0.9$. Table 8 shows S/N ratios required for a three-tone system using 1-to-1 tone and command correspondence and a four-tone system using a pair of independent two-tone functions per command.

The signal requirements are thus comparable within 0.6 db so that the additional reliability afforded (since one channel can fail completely with no reduction in command capability) can be gained with one additional channel, some simple diode logic, and no increase in required transmitter power.

An alternative advantage of this technique is that it improves command capacity by providing as many as $2^N - 1$ command functions for N tones if some commands are allowed to require only one tone for activation.

3. Systems Operation

A number of major assemblies are required as a part of, or in support of, the command and telemetry systems. Some of these assemblies are a part of the spacecraft,

Table 8. Comparison of S/N requirements for three- and four-tone systems

Noise bandwidth, cps	Required S/N at detector, db		Relative available S/N for four-tone system[a] (1.4-db depression)
	Three-tone system	Four-tone system	
1	14.6	13.8	13.2
5	15	14.2	13.6
10	15.2	14.4	13.8

[a]Assumes same rms RF modulation as for three-tone system; rms = 0.8 radian.

UNCLASSIFIED ~~CONFIDENTIAL~~
Classification Changed to UNCLASSIFIED
Authority SPLEPD 20 dtd 29 Jan 1961
Date 11/5/62
By V. Pritchard

some part of the various Deep Space Net Stations, and others are used in conjunction with preparation and firing operations at JPL, AMR, and elsewhere as required.

Ground command equipment. This equipment encodes the commands in tone form suitable for modulating the ground-based transmitters and test equipment. It includes tone generators and suitable monitoring equipment necessary to establish their functioning within tolerance. This equipment will be built into appropriate field stations and test consoles.

Command decoder. This spacecraft assembly receives and demodulates the command information, the specific command information goes to the controller which distributes it as appropriate.

Spacecraft telemetry encoder. This spacecraft assembly contains equipment for collecting, multiplying, and encoding scientific and engineering data. The output of this unit modulates the transmitter.

Telemetry data presentation console. This unit demodulates the output of the ground receiver and provides a display of this data. All of the engineering data is decommutated as a subcarrier oscillator frequency for each measurement and is presented and held between samples for each measurement on a data display console. In addition, all of the engineering and scientific data is presented as an oscillograph recording and the demodulated scientific data is available to more comprehensive scientific data presentation or analysis equipment.

Trailer-mounted telemetry field station. These stations always operate in conjunction with mobile launch-type checkout receiving stations. This station provides limited data presentation of the type previously described. The unit provides recording for preflight systems tests and the launch phase of flight. The station also handles and records data regarding the performance of the associated ground receiver.

Telemetry DSN recording station. This assembly is permanently installed in the various Deep Space Net Stations. This station's primary function is to record on magnetic tape the telemetry data from the receiver. In addition, it has appropriate test equipment, very limited data demodulation capability, and an oscillograph.

Telemetry modulator for pole beacon. This unit provides data encoding in a manner to simulate the spacecraft telemetry data encoder. It is used to modulate the pole beacon transmitter and the combination is used to check out and calibrate the various DSN stations and other stations which do not have access to the actual spacecraft transponder.

Spacecraft telemetry test and calibration unit. This unit is a collection of test equipment housed in a portable case. The equipment is used to check out and calibrate spacecraft telemetry encoding equipment in the telemetry laboratory and in spacecraft assembly areas.

Command system test unit. This unit is a collection of test equipment housed in a portable case. It is used to test and calibrate the spacecraft command decoder and the ground command encoder. It will be used in the laboratory, at spacecraft assembly areas, and at field stations having command capability.

Data reduction laboratory. This is the JPL data reduction laboratory which will be used in conjunction with system qualification tests. The data reduction laboratory will record and reduce systems tests at JPL and will reduce data taken during flight.

D. Guidance

Attitude stabilization and mid-course guidance maneuvers require the accurate determination of earth and sun lines. The required accuracy of 0.1 degree is highest just prior to a guidance maneuver. At all other times the required accuracy is much less stringent, on the order of ±2 degrees.

During the course of a mission, the earth-probe-sun angle must be held within limits of ±45 degrees about a nominal of 90 degrees (which would mean that the earth will nominally be seen by the probe as a partially illuminated sphere). At first glance, this condition appears to be a serious objection to the application of visible light detection (as opposed to infrared) since it would inherently produce an offset error from the true center of the earth in one axis. On closer inspection, however, this apparent objection disappears for the case of accurately determining a three-axis angular reference system in

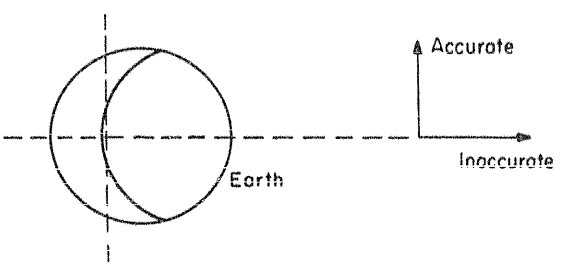

Classification Changed to UNCLASSIFIED
Date 11-5-62
Authority JPL-EPD "20 dtd 2 Jan 1961
By V Pritchard

space. Since the sun-earth two-body system provides four axes of information, the redundant axis then is the inaccurate earth axis.

Although this axis is required for antenna orientation, the accuracy tolerance is wide. Elimination of the need for infrared observation of the earth permits the application of very sensitive detectors which require no cooling or special handling.

1. Earth Seeker

The current earth seeker design consists of three ¾-inch-diameter photomultiplier tubes mounted in μ-metal shields. The field of view is constrained by a cover in which slits are cut. The complete unit including preamplifiers will weigh about 1 pound.

A shutter is provided to shade the detectors if the sun should come into the field of view. A diffusion device is included to help protect the tube cathode from direct sunlight. Tests are presently being conducted to ascertain if direct sunlight can be tolerated by the tubes for any prolonged period. Recent tests indicate the photomultiplier was undamaged if all voltage excitation was removed.

A filter unit is included to provide at least two points on the trajectory where actual light flux, to the tubes, is equal to a single constant. On a lunar mission the earth light flux at mid-course distance is 5 times the value received at terminal maneuver distance. This amount of variation would probably cause a change in the null position of the device by a significant amount. Since the device has not been tested, this effect can only be estimated. At worst, the expected value of null shift due to large gain changes and light input changes should only be of the order of 1 degree.

The sensor as designed has the estimated capability of locking on the half-illuminated earth from a distance of 10 million miles. At this distance the seeker will be operating on a light flux of 1.76×10^{-9} watts/cm^2, and actual input to each detector will be nominally $\approx 8 \times 10^{-11}$ watts. Tube output will be about 0.4 microampere, with a dark current of about 0.02 microampere, for a signal-to-noise ratio of 20. At this point the earth is approximately 400 times brighter than a first-order magnitude star.

A backup earth seeker is being fabricated which employs photoconductive detectors (cadmium selenide) in place of the multiplier phototubes. These are compact and have the advantage of being able to operate satisfactorily after exposure to direct sunlight. Their response time is quite long at low light levels, however, and some doubt exists as to their ability to sense the earth beyond 10^7 miles.

2. Sun Seeker

The sun seeker, schematically described in *SPS 6*, will be physically composed of many parts strategically placed around the payload to obtain the required spherical field of view. Detectors will be cadmium selenide photoconductors. Tests on these types have been completed.

Additional system study is required to find an optimum location for the sun sensor. The current configuration under investigation involves the use of a split primary axis sensor mounted on the main body of spacecraft. Less critical secondary sensor elements will be installed at convenient locations to complete the spherical field requirement. Care will be necessary to insure that no detectors receive reflected light from any part of the spacecraft.

3. Gyro Procurement

The attitude control systems, based upon limit cycle operation, require the measurement of angular rates about each of the vehicle's three axes. In addition, angular displacement measurements about at least two of the axes are required in later system applications. Since rate information is required for all applications and angular position required in later vehicles, it is planned to use a configuration of gyro and associated electronics which will provide both types of information.

The gyro is a single-axis floated unit, with electronic circuits, which amplifies and demodulates the gyro signal generator output and applies the resulting current back to the gyro torquer. The feedback or torque rebalance current holds the gimbal at null, with the magnitude and polarity of current determined by the turning rate about the gyro input axis. Spurious torques, acting on the gyro float or gimbal, create an error which may add or subtract to the true rate sensed by the gyro.

The second mode of operation, angle-displacement measurement, is attained by adding an integration to the torque rebalance loop such that the voltage stored across the capacitor is proportional to the time integral of the net rate indicated by the gyro. In actual application, this mode will be used to establish the angles commanded for correction during the mid-course period. Rockets will be fired in such a manner as to drive the vehicle to a new position attitude about the pitch and yaw axes. The corrective command will be in the form of a fixed turn

UNCLASSIFIED CONFIDENTIAL
Classification Changed to UNCLASSIFIED
Authority JPL EPD #20 dtd 2 Jan 1961
Date 11/5/62
By V. Pritchard

rate applied about the pitch and yaw axes of the vehicle as required and held for a predetermined time, thus establishing the desired attitude.

At present the fixed turn rate commanded for the correction maneuver will be 720 deg/hr which is established by the application of calibrated current to the two windings (control field and pattern field) of the gyro torquer. During the rate sensing mode, the gyro will sense rates from its minimum threshold level of approximately 0.01 deg/hr to an estimated maximum of 10 deg/hr with a nominal value of 1 deg/hr (estimated).

Although the environment during the mission will be nearly ideal for optimum gyro operation (near zero vibration and gravity forces), the gyro must be rugged enough to survive the environment created by the launch vehicle (e.g., vibration, acceleration, and shock). Another constraint placed on the gyro will be the need for extended life, specifically in the motor bearings where a minimum life of 2000 hours is desirable.

Performance goals for the gyro include the following: (1) mass unbalance, either axis, less than 4 deg/hr; (2) mass unbalance randomness, less than 1 deg/hr; (3) fixed torques, less than 2 deg/hr; (4) fixed torque randomness, less than 1 deg/hr; and (5) anisoelasticity coefficient, 0.1 deg/hr/g^2. The gyro life is 2000 hours minimum, during which time gyro performance will conform to these specifications.

The Minneapolis-Honeywell gyro model GG49E6 has been selected for the first series of vehicles. The unit differs from the typical GG49 configuration in that a damping fluid having minimum viscosity has been selected (minimum damping) to eliminate the need for heaters, thus decreasing electrical power requirements. The fluid still provides the desired density for full flotation but the viscosity becomes very low. The damping of the loop is designed into the electronics.

Motor bearing preloads have been reduced considerably to provide all possible increase in life expectancy while still retaining the rigidity necessary to survive the launch environment.

At present 16 gyros, for use in flight systems, have been ordered from Minneapolis-Honeywell. Three more are being modified at JPL to provide backup and early system evaluation. Two units have been modified and evaluated previously to demonstrate the feasibility of the gyro and related electronics. The results attained were fully satisfactory for present system requirements.

Mounting brackets have been designed and are now being fabricated. Laboratory test equipment, which will be followed closely by the design of field test equipment, has been designed and is now being fabricated. The target date for completion of the test equipment and the first complete assembly is the first week of April.

4. Electronic Development

It was found that the preliminary switching amplifier circuit, shown schematically in *SPS 6*, did not function satisfactorily when subjected to temperatures near 60 or −10°C, the extreme limits specified for the spacecraft. Since the malfunctioning was directly attributable to large current gain changes in the preamplifier stage of the switching amplifier over the temperature range, a redesign of the preamplifier was undertaken. An improved version of the switching amplifier is shown schematically in Figure 32. It should be noted that the added stage of the negative input preamplifier causes equal polarity preamplifier outputs so that both timing circuits can be made identical. Such a change also more nearly equalizes the preamplifier gains in the two channels, and simplifies the fuel totalizer input circuitry. The circuit shown was tested at the extreme temperatures and performed in acceptable fashion. It was observed that the switching voltage varies by approximately 20% over the entire temperature range, and that the nominal 100-millisecond hold and lockout periods varied by approximately ±20 milliseconds as a result of component variations in the timing circuits. Neither of these effects will degrade attitude control system performance. Ground separation between the preamplifier and timing circuits eliminated parasitic feedback tending to produce self-sustaining oscillations at the nominal 10-cps frequency of the timing circuit.

Further progress toward environmental packaging of the first spacecraft attitude control system electronics package has been made. Layout of the five basic modules which (in addition to externally mounted hardware) comprise the system is being completed. Among these modules are the gyro package which contains a set of orthogonally mounted gyros and associated electronics, the gyro loop control module, the actuating amplifier module, the fuel totalizer module, and the system control module. Four of these modules will be interchangeable, and only the system control module will be altered according to mission requirements. Printed circuit boards for the fuel totalizer and actuating amplifier modules have been ordered, and assembly of these units will start in the near future. Layout drawings for the gyro loop control, gyro package electronics, and the first system control module will be completed shortly. The gyro package casting is presently being machined and will be available within the next 3 weeks. However, it is not

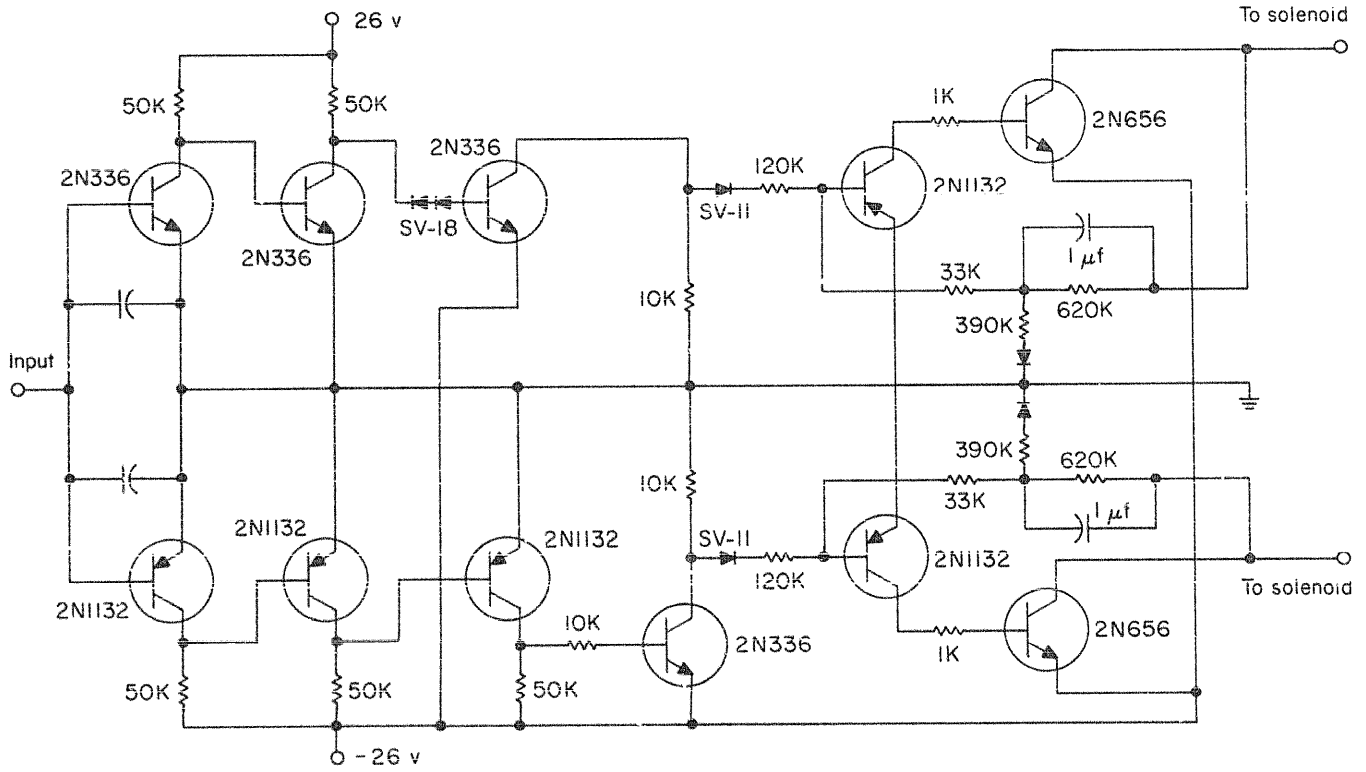

Figure 32. Switching amplifier

expected that the specially modified MIG gyros will arrive before the end of March 1960. A system interconnection diagram showing all pin assignments and a master cable harness is in the final stages of completion. Special wire with irradiated polyethylene insulation exhibiting superior qualities in a space environment will be used throughout. All internal connectors will be of the Cannon-D miniature type.

5. Thrust System Development

Space Programs Summary 6 illustrated the torque-test fixture which has satisfactorily been used to evaluate miniature nozzle designs. This fixture, as shown with the low-pressure plenum, provided data on water vapor systems which later led to a near optimum design of miniature nozzles. Recently the fixture was modified (Fig 33) to include a high-pressure nitrogen supply regulated to 15 psig. The fixture retains the features of a mercury float bearing capable of supporting a 20-pound load, the torque rebalance technique using a shaft-mounted Microsyn and torquer as the loop sensor and actuator, and the torque measuring capability in the range of 0.1 to 100 gm-cm.

The nozzle shown has a 0.025-inch-diameter orifice, an expansion ratio of 70, and an included angle of 42 degrees. Calculated thrust is 6 grams, with a 15-psi cham-

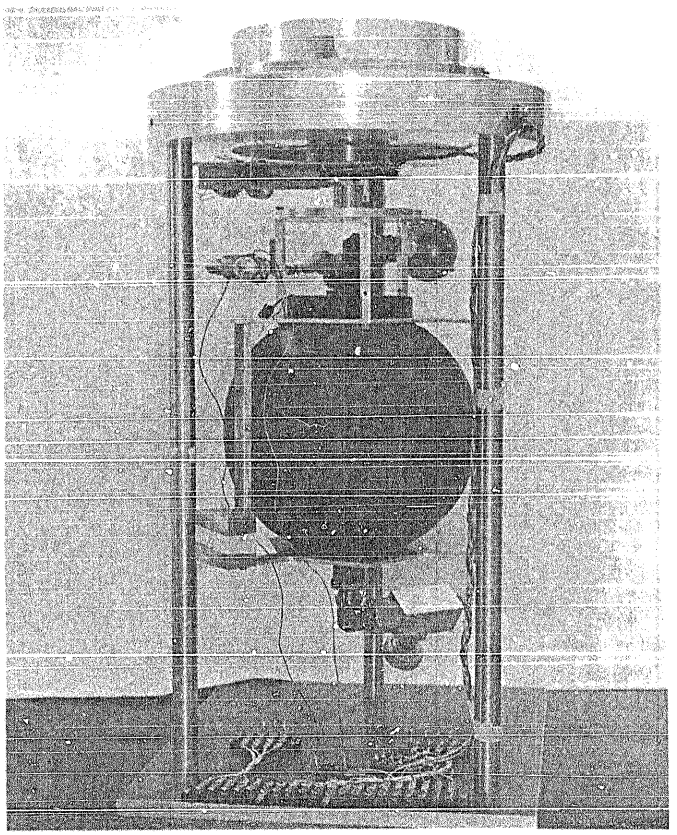

Figure 33. Torque test fixture

ber pressure and a 1.0 entrance coefficient. Experimental thrust measurements of 5.4 to 5.6 grams have confirmed the nozzle calculations and indicate an orifice coefficient of approximately 0.9. This high coefficient is indicative of streamline features designed into the nozzle. The excellent agreement between theoretical and experimental results has confirmed the application of classical nozzle equations to the design of miniature jet nozzles.

6. Functional Testing

Ideally, testing of an attitude control system can be accomplished only on a spacecraft in flight. The environmental parameters characteristic of space, namely, low gravitational forces, low aerodynamic friction, and near ultimate vacuum would indeed be difficult to simulate in the laboratory. In May of 1959 a visit was made to the ABMA facility in Huntsville, Alabama, to discuss attitude control concepts. ABMA at the time was working on a three-axis air bearing supported table which was contemplated for use in attitude control system evaluation. Mass unbalance difficulties arose due to table flexure which limited the utility of the ABMA table in early tests.

Shortly after the ABMA visit it was decided that a similar table would be extremely desirable in evaluating attitude control systems at JPL if the inherent difficulties of the ABMA table could be overcome and precise mass balance achieved. A study and design program was subsequently initiated. An artist's conception of the resulting design is shown in Figure 34.

The design objectives for the table structure were threefold. First, the structure had to be stiff so that deflection of the structure due to its own weight and mounted hardware would not contribute in excess of 10 gm-cm mass unbalance. Second, weight and inertia of the table were desired to be high in order to simulate anticipated spacecraft parameters. The table weight including the sphere is in excess of 800 pounds and inertias about the three major axes fall between 10 and 20 slug-ft^2. Third, the size of the table was limited so that operation in a 6-foot vacuum chamber would be possible in the future.

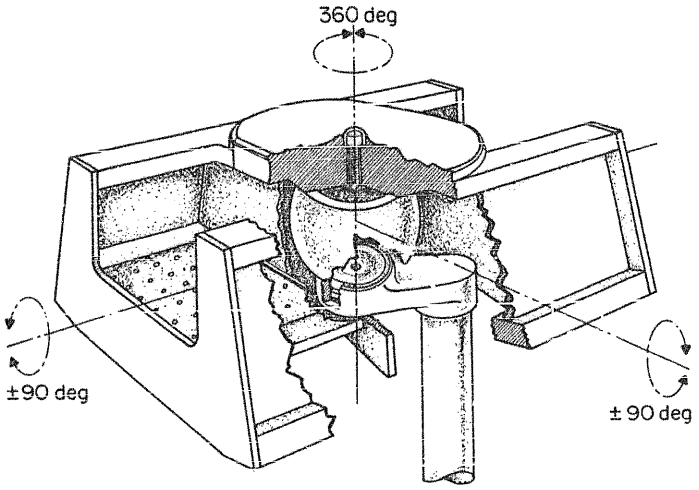

Figure 34. Spacecraft simulator

The air bearing shown in Figure 35 consists of a pad and a stainless steel spherical ball with a portion removed to provide for mounting. The ball is 10 inches in diameter and spherical to within ±30 microinches. The surface finish of the ball and pad is approximately 2 microinches. The pad has four radial grooves extending from the central gas port to a concentric groove. The table is lifted by an 80-psi nitrogen supply working between the pad and ball. In the resulting gas-lubricated bearing, coulomb friction has been eliminated and turbine torques have been minimized by the highly polished finish of the ball-pad combination. Gas flow rate is approximately 0.10 ft^3/min. At the present time the simulator is complete with the exception of several modifications yet required on the table. The ball has already been successfully air supported on the stand (Fig 36). Assembly of the ball to the table will take place during the latter part of January.

The basic attitude control system (which includes a three rate-gyro module, earth sensor, sensor modules, switching and control amplifiers, fuel totalizer, fuel tanks, regulator and control jets) will be mounted rigidly to the table. Mass balance of these components in all orientations of the table is essential within precise tolerances. One interesting mass balance problem already encountered concerns the fuel-tank mounting detail. Two tanks manifolded together are mounted symmetrically about the rotational center of the table. Consideration must be given to the following parameters to achieve acceptable mass balance: (1) mass and volumetric distribution must be identical; (2) the tanks must be supported in such a manner that pressurizing and depressurizing do not contribute to unbalance through expansion and contraction of the vessel, and (3) the manifolding line between tanks must be as small a volume as possible.

When the table is driven into either of its 90-degree positions, it becomes necessary to rotate the supporting stand which is coupled to the base through ball bearings. Rotation of the stand may be accomplished manually or remotely by the geared motor mounted to the base.

a. Instrumentation. To facilitate the critical balance operation required to place the table into operation, automatic balancing equipment is being designed. The principal objective of this equipment will be to achieve a precise balance of the assembly in a minimum time.

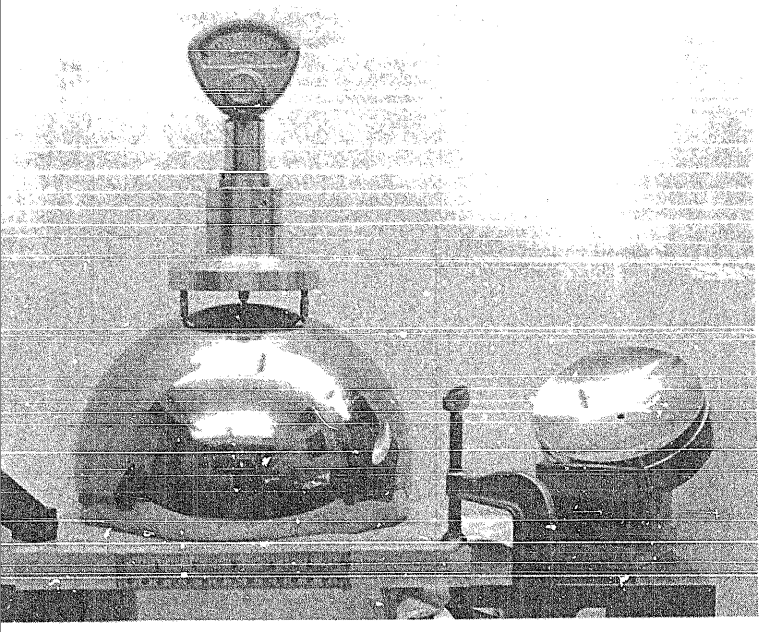

Figure 35. Simulator air bearing

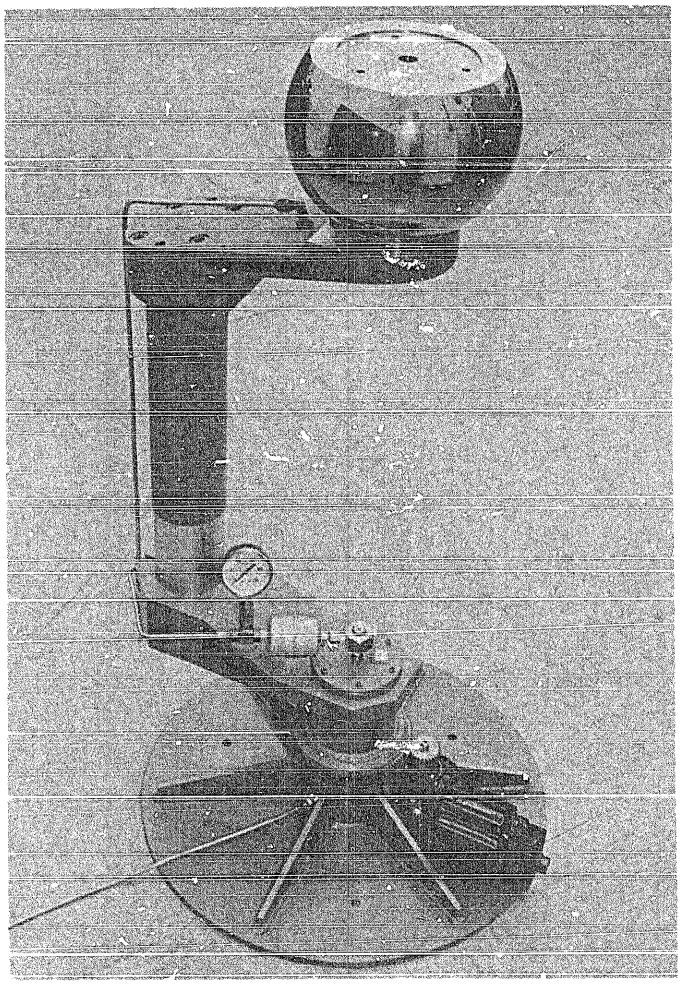

Figure 36. Simulator stand and air bearing

Since the criterion for balance is that the table has zero acceleration, it is necessary to sense either the table acceleration or one of its integrals. For the present case, the measurement of table velocity is most readily available from the rate gyros which are utilized in the attitude control system. The required accuracy of the balancing system must be at least 10 gm-cm. The response to a step input of unbalance torque must be such that the angular displacement of the table is small to insure that the gravity vector remain approximately constant.

The attitude control system rate gyro package which is used as a sensor for the single-axis balancing servo is shown in Figure 37. The rate gyro senses the velocity of the table and produces a voltage proportional to this velocity. This voltage is amplified and passed through an active lead network. The signal is then modulated, amplified, and applied to the control winding of a 400-cps gearhead servomotor (Size 8). The output shaft of the gearhead servomotor drives a lead screw which in turn positions a 100-gram weight. The position of this weight applies a balancing torque to the table.

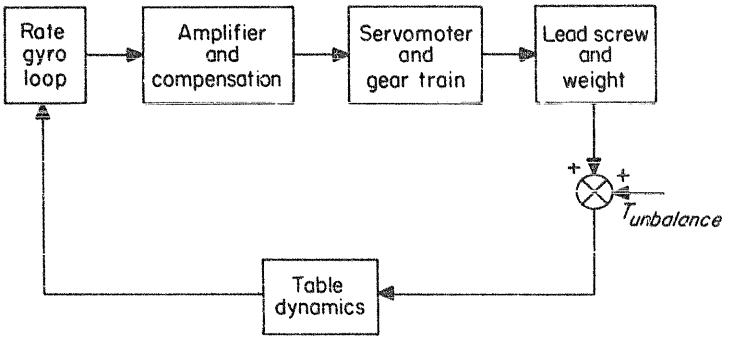

Figure 37. Single-axis balancing servo

In Figure 38, a block diagram of the linear servosystem with the appropriate transfer functions is given for a single-axis case. Because of the double integration in the loop, the system is a Type II servo. This system is being simulated on the analog computer, together with the appropriate nonlinearities such as motor dead zone, motor saturation, backlash, and gyro-loop dead zone. The data at present is incomplete, but indicates that the single axis will perform satisfactorily.

The three-axis balancing system will be mounted as shown in Figure 39. The procedure for balancing will consist of a manual balance to approximately 200 gm-cm. The table is then positioned in the x-z plane, horizontal to the earth's surface. The table is automatically balanced in this position using only the two balancing servos A and B parallel to the x and z axes, respectively.

ber pressure and a 1.0 entrance coefficient. Experimental thrust measurements of 5.4 to 5.6 grams have confirmed the nozzle calculations and indicate an orifice coefficient of approximately 0.9. This high coefficient is indicative of streamline features designed into the nozzle. The excellent agreement between theoretical and experimental results has confirmed the application of classical nozzle equations to the design of miniature jet nozzles.

6. Functional Testing

Ideally, testing of an attitude control system can be accomplished only on a spacecraft in flight. The environmental parameters characteristic of space, namely, low gravitational forces, low aerodynamic friction, and near ultimate vacuum would indeed be difficult to simulate in the laboratory. In May of 1959 a visit was made to the ABMA facility in Huntsville, Alabama, to discuss attitude control concepts. ABMA at the time was working on a three-axis air bearing supported table which was contemplated for use in attitude control system evaluation. Mass unbalance difficulties arose due to table flexure which limited the utility of the ABMA table in early tests.

Shortly after the ABMA visit it was decided that a similar table would be extremely desirable in evaluating attitude control systems at JPL if the inherent difficulties of the ABMA table could be overcome and precise mass balance achieved. A study and design program was subsequently initiated. An artist's conception of the resulting design is shown in Figure 34.

The design objectives for the table structure were threefold. First, the structure had to be stiff so that deflection of the structure due to its own weight and mounted hardware would not contribute in excess of 10 gm-cm mass unbalance. Second, weight and inertia of the table were desired to be high in order to simulate anticipated spacecraft parameters. The table weight including the sphere is in excess of 800 pounds and inertias about the three major axes fall between 10 and 20 slug-ft^2. Third, the size of the table was limited so that operation in a 6-foot vacuum chamber would be possible in the future.

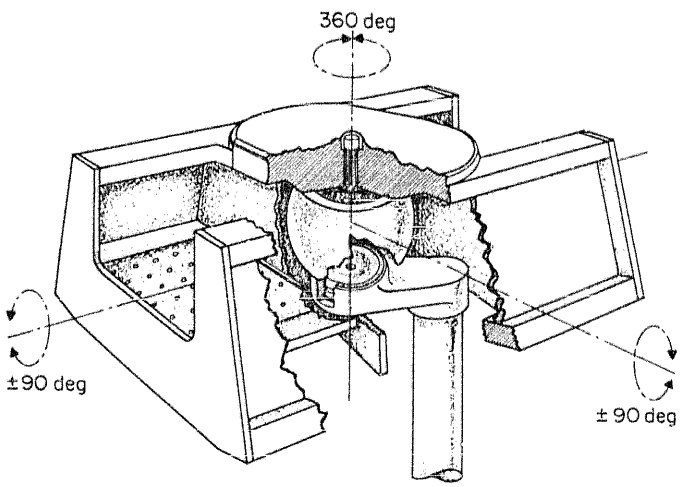

Figure 34. Spacecraft simulator

The air bearing shown in Figure 35 consists of a pad and a stainless steel spherical ball with a portion removed to provide for mounting. The ball is 10 inches in diameter and spherical to within ±30 microinches. The surface finish of the ball and pad is approximately 2 microinches. The pad has four radial grooves extending from the central gas port to a concentric groove. The table is lifted by an 80-psi nitrogen supply working between the pad and ball. In the resulting gas-lubricated bearing, coulomb friction has been eliminated and turbine torques have been minimized by the highly polished finish of the ball-pad combination. Gas flow rate is approximately 0.10 ft^3/min. At the present time the simulator is complete with the exception of several modifications yet required on the table. The ball has already been successfully air supported on the stand (Fig 36). Assembly of the ball to the table will take place during the latter part of January.

The basic attitude control system (which includes a three rate-gyro module, earth sensor, sensor modules, switching and control amplifiers, fuel totalizer, fuel tanks, regulator and control jets) will be mounted rigidly to the table. Mass balance of these components in all orientations of the table is essential within precise tolerances. One interesting mass balance problem already encountered concerns the fuel-tank mounting detail. Two tanks manifolded together are mounted symmetrically about the rotational center of the table. Consideration must be given to the following parameters to achieve acceptable mass balance: (1) mass and volumetric distribution must be identical; (2) the tanks must be supported in such a manner that pressurizing and depressurizing do not contribute to unbalance through expansion and contraction of the vessel, and (3) the manifolding line between tanks must be as small a volume as possible.

When the table is driven into either of its 90-degree positions, it becomes necessary to rotate the supporting stand which is coupled to the base through ball bearings. Rotation of the stand may be accomplished manually or remotely by the geared motor mounted to the base.

a. Instrumentation. To facilitate the critical balance operation required to place the table into operation, automatic balancing equipment is being designed. The principal objective of this equipment will be to achieve a precise balance of the assembly in a minimum time.

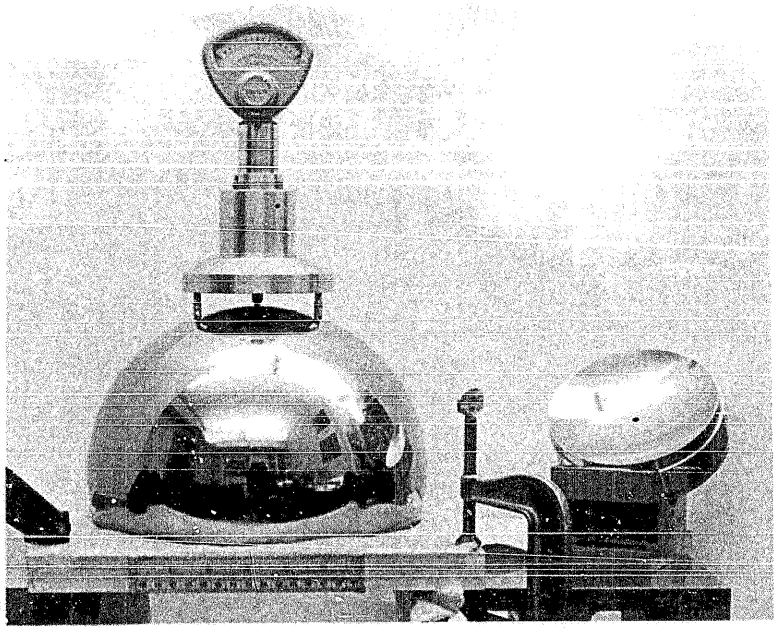

Figure 35. Simulator air bearing

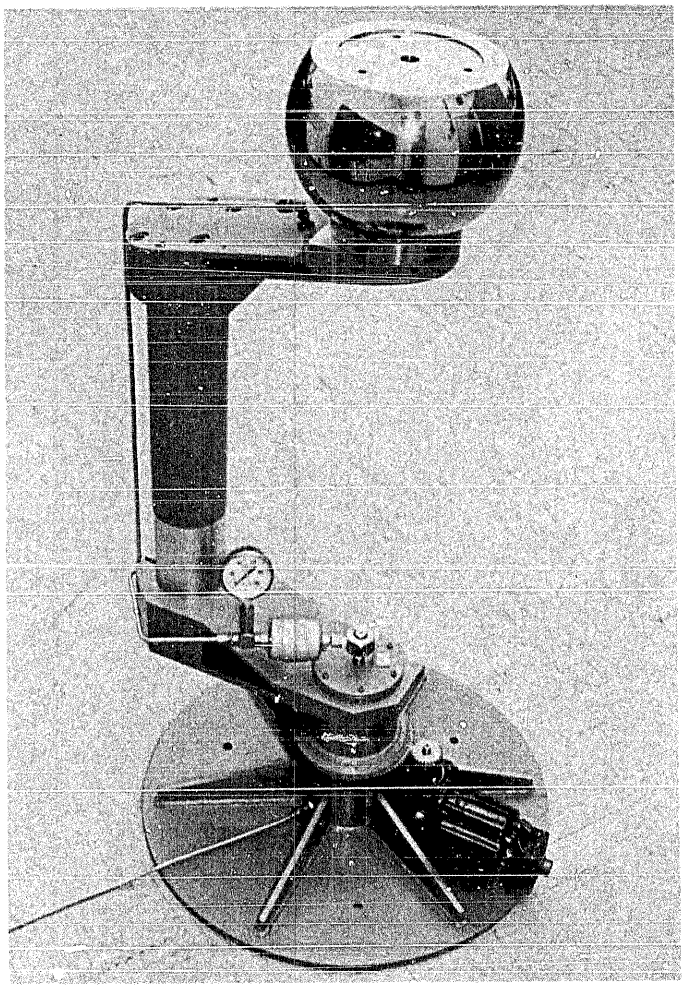

Figure 36. Simulator stand and air bearing

Since the criterion for balance is that the table has zero acceleration, it is necessary to sense either the table acceleration or one of its integrals. For the present case, the measurement of table velocity is most readily available from the rate gyros which are utilized in the attitude control system. The required accuracy of the balancing system must be at least 10 gm-cm. The response to a step input of unbalance torque must be such that the angular displacement of the table is small to insure that the gravity vector remain approximately constant.

The attitude control system rate gyro package which is used as a sensor for the single-axis balancing servo is shown in Figure 37. The rate gyro senses the velocity of the table and produces a voltage proportional to this velocity. This voltage is amplified and passed through an active lead network. The signal is then modulated, amplified, and applied to the control winding of a 400-cps gearhead servomotor (Size 8). The output shaft of the gearhead servomotor drives a lead screw which in turn positions a 100-gram weight. The position of this weight applies a balancing torque to the table.

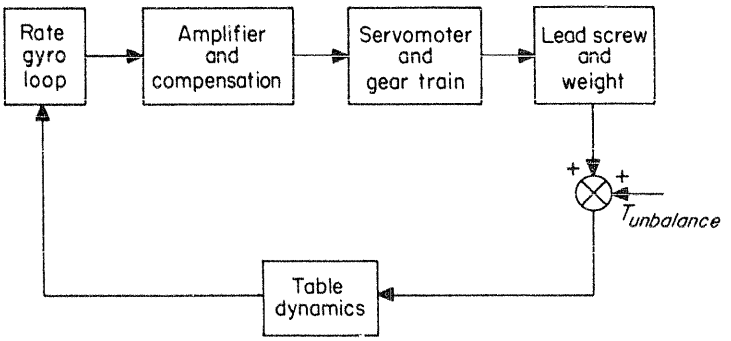

Figure 37. Single-axis balancing servo

In Figure 38, a block diagram of the linear servosystem with the appropriate transfer functions is given for a single-axis case. Because of the double integration in the loop, the system is a Type II servo. This system is being simulated on the analog computer, together with the appropriate nonlinearities such as motor dead zone, motor saturation, backlash, and gyro-loop dead zone. The data at present is incomplete, but indicates that the single axis will perform satisfactorily.

The three-axis balancing system will be mounted as shown in Figure 39. The procedure for balancing will consist of a manual balance to approximately 200 gm-cm. The table is then positioned in the x-z plane, horizontal to the earth's surface. The table is automatically balanced in this position using only the two balancing servos A and B parallel to the x and z axes, respectively.

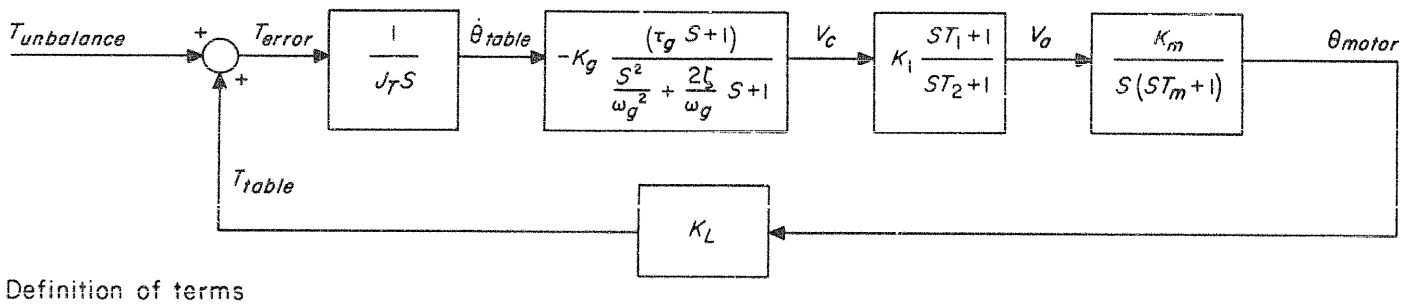

Definition of terms

$T_1 T_2$ = compensation time constant

J_T = table inertia

K_1 = amplifier gain volt/volt

K_g = gyro loop gain volt/rad/sec

ω_g = gyro loop resonant frequency

ζ = gyro loop damping factor

τ_g = gyro loop time constant

K_m = motor gain rad/sec/volt

T_m = motor mechanical time constant

K_L = gain of gear ratio, lead screw and weight

Figure 38. Linear servosystem

Since the gravity vector does not affect the y axis when the table is in this position the C servo is not required.

When the table is balanced in this position, the A and B balancing servos are de-energized and the table is then rotated 90 degrees about the x axis. In this position, the C servo is activated. It is controlled by the gyro which senses motion about the x axis since the only resultant unbalance of the table will cause rotation about the x axis alone.

This balancing procedure will be reiterative if the initial unbalances are of sufficient magnitude to cause resultant table displacements larger than 5 degrees of angle. In any event, the process will converge to a balanced condition and the reiterations may be used to secure a better balance. With this balancing system, the only limitation on balance of the spacecraft simulator will be the mass unbalance of the table and hardware and the nonlinearities in the balancing servo.

b. Simulator facility. A room is presently being prepared in which the simulator table will be installed. The room will be furnished with simulated sun and earth sources, and all room surfaces will be treated to prevent internal reflections. The sun will be simulated by a 1500-watt collimated light causing it to appear at an infinite distance. The size of the source as seen from the table will be the same as the sun seen from the earth or approximately 30 minutes of arc. A partition divides this room into control and operating areas. Small slits in this wall will provide observation stations for personnel. The simulator room will be sealed during operation in order to eliminate extraneous air drafts and to maintain total darkness except for the earth and sun sources.

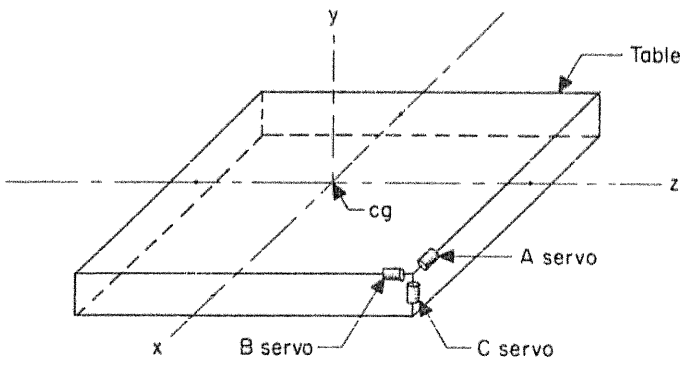

Figure 39. Three-axis balancing system

E. Power

In recent months the spacecraft electrical power system has been redesigned several times. To provide a clear understanding, an up-to-date engineering description of the spacecraft power system will follow.

The spacecraft electrical power system as planned for the initial flights provides 95 watts of regulated power at various ac and dc voltages as required. The primary power source is a sun-oriented array of 10 ft² photovoltaic solar-cell panels as shown in Figure 40. Two panels are used for the moon and Venus missions, whereas six panels are required at Mars. The solar panel output and the intensity of the sun's radiation decrease as a function of the square of the distance from the sun, as

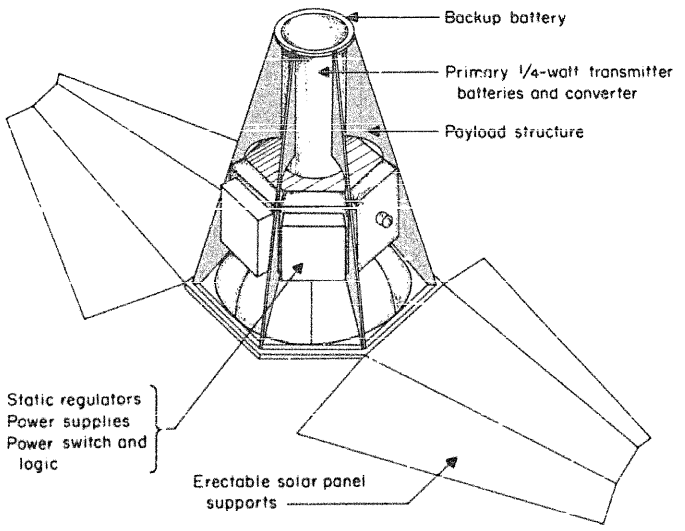

Figure 40. Spacecraft

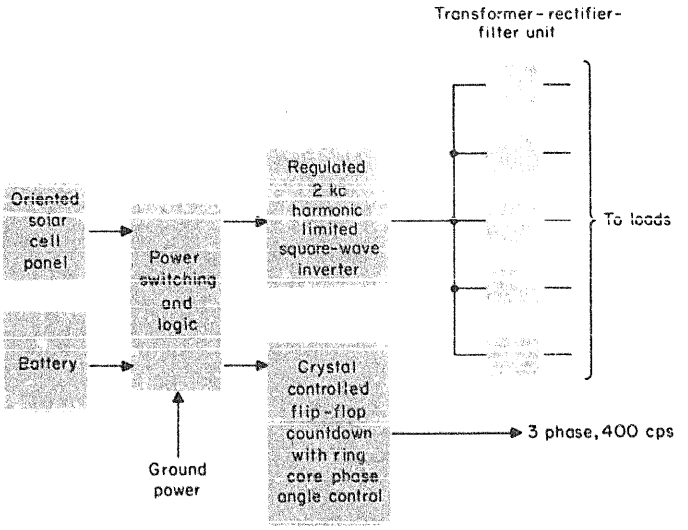

Figure 41. Electrical power system

shown in Table 9. Batteries provide power when the spacecraft is in the earth's shadow if takeoff occurs at night and emergency power if the attitude control or solar panel erection systems fail. A static transistor–magnetic power supply provides 400-cps power, as well as a variety of regulated dc voltages. Figure 41 presents a block diagram of the spacecraft electrical power system.

1. Photovoltaic

The sun-oriented silicon solar cells convert solar radiation to electrical energy. Each quantum of solar radiation which is absorbed and has an energy level greater than the gap between the valence band and the conduction band generates an electron-hole pair. The electrons flow to the *n*-region and the holes to the *p*-region of the photovoltaic *p-n* junction.

The solar cells are attached to the solar panels in the manner shown in Figure 42. Glass slides (6 mils thick) which have an antireflection coating on their outer surface and an ultraviolet reflective coating on their inner surface are attached to each individual 2 cm^2 solar cell with a special adhesive. The glass slide increases the emissivity and efficiency of the solar cell by causing it to radiate more energy and therefore operate at a lower temperature. The antireflection coating increases the amount of light absorbed by the solar cells and their electrical output. The ultraviolet coating reflects a low total energy portion of the solar spectrum to which the solar cell does not respond and which would probably damage the adhesive. The selection, application quality control, and evaluation of these adhesives is critical to the technical success of the solar panel. A great deal of advanced development has been conducted at JPL on the solar cell–glass slide adhesive problem.

Table 9. Spacecraft solar power system

Solar power system performance	A-1 Earth	A-2 Earth	A-3 Earth	A-4 Earth	A-5 Venus	A-6 Mars
Standard panel area, ft^2	10	10	10	10	10	10
Number of panels each flight	2	2	2	2	2	6
Unregulated output per panel, watts	70	70	70	70	110[a]	43[a]
Total unregulated solar panel output, watts	140	140	140	140	220	258
Power system output required,[b] watts	102	102	102	102	158	158
Power system output available, watts	95	95	95	95	149	175
Power system output margin, watts	−7	−7	−7	−7	−9	17
Sun distance, 10^6 miles	92.8	92.8	92.8	92.8	67.3	141.7
Estimated solar cell temperature, °C	39	39	39	39	93	−21

[a]Higher efficiency solar cells.

[b]Survey of 14 December 1959.

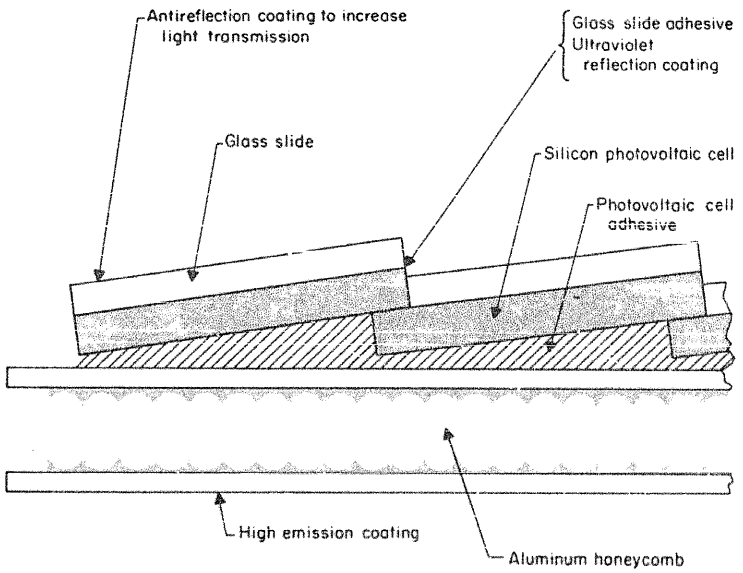

Figure 42. Solar panel cross section

In order to achieve the highest possible amount of power from a given number of solar cells, the operating point of the static inverter on the solar panel *E-I* curve has been carefully selected, as shown in Figure 43. It is intended to have the static inverter load line vary from the maximum power load line through the knee of the *E-I* curve to the lighter load, higher impedance load lines. Operating along this part of the *E-I* curve will present the static inverter with a more nearly constant voltage. If load variations do not exceed 20%, only one series dc-ac inverter may be required to provide ±2.5% voltage regulation. A single static inverter would achieve approximately 80% energy conversion; whereas if two series regulators are required, the conversion efficiency will fall to 70%. It will probably be necessary to use two static inverters for operation from the launch batteries. The watt-hr/lb performance of the battery is partially proportional to its allowable voltage regulation from ±1.5 to ±4 volts.

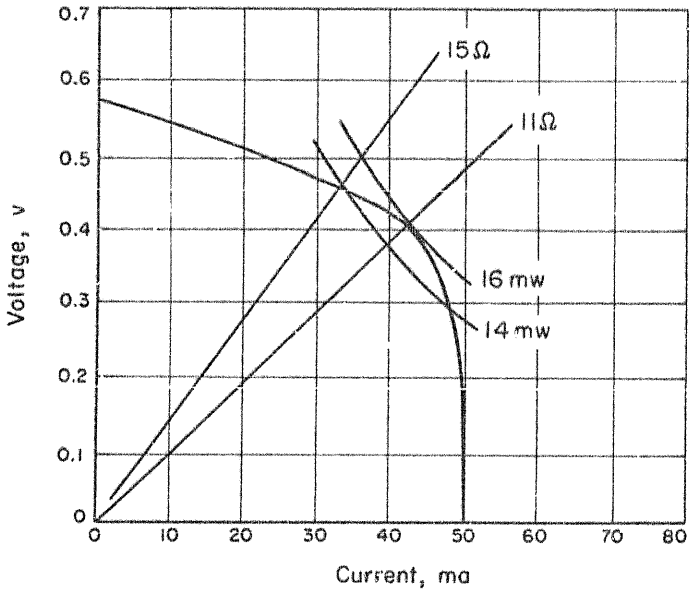

Figure 43. Solar cell *E-I* curve

The detailed power requirements of the estimated loads are presented in Table 10; the voltage accuracy requirements are also tabulated. A feedback voltage control loop is required for only one output. Every effort is being made to simplify the design of the static inverter to increase its reliability consistent with the conversion efficiency, and the voltage and frequency accuracy required.

A weight analysis of the spacecraft power system is presented in Table 11. The primary power-source solar panels will weigh 30 pounds, while the static inverter power regulator has a total allocated weight of 15 pounds.

To improve the dynamic (2 kc) impedance matching between the solar panels and the static inverter and its load, batteries may be placed in parallel with the solar panel. Preliminary tests indicate that it is doubtful if batteries can be successfully used in a simple, reliable manner for matching the dynamic impedance of solar panels to a 2 kc load. The use of capacitors in a similar manner in parallel with the input of the static inverter has been parti[illegible] investigated. In a similar phase Zener power diodes should be used to clamp the solar panel output voltage at the maximum efficiency–maximum load design point. The achievement of high efficiency conversion at ½ load is not nearly as important as the full load where the entire spacecraft system may be power-limited. Figure 43 illustrates the load-line impedance-matching problem.

2. Battery

A primary silver-zinc battery will be flown on Spacecrafts A-1 and A-2 to provide backup power in the event that the solar power system is inoperative for any reason. Whatever payload weight capability that is available will be used to provide backup battery capacity to operate the spacecraft for as long a period of time as possible. The characteristics of the 107-pound Eagle-Picher primary silver-zinc battery are shown in Table 12. Additional batteries of a comparable design may be provided in 25-pound increments if a suitable battery can be developed and is feasible for this application. An internal thermostat-controlled heater will probably be required to keep the backup batteries at operating temperature when they are not delivering power.

Table 10. Spacecraft power analysis[a]

Static converter name	Application	Input,[b] watts avg	Estimated efficiency, %	Volts out	Deviation, %	Frequency	Output,[c] watts avg
Commutator	¼-watt transmitter	(From separate 80-hr battery)	66	−12 4.75 100	±5 ±2 ±2	DC DC DC	0.84 0.95 0.83
	Transponder	11.7	68	20 −20	±5 ±5	DC DC	6.0 1.92
	¼-watt power amplifier	4.4	68	4.75 100	±2 ±2	DC DC	2.38 0.6
	3 watt	12.3	68	4.75 275	±2 ±2	DC DC	2.38 6.0
	10 watt[d]	22.0	68	4.75 275	±2 ±2	DC DC	14.25 0.83
		42.0[e]	68	500	±2	DC	28.57
Attitude control		Acquire[f] 39.0 Cruise 23.0	67	26 −26 26 ac 700 20	±5 ±5 ±5 ±5 ±5	DC DC 400 1554 1554	13.7 0.7 11.0 1.5 1.0
Data encoder (engineering telemetry) and command decoder	Engineering telemetry	11.0 0.71	— 70	31—23 −20	Raw power ±2.5	DC DC	— 0.5
	Command decoder	6.5	—	31—23	Raw power	DC	—
Controller timer		3.1	67	26 26 −26	±5 ±5 ±5	400 DC DC	0.052 1.04 1.04
		3.9	—	31—23	Raw power	DC	3.9
Scientific packages		7.1	85	28	±5	2400	3.0

[a]Input voltage is 31 to 23 volts.
[b]Total input at acquisition (2 hours) is 163.71 watts and at cruise is 147.7 watts.
[c]Total output at cruise is 105.98 watts.
[d]May be eliminated.
[e]8.3 watts during launch (17 minutes).
[f]21 watts during launch (17 minutes).

3. *Distribution System*

The power distribution system of the spacecraft (Fig 41) is comparable to the power distribution network of an electric power company. The same problems of grounding, fault clearance, conducted and radiated interference, power load cross-talk, efficiency, size, weight, and economy exist in both public utility and spacecraft power distribution networks. The ground rules for optimizing the two distribution systems, however, are quite different. For the spacecraft, the power distribution networks should be optimized with the various factors evaluated in accordance with the following relative priority: reliability, efficiency, conducted and radiated inter-

Table 11. Weight analysis of electrical power system for Spacecrafts A-1 through A-4[a]

Assembly	Weight, lb
Sun-oriented solar panel, 20 ft²	30
Launch and emergency battery	15
Power logic and switching	3
Regulated static inverter power supplies, ac and dc	15
	63

[a]On Spacecrafts A-1 and A-2 only, the payload weight capacity not required for other purposes will be used for the primary silver-zinc backup battery capacity. The weight capacity available for this backup battery is estimated to be 200 pounds.

Table 12. Characteristics of backup battery[a]

Manufacturer	Eagle-Picher
Type	Silver peroxide—zinc primary
Number of cells	16
Nominal voltage, volts	25.0
Weight (no heaters), pounds	107
Performance, watt-hr/lb	75
Pressure relief valve setting, psi	5 to 15 differential
Dimensions, inches	16.81 × 8 × 11.30
Discharge capacity in 80 hours, watt-hr	7000
Voltage regulation,[b] volts	−31 to 24

[a]At the present time, a Type I-A battery with no electrical heaters is to be used; later, however, heaters may be required, especially if power is not provided continuously.
[b]No load to full load plus temperature range (±15°F) with 80-hour discharge time.

ference in relation to the interference susceptibility of the most critical subsystem in the spacecraft, power load regulation cross-coupling, balancing of heat dissipation, weight, size, and economy.

The power distribution systems to be considered for the spacecraft can be classified according to the form in which power is conducted from the central power source or regulator to the individual load transformer-rectifier (T-R) and regulator units. These methods of power distribution are as follows: unregulated dc, pulse width modulated, regulated square-wave, regulated square-wave with no harmonics higher than the tenth, sine-wave with total rms harmonics limited to 5%, regulated common supply dc voltage, and regulated individual load dc. Figures 44a and b show block diagrams of two systems presently under study.

These seven different power distribution systems will be evaluated according to the relative priority assigned to the various evaluation factors. An actual operational mockup of the power system to permit interference tests is required for proper evaluation, in addition to the comparative component weight analysis of the power system.

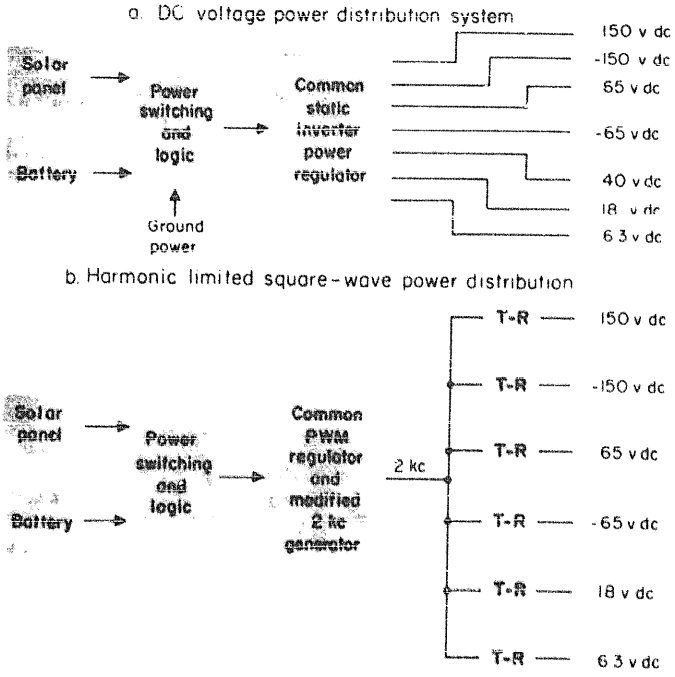

Figure 44. Power distribution networks

4. Regulated Power Supplies

Although interference tests are yet to be conducted on a power system mockup, it is believed that the spacecraft power distribution system will probably be a harmonic-limited square-wave system. A common pulse width modulated (PWM) regulator is utilized to provide regulated dc to the 2-kc square-wave static inverter, as shown in Figure 45. Either the output voltage of the most critical dc voltage is sensed and used to control the PWM regulation, or the regulated dc output is referenced to a Zener diode and this error signal is used to control the pulse width modulation.

If additional individual load regulation is required, it will be accomplished by utilizing conventional dissipative-type transistor regulator circuits. Compensated shunt-type power supply regulators with amplification can be used to provide extremely stable low-drift dc voltages as required. The efficiency of these regulators is approximately 40%; they will be used only where necessary.

The 400-cps power supply will utilize a 19.2-kc shock- and vibration-mounted crystal as a frequency reference element. Primary countdown circuits will be used to provide three-phase, two-phase, or single-phase 400-cps power control signals as required. Either silicon-controlled rectifiers or silicon transistors will be utilized as the solid-state power amplifier to generate 400-cps power. A typical schematic is shown in Figure 46.

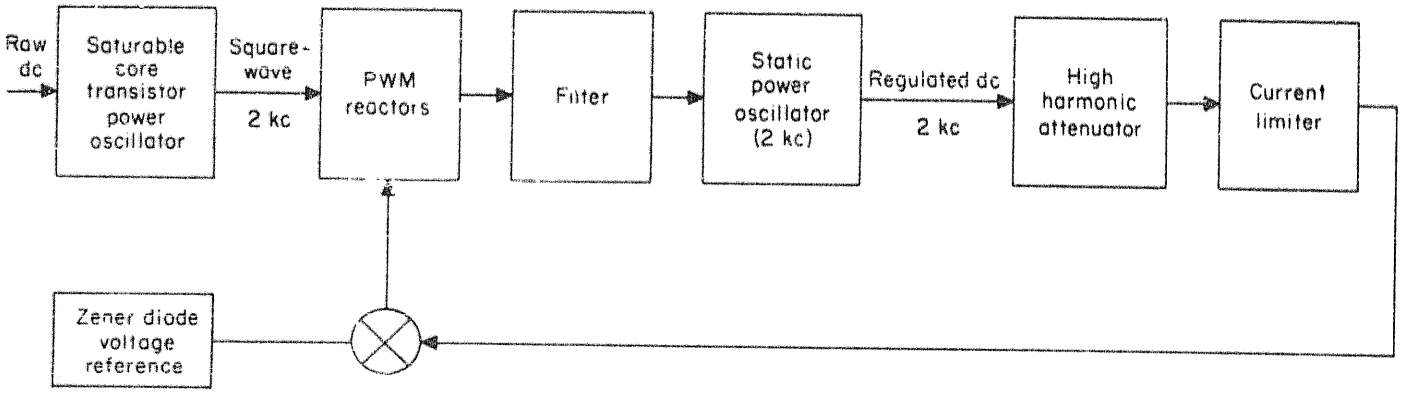

Figure 45. 2-kc square-wave PWM regulator

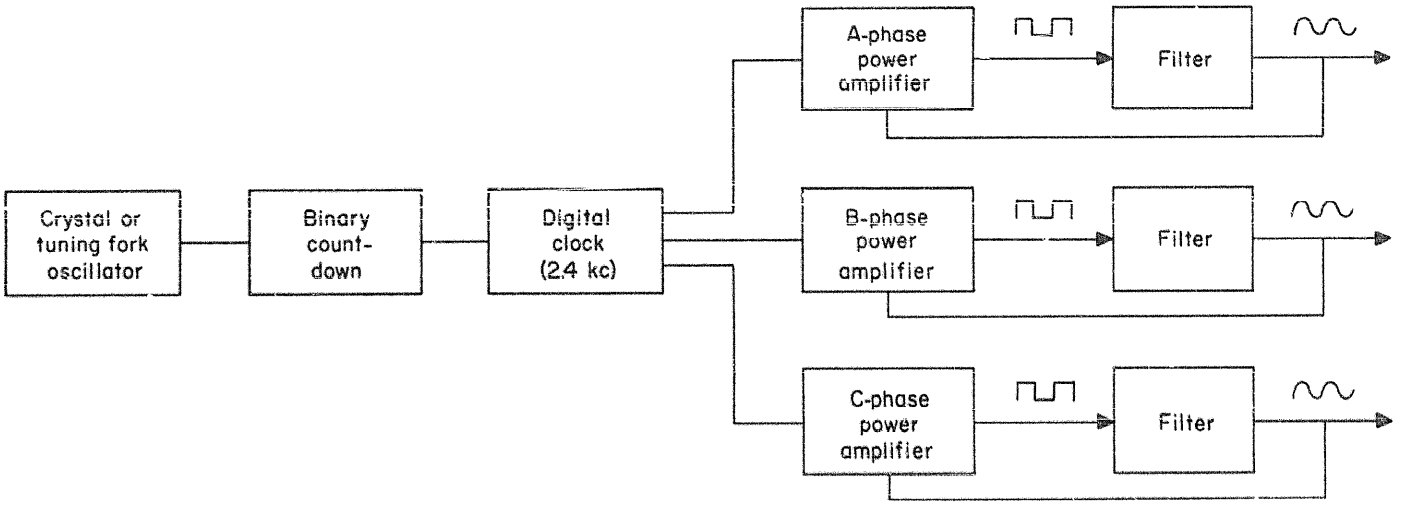

Figure 46. Typical three-phase static inverter

F. Packaging

Packaging for the spacecraft equipment has been influenced to a great extent by the need for a design which is versatile. This versatility is required in order to make the spacecraft capable of accepting equipment of various power dissipations, shapes, sizes, and operating environments. Nevertheless it was considered advantageous to achieve an integrated design by using modular packaging for the electronic equipment.

The basic shape of the electronic equipment compartment is as shown in Figure 47. The compartment, with the assemblies in the closed conditions, will be capable of retaining 1 atmosphere of pressure. For the initial missions, the compartment may not be sealed; however, it was felt that for subsequent missions it may be desirable to seal the compartment in order to accomplish the following.

Temperature control. Temperature limiting of the critical components could be accomplished by forced convection of air or other suitable gas contained within the spacecraft.

Electrical problems. Electrical problems associated with high-vacuum conditions can be avoided by a pressurized compartment.

Materials problems. Sublimation of some of the materials is known to occur under high-vacuum conditions; therefore, pressurization may be necessary.

In order to reduce the design and fabrication time, the subassembly chassis are uniform in profile and vary in width as is necessary. Cables will be run down the center of the assembly and connect to the spacecraft harness (Fig 47); critical cabling, however, could be isolated from the main trunk. Using subassembly chassis of uniform profile enables subassemblies to be interchanged from one assembly to another in order to accomplish mass and heat balance as required from flight to flight

Temperature control of the electronic equipment will be accomplished in the following manner for the initial flights. All heat dissipating parts will conduct heat to the subassembly chassis which, in turn, is in good thermal contact with the assembly chassis. The heat is then rejected at a rate dependent on the absorptivity and emissivity of the outer surface of the assembly chassis. This rate will be established to allow the equipment to operate under favorable temperature conditions.

a. Attitude control assembly. At the present time, design work for the attitude control assembly is nearing completion. This assembly will consist of six subassemblies: (1) system control, (2) gyro control, (3) gyro package, (4) actuation, (5) fuel totalizer, and (6) gas bottle. Subassembly chassis have been delivered for all of the subassemblies except the gyro package which is on order

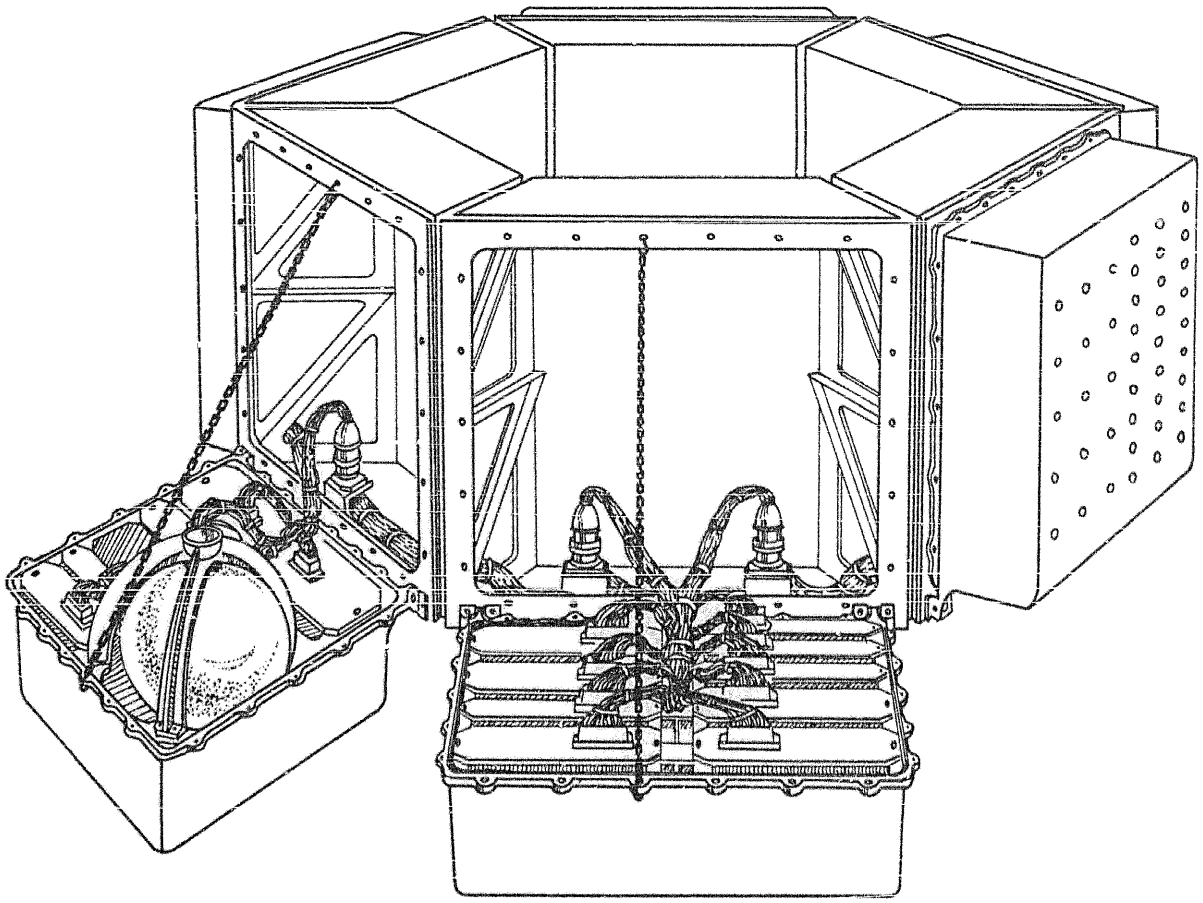

Figure 47. Spacecraft packaging

but has not yet been delivered. A prototype of the attitude control assembly is being fabricated at JPL for environmental testing.

b. Vibration tests—assembly housings. Vibration testing of the assembly housings has been completed. These tests were conducted with both the aluminum and magnesium cast housings, of varying wall thickness, both loaded and unloaded. In general, the unloaded housings had their first primary resonance in the area of 500 cps; again in general, the loaded housings had their first primary resonance at approximately 1000 cps. On the basis of these vibration tests, the nominal wall thickness of the assembly housings is being reduced from 0.150 to 0.120 inch.

Tests still to be performed on the assembly housings are the proof pressure and the leak rate tests.

G. Orbit Determination

The direction and magnitude of the correcting impulse for a mid-course or retro-maneuver is determined from radio tracking data. The radio tracking data is contaminated by random noise from many sources; for example, angle tracking data is subject to random errors caused by mechanical deformation of the tracking antennas and by receiver noise which causes jitter in the antenna servos. A digital computer program, described in *SPS 2*, was used to determine the injection conditions for the orbit which fits the measured data with the least square error. These estimates of the injection errors can be used to determine the mid-course correction. Therefore, for error analysis, it is necessary to know how accurately the orbit can be determined from the measured data. A method of finding the accuracy of orbit determination was described in *SPS 5*. This method has been programmed on the digital computer, and some preliminary results were described in *SPS 6*. Some recent results are described herein. The accuracy of orbit determination is studied as a function of the magnitude of the noise in various data types. Some preliminary results are shown concerning orbit redetermination after a mid-course maneuver. Also, it is shown that the use of range data results in very accurate orbit determination.

For these studies a 51-hour lunar trajectory has been used. The powered flight portion of this trajectory includes a coasting period between second-stage burnout and third-stage ignition. Third-stage burnout occurs over the South Atlantic Ocean. The probe's closest approach to the surface of the moon (300 miles) should occur after the probe is in flight about 51 hours.

It is assumed that while the probe is on this trajectory it is tracked by the JPL (downrange-type) station at Johannesburg, South Africa, and by the Deep-Space Net Station at Goldstone, California. Table 13 shows the assumed characteristics of the noise for each station.

Table 13. Assumed noise characteristics

Station	Maximum range, miles	Type of data	σ	T, minutes
Johannesburg	50,000	Elevation angle, degrees	0.1	$<1/6$
			0.01	1/2
			0.1	60
		Azimuth angle, degrees	Same as elevation	
		Range rate, meters/sec	1	$<1/6$
Goldstone	>250,000	Declination, degrees	0.03	$<1/6$
			0.01	1/2
			0.01	300
		Hour angle, degrees	Same as declination	
		Range rate, meters/sec	1	$<1/6$

(Here σ^2 is the mean square value of a particular kind of noise, and T is the time interval in minutes over which the noise is assumed to be perfectly correlated.) The assumptions concerning the characteristics of the noise components are explained in more detail in *SPS 6*. For both stations, the high-frequency angle noise ($T < 1/6$) is due to servo jitter. The component with $T = 1/2$ is due to uncertainties in the atmospheric refraction correction. The very low frequency error is due to structural deflections of the antenna. The doppler accuracy is limited by the transmitter frequency stability and the probe acceleration or roundoff error in counting to the nearest cycle. It is assumed that each type of data is sampled once every 10 seconds.

Figure 48 shows the accuracy of orbit determination as a function of time t measured from injection. The ordinate λ is the length of the semimajor axis of the 40% probability ellipse of miss components at closest lunar

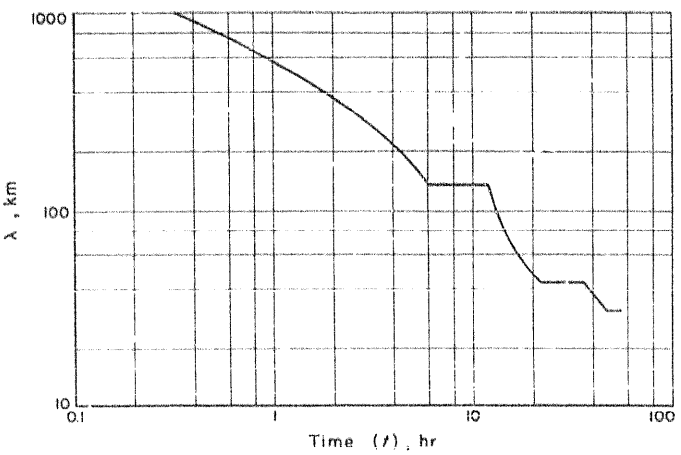

Figure 48. Accuracy of orbit determination of 51-hour lunar trajectory

approach. In Figure 48, Johannesburg tracks from shortly after injection until the probe goes out of range at $t = 6$ hours. The data from Johannesburg reduces λ to 104 km. Goldstone acquires at $t = 12$ hours and data taken during the first pass reduces λ to 43 km. Data taken during the second pass over Goldstone reduces λ to 31 km. At closest approach the probe is below the horizon at Goldstone. Suppose that a mid-course maneuver is to be made at some time $t = t_g$ in order to null the miss components at closest approach. Since the correcting velocity increment is computed from the radio tracking estimates of the orbit, the accuracy of the mid-course guidance cannot be better than $\lambda(t_g)$ as shown in Figure 48.

Figure 49 shows how the accuracy of orbit determination on the 51-hour trajectory varies with the magnitude of the noise in the range rate data. The ordinate of the graph is the value of λ at 20 hours, $\lambda(20)$, and the abscissa is the value of σ for the range rate data, $\sigma_{\dot{r}}$. The value of λ at 20 hours is chosen because considerations of fuel economy, component error, etc., indicate that the optimum t_g is between 15 and 20 hours for this trajectory. It is assumed that $\sigma_{\dot{r}}$ is the same for both stations and that $T < 1/6$ minutes as in Table 13. The noise in the angle data is the same as in Table 13. Note that, in Figure 49 when $\sigma_{\dot{r}} = 1$ meter/sec, $\lambda(20) = 49$ km which agrees with Figure 48. As $\sigma_{\dot{r}}$ becomes larger in Figure 49, the range data contributes less to the overall orbit determination. The curve approaches an asymptote $\lambda(20) = 1100$ km which is the value of $\lambda(20)$ if only angle data is used. It would be very difficult to build a two-way doppler system with $\sigma_{\dot{r}} < 0.2$ meter/sec.

Figure 50 shows the effect of varying the magnitude of the low-frequency angle noise at Goldstone on $\lambda(20)$. The value of σ for the low-frequency component of noise in hour angle and declination is σ_α. All other noise components are the same as in Table 13. The curve approaches an upper asymptote $\lambda(20) = 90$ km when the angle accuracy is so poor that the data is useless. The curve approaches a lower asymptote determined by the other two noise sources in the Goldstone angle data. The lower asymptote is not shown on this graph.

Figure 51 shows the effect of varying the magnitude of the low frequency angle noise at Johannesburg on $\lambda(20)$. The value of σ for the low-frequency component of noise in elevation and azimuth is σ_γ. All other noise components are the same as in Table 13. The curve has an upper and lower asymptote as for σ_α.

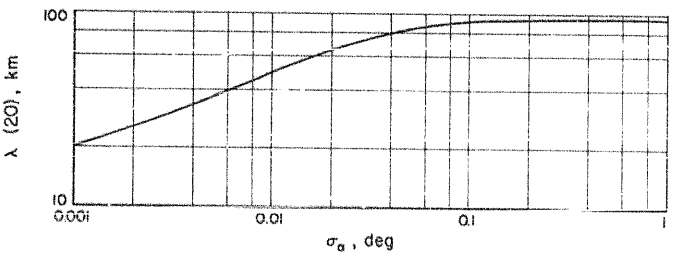

Figure 50. Effect of σ_α on accuracy of orbit determination

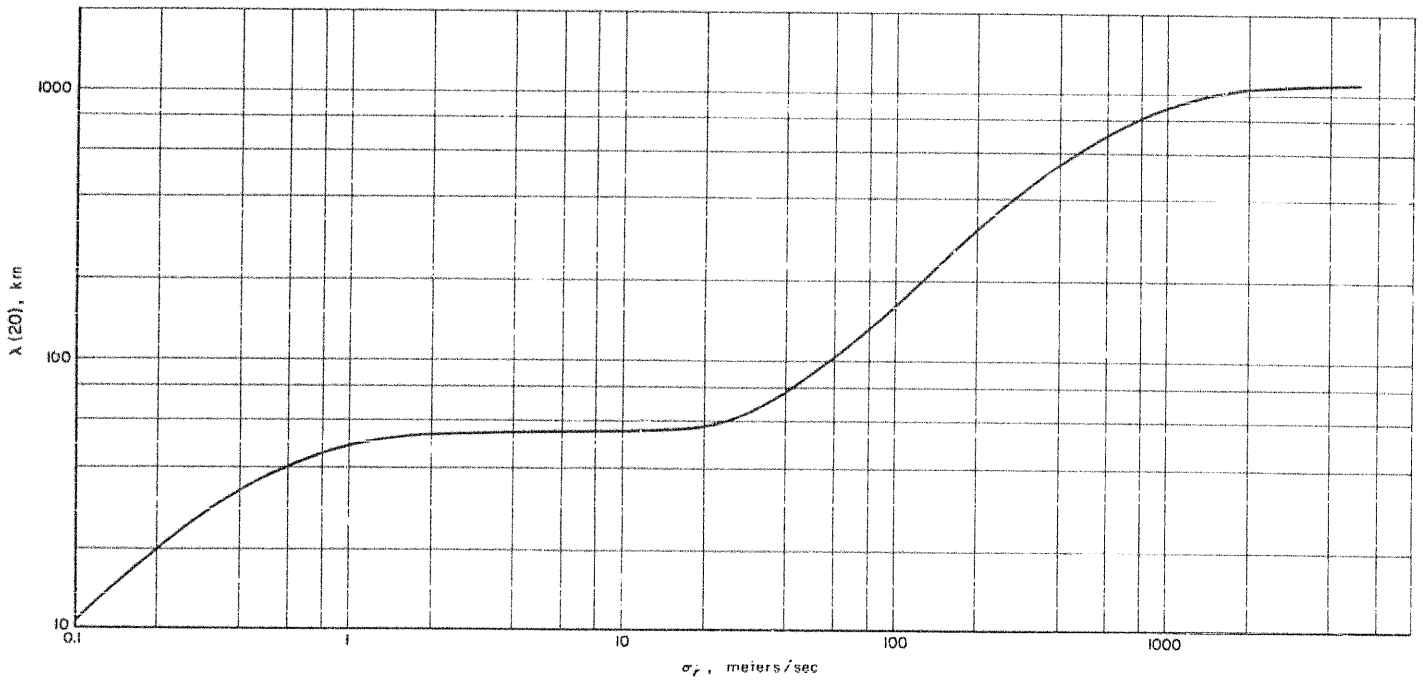

Figure 49. Effect of $\sigma_{\dot{r}}$ on accuracy of orbit determination

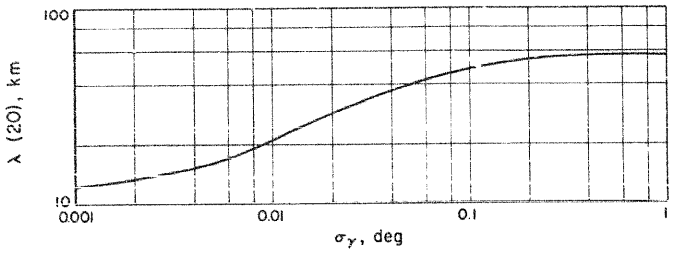

Figure 51. Effect of σ_γ on accuracy of orbit determination

Figure 52 shows $\lambda(t)$ when there is a mid-course maneuver. The solid curve in Figure 52 is the same curve as in Figure 48. It is assumed that a mid-course maneuver is made at $t_g = 9$ hours, although this is not the optimum time. Due to component errors in the mid-course guidance system, there will be some uncertainty in the direction and magnitude of the velocity vector applied to the probe. Using typical values for these uncertainties, the orbit determination degenerates at t_g as shown by the dashed curve in the figure. Subsequent tracking reduces λ considerably. For some missions, it may be necessary to redetermine the orbit quite accurately after a mid-course maneuver in order to calculate the impulse for a retro-maneuver or as part of a scientific experiment.

Figure 53 shows $\lambda(t)$ when range data from both stations is utilized in addition to angle and range rate. It is assumed for the range data that $\sigma = 10$ minutes and $T > 1/6$ minute. All other noise components are the same as in Table 13. It can be seen that range data is very useful in determining the orbits.

At the present time, the effect of range data is being studied more thoroughly. Also being studied are the effects of additional stations and different station configurations.

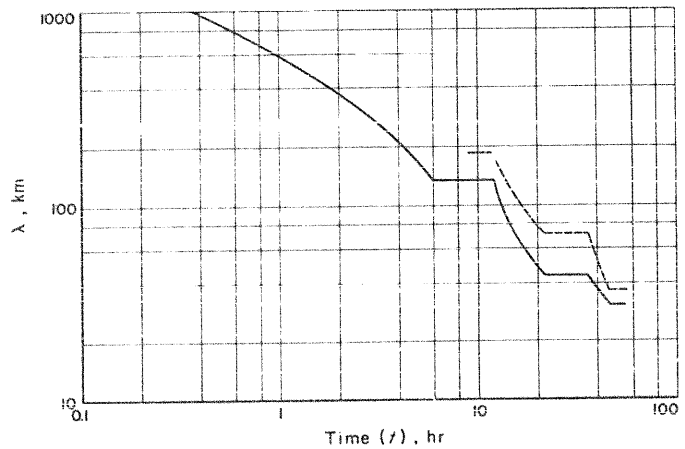

Figure 52. Accuracy of orbit determination with mid-course maneuver

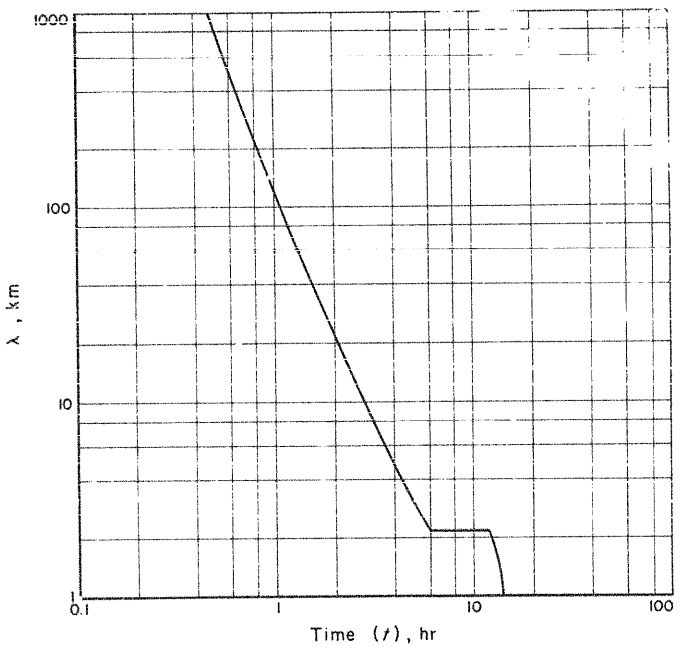

Figure 53. Accuracy of orbit determination when range data is used

UNCLASSIFIED
CONFIDENTIAL

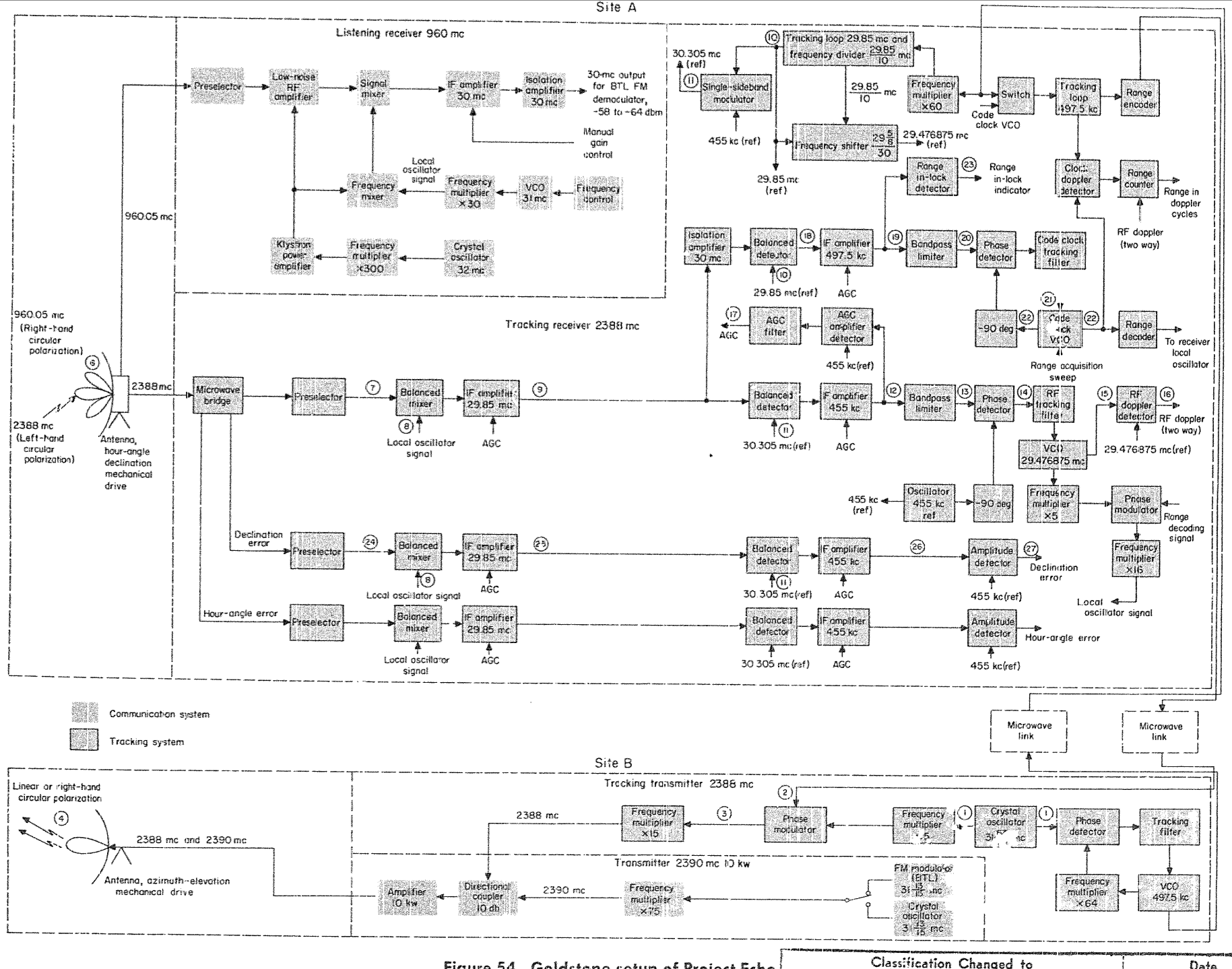

Figure 54. Goldstone setup of Project Echo

Classification Changed to UNCLASSIFIED
Date 9-1-60
Authority Orl Newlan 9-1-60
By Jack Lowe

UNCLASSIFIED
CONFIDENTIAL

III. PROJECT ECHO

The utilization of earth satellites has been proposed as a possible technique for improving global communications. These communications satellites fall into two general categories: passive repeaters and active repeaters. Project Echo utilizes a passive repeater in the form of a 100-foot-diameter balloon. Project Echo is a NASA program; however, other agencies and organizations have been invited to utilize the 100-foot balloon to perform communications experiments. The official NASA transmit/receive stations are located at Goldstone, California, and Holmdel, New Jersey (*SPS 6*). The Goldstone station is operated by the Jet Propulsion Laboratory, and the Holmdel station is under the cognizance of the Bell Telephone Laboratories (BTL).

The Goldstone and Holmdel transmit/receive stations are described functionally in *SPS 6*. The two Goldstone antennas operate together, and they may be positioned (1) optically, (2) digitally, from computed trajectory data, or (3) by radio means, automatic tracking on the reflected RF signal. The Holmdel antennas also operate together, and they can be positioned optically or digitally. The Goldstone transmitter frequency is 2390 mc, whereas the Holmdel transmitter frequency is 960.05 mc. Therefore, the east-to-west coast link is on 960 mc, and the west-to-east coast link is on 2390 mc.

The Goldstone station will comprise a 960-mc listening receiver, a 2388-mc tracking receiver, and a 2390/2388-mc 10-kw transmitter for Project Echo (*SPS 6*). The 960-mc listening receiver will amplify and demodulate the voice signal transmitted from Holmdel, New Jersey, via the passive communications satellite. The 10-kw 2390-mc transmitter will be voice-modulated, and the signal will be beamed at the passive communications satellite for reception at Holmdel. A 1-kw CW 2388-mc transmitter will provide a balloon-reflected signal for the Goldstone 2388-mc tracking receiver.

The 2388-mc tracking receiver, operating in conjunction with the simultaneous-lobing antenna feed and microwave bridge, will provide the dc control signals to the servosystem for automatic positioning of the antenna in angle. A revised functional block diagram of the Goldstone tracking and communications system for Project Echo is shown in Figure 54. The waveform equations which describe the operation of the 2388-mc CW doppler-radar were presented in *SPS 6*.

A. Moon Bounce Experiments

Three preliminary communications experiments have been performed to date between the Goldstone and Holmdel stations using the moon as a passive repeater in an east-to-west transmission at 960.05 mc. The first transmission tests were made on 23 and 24 November 1959, followed by further experiments on 2 December 1959, and 6 January 1960. During the approximate 8 hours that the moon was mutually visible, the first half of this period was used by BTL for their wide deviation FM transmission, while the second half of the experiment was used

by JPL for phase-coherent transmission with phase modulation.

During the first experiment on 23 and 24 November, the 960.05 mc low-noise listening receiver at Goldstone was operated in conjunction with Bell Telephone Laboratory FM demodulator. During this experiment some trouble was experienced at Holmdel with RF arcing in the high-power transmission line between the 10-kw transmitter and its antenna.

During the test of 23 December, the moon was angle-tracked automatically using the TRAC(E) tracking receiver (*SPS 1* through *4*) which was installed at Goldstone for the *Juno II* program and used for tracking *Pioneer* probes *III* and *IV*. The angle tracking experiment was successful, and the angle data recorded during the test is being reduced at the present time.

During the JPL portion of the 6 January moon bounce test, the 960.05-mc low-noise listening receiver was operated as a phase-coherent system with a closed-loop-noise bandwidth of 16 cps at strong signal levels. Recordings were made of audio tone and voice modulation, as well as the depth and frequency of the signal fading. Although rather severe signal fading was apparent, clear voice transmission was accomplished. The results of the 6 January moon bounce tests will be presented in a later report.

B. Transmitter Exciter

A phase-stable crystal-controlled 960.05-mc exciter has been developed for use in the preliminary Project Echo experiments utilizing the moon as a passive reflecting sphere. This exciter was used in conjunction with the BTL 10-kw amplifier to provide a phase-modulated transmission from Holmdel, New Jersey, to Goldstone, California, via the moon during a portion of the tests performed on 23 December 1959 and 6 January 1960.

The module arrangement for the exciter is illustrated in Figure 55. The *Juno II* transmitter shown is a phase-stable crystal-controlled signal source capable of deliver-

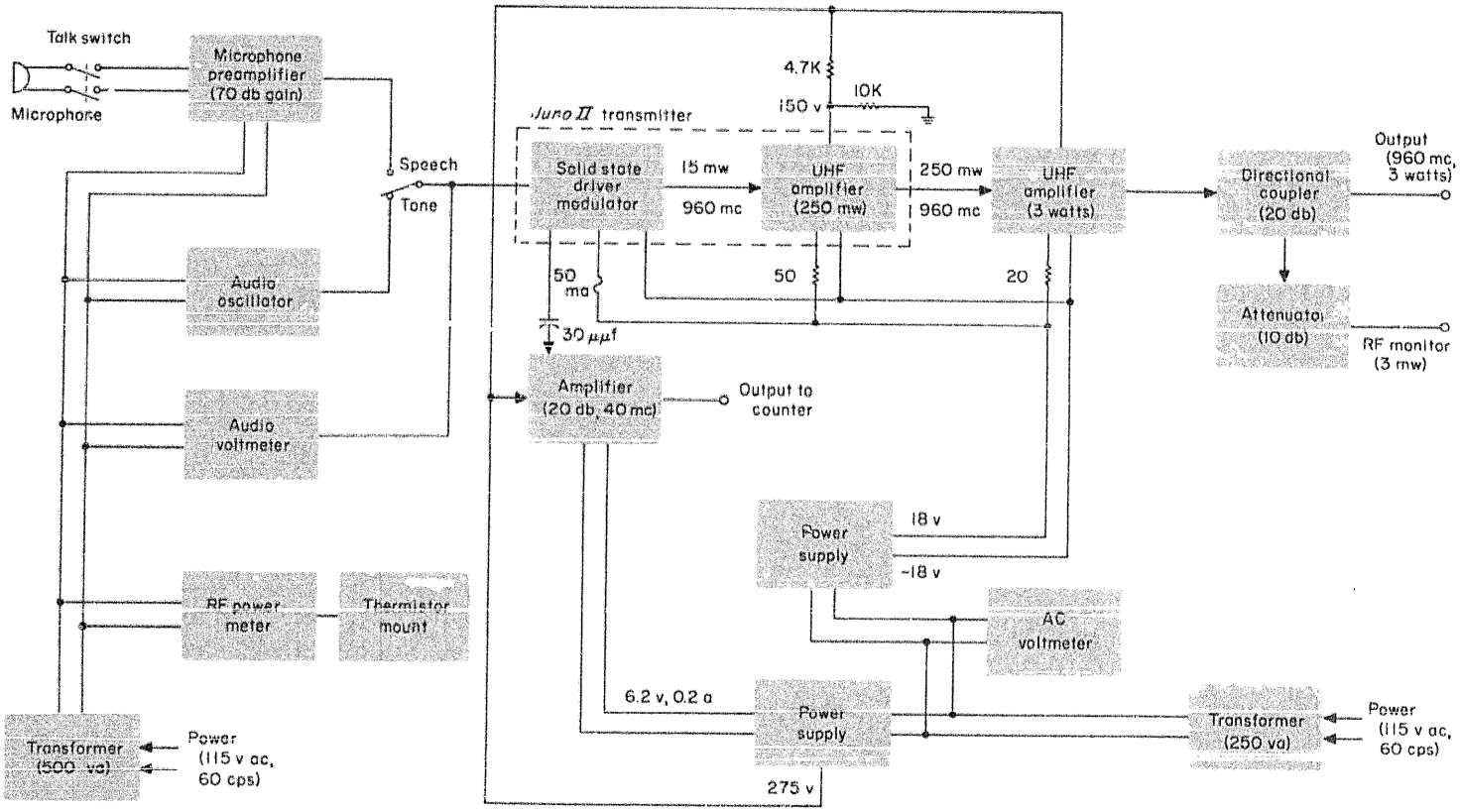

Figure 55. 3-watt exciter

ing 250 milliwatts of power at 960 mc (*SRS 1, 2,* and 3). The unit may be phase-modulated in excess of 1 radian over the complete audio range. The *Juno II* transmitter is followed by a 3-watt 960-mc cavity amplifier developed for airborne applications (*SPS 5*), which provides adequate power to meet the drive requirements of the JPL 10-kw klystron amplifier. A solid-state power supply provides the required dc current for the UHF amplifier vacuum-tube heaters so as to avoid spurious phase modulation at the power-line frequency.

Tests made at JPL, Pasadena, with this exciter included: (1) phase stability tests in conjunction with a phase-stable 960-mc receiver, and (2) modulation tests with a 960.05-mc phase-coherent receiver which is similar to the Goldstone receiver and is capable of detecting audio speech signals (Fig. 56). The measured rms phase error of the 3-watt exciter unit was 1.5 degrees when the receiver was operated with a 15-cps closed-loop bandwidth. The measured audio response, using the laboratory phase-coherent receiver and tone modulating the exciter, is shown in Figure 56. When the temperature of the exciter was varied over a range of 10 to 55°C, the modulation index did not vary more than ±2 degrees, and the power output was constant within ±½ db. For a temperature variation of ±5°C, the change in carrier frequency did not exceed ±1 part in 10^6. Operation of the exciter during the moon bounce tests of 23 December 1959 and 6 January 1960 was completely satisfactory.

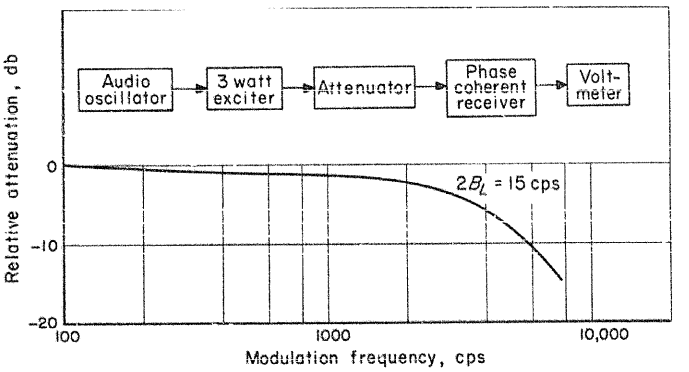

Figure 56. Audio response of phase coherent receiver using 3-watt exciter

IV. VEGA PROGRAM

With the cancellation of the *Vega* program, several areas of research and development have been discontinued. Concluding reports on those projects are presented in this section. Other studies, as stated in the Synopsis, will be continued in Volume II of the *Research Summary 36-1*.

A. Spacecraft

1. Telemetry Antenna

At the time of *Vega* cancellation, development of the third-stage telemetry antenna system had reached the stage of preliminary radiation pattern measurements to determine a suitable configuration. An essentially omnidirectional pattern was desirable since the antenna was to provide satisfactory coverage for a variety of possible missions and trajectories. It was also desirable to have uninterrupted telemetry reception in the event of vehicle guidance failure. Therefore, very low pattern levels over a substantial solid angle were avoided. A resonant quarter-wavelength stub antenna was chosen for the radiating element since it exhibited a resemblance to the desired omnidirectional antenna and was a very simple antenna to construct.

A quarter-scale model of the antenna and ground plane is shown in Figure 57. Figure 58 shows two of these antennas mounted on a quarter-scale model of the *Vega* vehicle (after first-stage separation). Radiation patterns have been taken with this configuration with both antennas driven in phase, with the antennas driven 180 degrees out of phase, with the antennas driven 270 degrees out of phase, and with only one antenna driven. Preliminary evaluation of the patterns indicated that two antennas driven in phase covered 25% more solid angle area than the single antenna, 100% more than the two antennas driven 180 degrees out of phase, and 30% more than the two antennas driven 270 degrees out of phase,

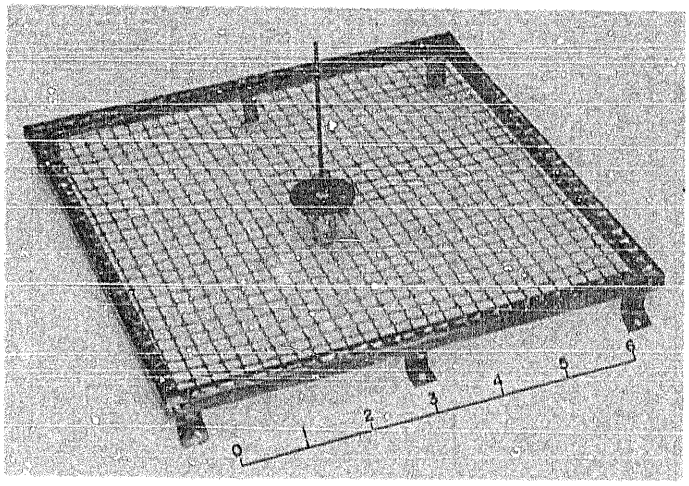

Figure 57. Third-stage telemetering antenna, ¼-scale model

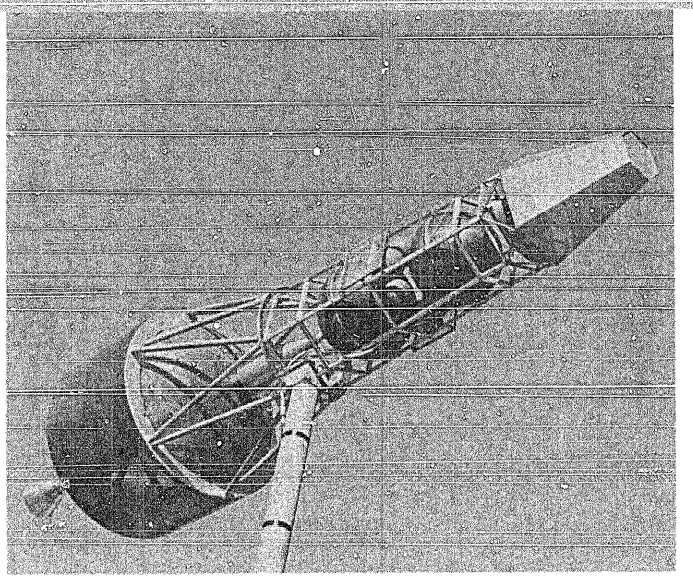

Figure 58. Third-stage telemetering antenna, mounted on spacecraft mockup

above the −10 db level relative to a half-wave dipole. The two antennas driven in phase covered 80% of the total 4π solid angle down to this level.

Measurements of impedance vs length of the ¼-inch-diameter unmatched stub showed the resonant length to be 0.231λ. The resonant resistance was determined to be 26 ohms. Hence, a simple $\lambda/4$ coaxial matching section of 36-ohm characteristic impedance would be required to match the antenna into a 50-ohm transmission line. Cancellation of the program occurred before fabrication of a full-scale prototype with matching section was completed. No further work on the development of this antenna will be done.

2. Controller

The controller is a device whose primary purpose was to coordinate the intersystem activities of the spacecraft. To this end the controller was to perform the following general functions:

(1) Generate timing information.

(2) Receive information and/or commands from: (a) earth-based control during preflight system tests, (b) earth-based radio control during flight (c) timer, and (d) on-board systems to indicate the existence of conditions requiring action by other systems.

(3) When required, generate commands based upon information from the sources shown in Item (2).

(4) Route the commands to the appropriate spacecraft systems for action.

The specific functions of the controller based on a *Vega*-boosted direct ascent were planned: (1) to provide timing pulses for the stepping switches of the telemetry, and (2) to initiate a flight sequence by generating commands based on timing information from the timer of the controller.

A tentative flight sequence was prepared for a *Vega*-boosted direct ascent (Table 14). The times listed were intended to give an idea of the relative sequence of events.

Table 14. Flight sequence for Vega-based spacecraft

Time	Type[a]	Org[b]	Des[b]	Occurrence or command
X	I	EA	CL	Launch has occurred
X	C	CL	CL	Start timer
X + 17 min	T	CL	ST	Unfold solar panels
X + 17 min	T	CL	ST	Extend boom
X + 17 min	T	CL	SC	Turn on solar corpuscular radiation experiment
X + 19 min	T	CL	AC	Turn on attitude control power
X + 19 min	T	CL	AC	Acquire the sun
X + 2 hr	T	CL	ST	Unlatch antenna
X + 2 hr	T	CL	AC	Position antenna
X + 2 hr	T	CL	AC	Acquire the earth
X + 2 mo	T	CL	RF	Turn off transmitter
—	C	ER	RF	Transfer from crystal-controlled to receiver-controlled operation
—	C	ER	AC	Roll-lock overide[c]
—	C	ER	AC	Earth-sensor angle override[d]

[a] Indicates the type or nature of an occurrence, where I is initial command, C is a command resulting from a non-timed event, and T is a command resulting from generated time information.

[b] Org indicates the system originating the occurrence or command, and Des, the system receiving and acting upon the information or command. The symbols are identified as follows: AC, attitude control; CL, controller; EA, earth checkout and launch except via RF link; ER, earth control via RF link; RF, communication; SC, scientific instruments; and ST, structures.

[c] Command from earth which will cause the spacecraft to resume rolling in search of earth when the spacecraft has locked in roll on something other than earth.

[d] Command from earth which will cause the earth sensor to change its angle with respect to the roll axis. This command may be used for the purpose of breaking a lock on something other than earth, and also allows setting the earth-sensor angle to some position other than an advance-programmed angle in the event the vehicle does not follow the expected trajectory.

IV. VEGA PROGRAM

With the cancellation of the *Vega* program, several areas of research and development have been discontinued. Concluding reports on those projects are presented in this section. Other studies, as stated in the Synopsis, will be continued in Volume II of the *Research Summary 36-1*.

A. Spacecraft

1. Telemetry Antenna

At the time of *Vega* cancellation, development of the third-stage telemetry antenna system had reached the stage of preliminary radiation pattern measurements to determine a suitable configuration. An essentially omnidirectional pattern was desirable since the antenna was to provide satisfactory coverage for a variety of possible missions and trajectories. It was also desirable to have uninterrupted telemetry reception in the event of vehicle guidance failure. Therefore, very low pattern levels over a substantial solid angle were avoided. A resonant quarter-wavelength stub antenna was chosen for the radiating element since it exhibited a resemblance to the desired omnidirectional antenna and was a very simple antenna to construct.

A quarter-scale model of the antenna and ground plane is shown in Figure 57. Figure 58 shows two of these antennas mounted on a quarter-scale model of the *Vega* vehicle (after first-stage separation). Radiation patterns have been taken with this configuration with both antennas driven in phase, with the antennas driven 180 degrees out of phase, with the antennas driven 270 degrees

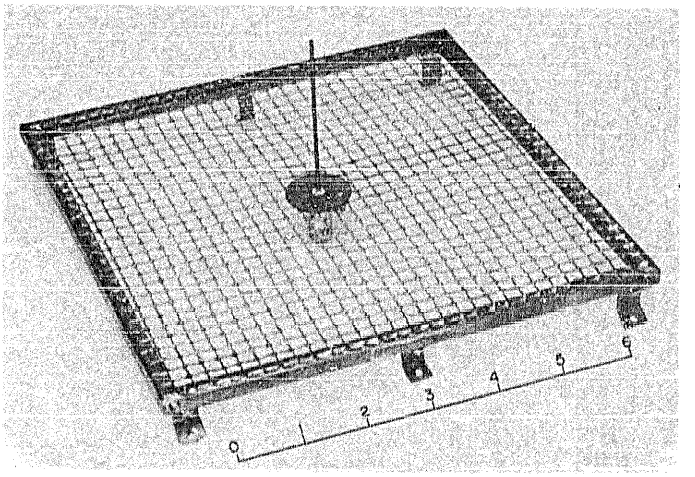

Figure 57. Third-stage telemetering antenna, ¼-scale model

out of phase, and with only one antenna driven. Preliminary evaluation of the patterns indicated that two antennas driven in phase covered 25% more solid angle area than the single antenna, 100% more than the two antennas driven 180 degrees out of phase, and 30% more than the two antennas driven 270 degrees out of phase,

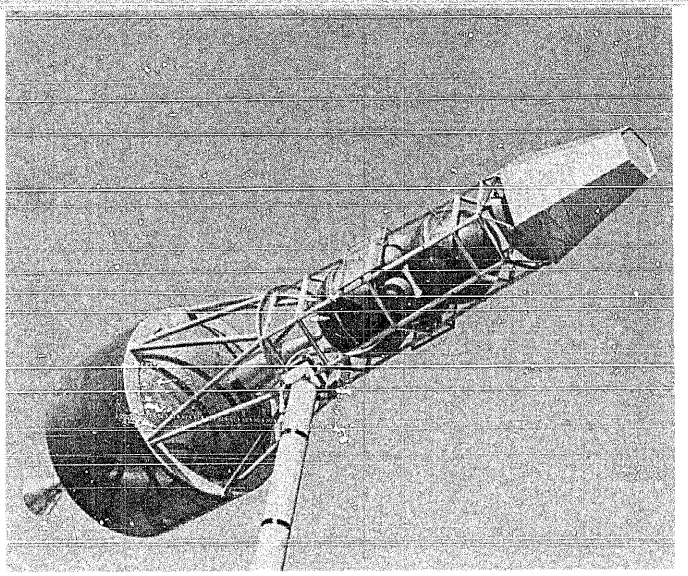

Figure 58. Third-stage telemetering antenna, mounted on spacecraft mockup

above the −10 db level relative to a half-wave dipole. The two antennas driven in phase covered 80% of the total 4π solid angle down to this level.

Measurements of impedance vs length of the ¼-inch-diameter unmatched stub showed the resonant length to be 0.231λ. The resonant resistance was determined to be 26 ohms. Hence, a simple $\lambda/4$ coaxial matching section of 36-ohm characteristic impedance would be required to match the antenna into a 50-ohm transmission line. Cancellation of the program occurred before fabrication of a full-scale prototype with matching section was completed. No further work on the development of this antenna will be done.

2. Controller

The controller is a device whose primary purpose was to coordinate the intersystem activities of the spacecraft. To this end the controller was to perform the following general functions:

(1) Generate timing information.

(2) Receive information and/or commands from: (a) earth-based control during preflight system tests, (b) earth-based radio control during flight, (c) timer, and (d) on-board systems to indicate the existence of conditions requiring action by other systems.

(3) When required, generate commands based upon information from the sources shown in Item (2).

(4) Route the commands to the appropriate spacecraft systems for action.

The specific functions of the controller based on a *Vega*-boosted direct ascent were planned: (1) to provide timing pulses for the stepping switches of the telemetry, and (2) to initiate a flight sequence by generating commands based on timing information from the timer of the controller.

A tentative flight sequence was prepared for a *Vega*-boosted direct ascent (Table 14). The times listed were intended to give an idea of the relative sequence of events.

Table 14. Flight sequence for *Vega*-based spacecraft

Time	Type[a]	Org[b]	Des[b]	Occurrence or command
X	I	EA	CL	Launch has occurred
X	C	CL	CL	Start timer
X + 17 min	T	CL	ST	Unfold solar panels
X + 17 min	T	CL	ST	Extend boom
X + 17 min	T	CL	SC	Turn on solar corpuscular radiation experiment
X + 19 min	T	CL	AC	Turn on attitude control power
X + 19 min	T	CL	AC	Acquire the sun
X + 2 hr	T	CL	ST	Unlatch antenna
X + 2 hr	T	CL	AC	Position antenna
X + 2 hr	T	CL	AC	Acquire the earth
X + 2 mo	T	CL	RF	Turn off transmitter
—	C	ER	RF	Transfer from crystal-controlled to receiver-controlled operation
—	C	ER	AC	Roll-lock override[c]
—	C	ER	AC	Earth-sensor angle override[d]

[a] Indicates the type or nature of an occurrence, where I is initial command, C is a command resulting from a non-timed event, and T is a command resulting from generated time information.

[b] Org indicates the system originating the occurrence or command, and Des, the system receiving and acting upon the information or command. The symbols are identified as follows: AC, attitude control; CL, controller; EA, earth checkout and launch except via RF link; ER, earth control via RF link; RF, communication; SC, scientific instruments; and ST, structures.

[c] Command from earth which will cause the spacecraft to resume rolling in search of earth when the spacecraft has locked in roll on something other than earth.

[d] Command from earth which will cause the earth sensor to change its angle with respect to the roll axis. This command may be used for the purpose of breaking a lock on something other than earth, and also allows setting the earth-sensor angle to some position other than an advance-programmed angle in the event the vehicle does not follow the expected trajectory.

B. Guidance and Control

1. Injection Guidance

a. Injection guidance equations. This report concludes the *Vega* guidance equation analysis with a description of how the optimum coefficients in the equations were obtained. The results of a perturbation study are tabulated for two typical lunar trajectories, a direct ascent and a coasting orbit, using these coefficients.

It was stated (*SPS 6*) that guidance equations for the precoast stages of a *Vega* coasting orbit lunar trajectory should be based on nulling deviations in the conic parameters at second-stage shutoff in order to achieve a circular coasting orbit. Subsequent studies have shown, however, that smaller injection errors are obtained when the predicted target error equations are mechanized for guidance during the lower stages as well as in the third stage. To do this, one set of coefficients is used for sustainer and second stage to null the target miss distance due to coordinate deviations at second-stage shutoff, assuming a standard third stage. A different set of guidance coefficients is used for third stage based on nulling target miss distance due to injection deviations.

As one might expect, this leads to a less circular coasting orbit but results in the vehicle having a more nearly standard position and velocity when the third stage ignites at a fixed master time from launch, rather than after a fixed coasting period. This is important, since the cleared integrators before third-stage ignition have no residual error signals present to indicate the vehicle is not flying the standard trajectory. As a result, the third-stage guidance can null only those measured perturbations which arise during the third-stage burning.

The significance of this is demonstrated by the following example. For two trajectories whose only perturbation was a 2% error in booster flow rate, the calculated lunar target miss distance using coefficients for controlling circularity of coasting orbit was 1716 nautical miles compared to 910 nautical miles when the miss vector was nulled.

For the direct ascent case, it was found that there was no significant advantage to using more than one set of coefficients for all stages when the set chosen was based on nulling the lunar miss vector due to injection deviations in velocity and position. It is assumed here that the integrators are not cleared between stages.

Guidance equations. The coordinate system for the *Vega* guidance study is shown in Figure 59. Elevation guidance consists of nulling an error signal V_N, which can be defined as follows:

$$V_N(t) = \delta\dot{P}_m(t) + \frac{1}{\tau_E}\delta Q_m(t) \qquad (1)$$

where $\delta\dot{P}_m(t) = \dot{P}_m(t) - \dot{P}_m(t)_{std}$ is the deviation from the standard measured velocity in an arbitrary P direction, and $\delta Q_m(t) = Q_m(t) - Q_m(t)_{std}$ is the measured displacement deviation from standard in an arbitrary Q direction. The quantities $\dot{P}_m(t)$ and $Q_m(t)$ are obtained in the vehicle by integration of the outputs of the orthogonal A and B accelerometers in the trajectory plane and multiplying these integrator outputs by the appropriate direction cosines. The corresponding standard values are obtained from the elevation guidance program.

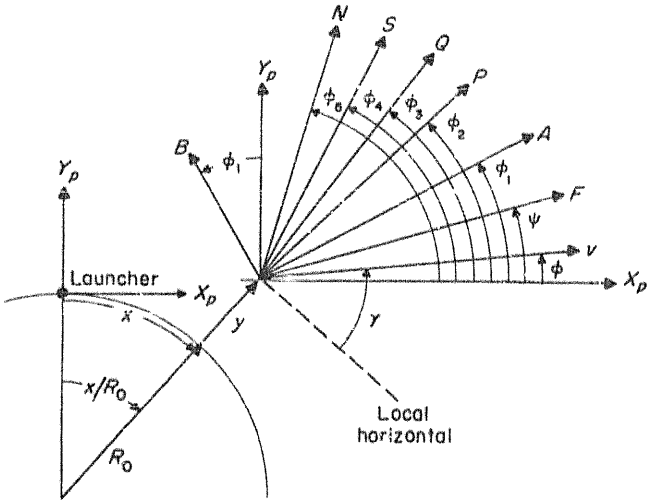

X_p, Y_p = inertial plumb line system erected at launch
A, B = platform fixed accelerometer axes
v = inertial velocity of cg
F = thrust line
P, Q = space fixed elevation guidance directions
S, N = space fixed shutoff equation directions
x = downrange distance from launch site
y = altitude above spherical earth
R_0 = radius of spherical earth (20,902,910 ft)
γ = inertial path angle above local horizontal

Figure 59. Coordinate system for *Vega*

The shutoff equation is similar in form except that the standard coordinates are referenced to a fixed rather than a changing time. The shutoff signal V_S is

$$V_S(t) = \dot{S}_m(t) - \dot{S}_m(t_{ss})_{std} + \frac{1}{\tau_S}\{[N_m(t) - N_m(t_{ss})_{std}] + \dot{N}_m(t_{ss})_{std}[t - t_{ss}]\} \quad (2)$$

where t_{ss} is the standard shutoff time. A term proportional to time-to-go to standard shutoff time is now required. It can be shown that this equation is essentially equivalent to nulling a linear combination of time varying quantities at the standard shutoff time. The motor is shut off when $V_S(t)$ reaches zero, so that on a standard trajectory $V_S(t_{ss}) = 0$. Analogous to P and Q in the elevation guidance equation, S and N are arbitrarily selected axes along which it is desired to null deviations in velocity and position. A time varying program is not required because the V_S equation need only be nulled once during each stage—at the motor shutoff time.

The quantities $1/\tau_E$ and $1/\tau_S$ can be interpreted as weighting factors between position and velocity deviations. In each case τ has the dimension of time; thus, it can be seen that both V_N and V_S have the dimensions of velocity.

The problem is to determine τ_E, τ_S, and the P, Q, S and N directions. The guidance equations that are mechanized in VIGS are somewhat different in form from those just shown, but are equivalent.

The elevation guidance equation in the VIGS mechanization is

$$V_N(t) = E_1\dot{A}_m(t) + E_2\dot{B}_m(t) + E_3A_m(t) + E_4B_m(t) - P_p(t) \quad (3)$$

where $P_p(t)$ is the programmed simulation of the standard trajectory

$$P_p(t) = E_1\dot{A}_{m\,std} + E_2\dot{B}_{m\,std} + E_3A_{m\,std} + E_4B_{m\,std} \quad (4)$$

Thus,

$$\left.\begin{aligned} E_1 &= \cos(\phi_2 - \phi_1) \\ E_2 &= \sin(\phi_2 - \phi_1) \\ E_3 &= -\frac{1}{\tau_E}\cos(\phi_3 - \phi_1) \\ E_4 &= \frac{1}{\tau_E}\sin(\phi_3 - \phi_1) \end{aligned}\right\} \quad (5)$$

The shutoff equation is

$$V_S(t) = K_1\dot{A}_m(t) + K_2\dot{B}_m + K_3A_m + K_4B_m + K_5t + K_6 \quad (6)$$

Thus,

$$\left.\begin{aligned} K_1 &= \cos(\phi_4 - \phi_1) \\ K_2 &= \sin(\phi_4 - \phi_1) \\ K_3 &= -\frac{1}{\tau_S}\cos(\phi_5 - \phi_1) \\ K_4 &= \frac{1}{\tau_S}\sin(\phi_5 - \phi_1) \end{aligned}\right\} \quad (7)$$

K_5 is $-(K_1\dot{A}_{mss} + K_2\dot{B}_{mss})$ and K_6 is evaluated so that $V_S(t_{ss}) = 0$ on the standard trajectory

$$K_6 = -(K_1\dot{A}_{mss} + K_2\dot{B}_{mss} + K_3A_{mss} + K_4B_{mss} + K_5t_{ss}) \quad (8)$$

Nulling lunar miss vector. The miss vector $\vec{B}$ has components $\vec{B}\cdot\vec{R}$ and $\vec{B}\cdot\vec{T}$ along the orthogonal unit vectors $\vec{R}$ and $\vec{T}$ in a plane normal to the trajectory's incoming asymptote. If the first-order partial derivatives of $\vec{B}\cdot\vec{R}$ and $\vec{B}\cdot\vec{T}$, with respect to the plumb-line displacement and velocity components, are known at a given time during flight, the coefficients for the elevation guidance and shutoff equations can be calculated to null deviations in these components of $\vec{B}$ in the following manner. Let these partial derivatives be denoted as a_i and b_i. Consider the equations for the first-order approximation to the miss components:

$$\begin{pmatrix} \Delta\vec{B}\cdot\vec{R} \\ \Delta\vec{B}\cdot\vec{T} \end{pmatrix} = \begin{bmatrix} a_1 & a_2 & a_3 & a_4 \\ b_1 & b_2 & b_3 & b_4 \end{bmatrix}\begin{bmatrix} \delta X_p \\ \delta Y_p \\ \delta\dot{X}_p \\ \delta\dot{Y}_p \end{bmatrix} = \begin{bmatrix} f_1 & f_2 & f_3 & f_4 \\ h_1 & h_2 & h_3 & h_4 \end{bmatrix}\begin{bmatrix} \delta A \\ \delta B \\ \delta\dot{A} \\ \delta\dot{B} \end{bmatrix} \quad (9)$$

where the f_i and h_i are related to the a_i and b_i terms by a rotation through the angle ϕ_1. Now, it remains only to express each of these miss distances in the same form as Equations (1) and (2), i.e.,

$$\frac{\Delta B\cdot R}{(f_3^2 + f_4^2)^{1/2}} = \frac{f_3\delta\dot{A} + f_4\delta\dot{B}}{(f_3^2 + f_4^2)^{1/2}} + \left(\frac{f_1^2 + f_2^2}{f_3^2 + f_4^2}\right)^{1/2}\cdot\left[\frac{f_1\delta\dot{A}}{(f_1^2 + f_2^2)^{1/2}} + \frac{f_2\delta\dot{B}}{(f_1^2 + f_2^2)^{1/2}}\right] \quad (10)$$

(with a similar expression involving $\Delta\vec{B}\cdot\vec{T}$) and equate the right-hand side of Equation (10) to V_N or V_S, as desired. The choice here is arbitrary if no constraints are placed on the orientation of P, Q, S or N or the magnitude of τ. For guidance purposes, however, it is desirable that P be approximately perpendicular to the missile roll axis or thrust direction. Using Equation (10) for the elevation guidance signal together with this constraint (namely, that the direction cosine coefficients of $\delta\dot{A}$ and $\delta\dot{B}$ are

now specified) requires that the R–T coordinate system be rotated through some angle ρ to a new R'–T' system with different partials given by

$$\begin{bmatrix} f_i' \\ b_i' \end{bmatrix} = \begin{bmatrix} \cos\rho & \sin\rho \\ -\sin\rho & \cos\rho \end{bmatrix} \begin{bmatrix} f_i \\ b_i \end{bmatrix}_{i=1,2,3,4} \tag{11}$$

subject to the fixed orientation of $\vec{P}$, i.e.,

$$\tan(\phi_2 - \phi_1) = \frac{f_3'}{f_4'} = \frac{\cos\rho\, f_3 + \sin\rho\, b_3}{\cos\rho\, f_4 + \sin\rho\, b_4} \tag{12}$$

Equation (12) is solved for ρ, which when substituted into Equation (11) yields the f_i' and h_i'. These are then used to determine ϕ_3 and τ_3 by the relationships

$$\tan\phi_3 = \frac{f_2'}{f_1'} \tag{13}$$

$$\tau_E = \left(\frac{f_3'^2 + f_4'^2}{f_1'^2 + f_2'^2}\right)^{1/2} \tag{14}$$

With ϕ_2, ϕ_3 and τ_E now calculated, it is a simple matter to plug them into Equation (5) to obtain the E_i.

It is not necessary to compute the angle of orientation of $\vec{S}$ and $\vec{N}$ in the shutoff equation. By analogy to the foregoing analysis, the shutoff equation is

$$V_S = \frac{\Delta\vec{B}\cdot\vec{T}}{(b_3'^2 + b_4'^2)^{1/2}} = K_1A + K_2B + K_3\dot{A} + K_4\dot{B} + K_5\dot{t} + K_6 \tag{15}$$

where the K_i are now given by

$$\left.\begin{aligned} K_1 &= \frac{b_3'}{(b_3'^2 + b_4'^2)^{1/2}} \\ K_2 &= \frac{b_4'}{(b_3'^2 + b_4'^2)^{1/2}} \\ K_3 &= \frac{b_1'}{(b_3'^2 + b_4'^2)^{1/2}} \\ K_4 &= \frac{b_2'}{(b_3'^2 + b_4'^2)^{1/2}} \end{aligned}\right\} \tag{16}$$

and the K_5 and K_6 are obtained just as in Equation (6).

Results. The lunar miss distance and injection coordinate deviations resulting from a number of perturbations are listed in Table 15 for a 36-hour direct ascent and a 63-hour parking orbit trajectory. The coordinates x, y, v, γ are defined in Figure 59. The value given for the miss distance $\Delta|\vec{B}|$ assumes that there is no midcourse guidance correction applied after injection.

b. Error analysis. A closed-loop analysis of the effect of component errors in the *Vega* injection guidance system has been completed. This closed-loop analysis used a two-dimensional digital trajectory program with guidance. The effects of the component errors were found by the following method:

$$\frac{\partial\vec{B}}{\partial E_i} = \frac{\partial\vec{B}}{\partial C_j}\cdot\frac{\partial C_j}{\partial E_i}$$

where $\vec{B}$ is the miss vector; C_j, the jth guidance parameter (e.g., guidance coefficients, platform orientation, etc.); E_i, the ith component error (e.g., accelerometer null shift, integrator drift, etc.); $\partial\vec{B}/\partial C_j$ is evaluated by perturbing the parameter C_j and comparing the resulting trajectory to the standard; and $\partial C_j/\partial E_i$ is defined by the error equations.

The trajectory used for the closed-loop error analysis was a 36-hour direct-ascent lunar impact trajectory. Table 16 shows the miss distance

$$\vec{B} = \frac{\partial\vec{B}}{\partial C_j}\cdot\frac{\partial C_j}{\partial E_i}\cdot E_i$$

calculated for the following three cases:

(1) Open-loop error analysis
(2) Closed-loop error analysis with the shutoff computer and autopilot
(3) Closed-loop error analysis with the shutoff and elevation guidance computers.

These results show that the open-loop error analysis results are close enough to the closed-loop results to be significant.

2. Mid-Course Guidance

a. Lunar mid-course maneuvers. Lunar mission studies have indicated that the choice of mid-course guidance point as a function of trajectory will govern the useful payload weight (Figs 60 and 61).

The required rms velocity capability, for several trajectories, as functions of time of application of mid-course maneuver is shown in Figure 60. Consideration of computer approximation errors would only shift the curves upward slightly and would not change their character.

On the basis of these studies, it has been concluded that the mid-course correction should take place between 10 and 20 hours after injection, for the range of trajectories studied. This is convenient for two reasons: first, it will take 10 to 20 hours to establish the orbit and calculate the required maneuver and, second, if the firings are southeast from Cape Canaveral, the probe will pass over the Goldstone tracking site during this period. Thus the Goldstone tracking site will be able to command and observe the maneuver.

Figure 61 is a plot of separated spacecraft weight and useful payload as a function of trajectory length. Useful

Classification Changed to UNCLASSIFIED
Authority JPL-EPD #20 2 Jan 1961
Date 11-3-62
By V. Pritchard
CONFIDENTIAL UNCLASSIFIED

Table 15. Lunar miss distance and injection coordinate deviations for two perturbed trajectories

Nature of perturbation	Trajectory	$\Delta\|\vec{B}\|$, km	Δx, km	Δy, km	Δv, meters/sec	$\Delta\gamma$, radians
Booster: standard Sustainer: standard Second stage: standard Third stage: 3-σ propellant flow-rate variation of 1.7%	36-hour direct ascent 63-hour coasting	79.4 523	6.47 6.32	3.14 0.83	−3.12 −1.30	0.0006 0.0010
Booster: standard Sustainer: standard Second stage: 2% flow-rate variation Third stage: standard	36-hour direct ascent 63-hour coasting	510 1062	6.04 −0.44	1.05 9.70	−4.06 −8.51	0.0005 0.0008
Booster: standard Sustainer: standard Second stage: 3-σ variation in specific impulse of 1.5% Third stage: standard	36-hour direct ascent 63-hour coasting	42.7 550	3.42 −0.24	1.64 4.92	−1.63 −4.35	0.0003 0.0004
Booster: standard Sustainer: standard Second stage: 0.5-degree thrust attitude error Third stage: 0.5-degree thrust attitude error	36-hour direct ascent 63-hour coasting	157 6058	2.73 −26.87	2.78 33.53	−2.91 −27.20	0.0005 0.0043
Booster: standard Sustainer: 0.82% flow-rate variation Second stage: 0.82% flow-rate variation Third stage: 0.70% flow-rate variation	36-hour direct ascent 63-hour coasting	617 216	17.16 6.83	6.39 −1.02	−9.43 0.39	0.0016 0.0005
Booster: 2% flow-rate variation Sustainer: 2% flow-rate variation Second stage: standard Third stage: standard	36-hour direct ascent 63-hour coasting	1398 1368	−5.27 −8.85	17.68 2.79	−14.84 −3.92	0.0018 −0.0007
Booster: 2% flow-rate error Sustainer: 2% flow-rate error Second stage: 0.82% flow-rate error; 0.5-degree thrust attitude error Third stage: 0.70% flow-rate error; 0.5-degree thrust attitude error	36-hour direct ascent[a] 63-hour coasting[a]	1436 1617	−0.71 −2.70	20.60 2.48	−19.14 −4.15	0.0025 −0.0002

[a]Several 3-σ errors make this an extreme perturbation case.

payload is defined as separated spacecraft weight minus the weight of the mid-course rocket and propellant. The following parameters have been assumed in these calculations: a specific impulse of 230 seconds and a mass ratio of 6.0. The calculations were made for two different types of mid-course systems:

(1) The correction made in the critical plane to adjust the miss-components ΔM_1 and ΔM_2.

(2) The correction made in a direction to adjust ΔM_1, ΔM_2 and time of flight variation ΔT_f. (Any direction may be required depending on the maneuver point and the numerical values of ΔM_1, ΔM_2 and ΔT_f.)

The curves indicate that maximum useful payload occurs for trajectory lengths of 60 to 80 hours; the curves also indicate the additional weight penalty to adjust ΔT_f in addition to the miss-component ΔM_1 to ΔM_2. Maximum useful payload is, of course, only one parameter involved in the choice of a trajectory for a given mission.

b. Attitude control. The complete mathematical model for the *Vega* third-stage dynamics has been incorporated in the control-loop studies. The model contains the effects of fuel sloshing, motor inertia and vehicle flexibility. The guidance loop has been closed around the attitude loop, and the gain margin evaluated for various flight times.

The autopilot insures stability of the system for all flight conditions if the guidance gain is kept below a certain value. This value of guidance gain is at least a factor of 4.5 above the nominal gain required. Given another angular reference, the autopilot system of the 6K-stage does not depend on the VIGS guidance system for proper operation. Study of this autopilot has ceased with the cancellation of the *Vega* program.

Classification Change
UNCLASSIFIED
Authority
JPL-EPD #20 2 Jan 1961
Date 11/5/62
By V. Puitcho

Table 16. Component error analysis of 36-hour lunar trajectory

Error source	1-σ error	Lunar miss, nautical miles		
		Open loop	Closed loop	
			Shutoff and autopilot	Shutoff and elevation
Accelerometer scale factor, absolute	0.02%	74.9	66.3	120.7
Accelerometer scale factor, stability	0.02%	208.1	204.7	236.0
Accelerometer null shift, absolute	3×10^{-4} g	428.8	455.8	487.3
Accelerometer null shift, stability	10^{-4} g	78.3	77.1	83.5
Accelerometer non-orthogonality	3×10^{-4} rad	390.5	428.1	440.1
Platform erection mixing error	3×10^{-4} rad	158.9	140.8	256.1
Integrator scale factor, stability	0.025%	276.7	272.1	314.3
Integrator drift, absolute	$\frac{1}{3}$ mv/min	102.6	95.1	96.6
Integrator drift, stability	1 mv/min	324.2	319.3	346.7
Total error	rms total	780.3	805.1	895.7

The mid-course attitude control system controls the vehicle attitude in such a manner that the velocity change vector of the mid-course rocket is properly directed.

Prior to ignition of the mid-course motor, the vehicle performs an attitude maneuver to aline the axis of the motor with the desired line of action of the thrust vector. The rocket motor is then ignited and the attitude control maintains the direction of the mid-course motor within certain tolerances.

Maintaining the direction of the mid-course motor may be accomplished by maintaining the attitude of the spacecraft. However, due primarily to uncertainty of the location of the center of mass of the spacecraft, this method of control involves errors of the order of 1 degree (2-σ) because for any situation where the spacecraft does not undergo continuous angular acceleration, the thrust vector of the mid-course rocket becomes alined with the center of mass of the spacecraft. An alternate approach to holding the attitude of the spacecraft constant is to hold the direction of the mid-course thrust vector constant, controlling the attitude of the spacecraft in such a manner that its center of mass moves into alinement with the thrust vector of the mid-course rocket.

The dynamics of the spacecraft include a flexible 15-foot boom with a massive package at its extremity

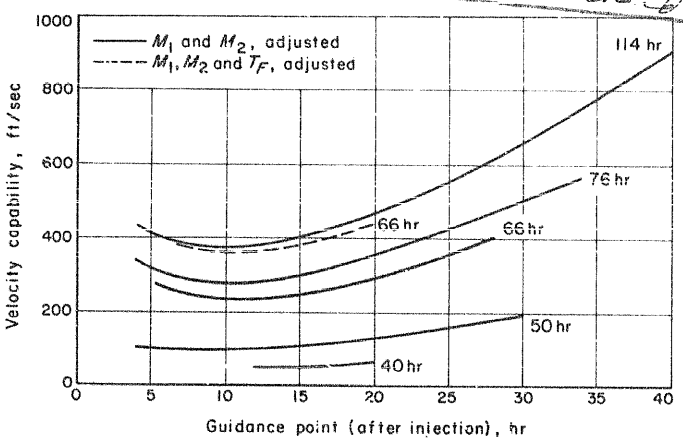

Figure 60. Required velocity vs lunar guidance points

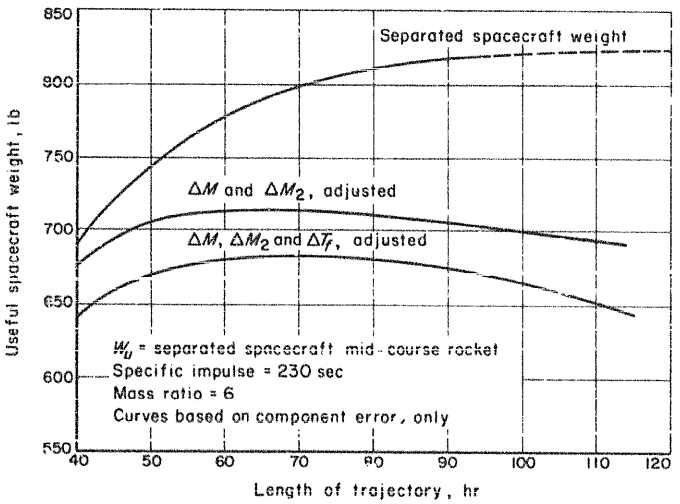

Figure 61. Spacecraft weight vs length of trajectory

extended from the spacecraft. It is believed that the describing-function approach will be used to study on-off control system configurations. System stability will be checked with the analog computer.

Two control systems are being considered. The first is an on-off system using hot gas bled from the mid-course motor combustion chamber. This system has the advantage of simplicity, in that the existing coasting-flight attitude control circuitry can be utilized, but suffers because no easy way is seen to determine the direction of the resultant thrust vector. The second system uses a gimbaled mid-course rocket motor. This system has the advantages of linearity and ease in determining the direction of the thrust vector, but requires electronics separate from the existing coasting-flight attitude control system.

Reference

1. Schwartz, M., *Information Transmission, Modulation, and Noise*, McGraw-Hill Book Company, Inc., New York, N. Y., 1959.